Investigation of Radiation Shielding Efficacy of Vanadium–Tellurite–Antimonite Semiconducting Glasses

Yasser Rammah (dr_yasser1974@yahoo.com)
Menoufia University https://orcid.org/0000-0003-3106-5571
I.O. Olarinoye
Federal University of Technology Minna
F.I. El-Agawany
Menoufia University
K A Mahmoud
Ural Federal University named after the first President of Russia B N Yeltsin: Ural'skij federal'nyj universitet imeni pervogo Prezidenta Rossii B N El'cina
Iskender Akkurt
Suleyman Demirel University: Suleyman Demirel Universitesi
El Sayed Yousef
King Khalid University

Research Article

Keywords: Vanadio-tellurite glasses, Shielding properties, Monte Carlo simulation, SRIM

Posted Date: November 13th, 2020

DOI: https://doi.org/10.21203/rs.3.rs-104534/v1

Investigation of radiation shielding efficacy of vanadium–tellurite–antimonite semiconducting glasses

Y.S. Rammah[1,*], I.O. Olarinoye[2], F.I. El-Agawany[1], K A Mahmoud[3,4], Iskender Akkurt[5], El Sayed Yousef [6,7]

[1]Menoufia University, Faculty of Science, Physics Department, 32511 Shebin El Koom, Egypt.

[2]Department of Physics, School of Physical Sciences, Federal University of Technology, Minna, Nigeria

[3]Ural Federal University, 19 Mira St, 620002, Yekaterinburg, Russia.

[4]Nuclear Materials Authority, P. O. Box 530, El Maadi, Cairo, Egypt.

[5]Süleyman Demirel University, Faculty of Arts and Sciences, Physics Department, Isparta-Turkey

[6]Research Center for Advanced Materials Science (RCAMS), King Khalid University, P. O. Box 9004, Abha 61413, Saudi Arabia.

[7]Physics Dep., Faculty of Science, King Khalid University, P. O. Box 9004, Abha 61413, Saudi Arabia

Corresponding author: Y.S. Rammah (dr_yasser1974@yahoo.com)

Abstract

Effects of antimony trioxide (Sb_2O_3) on neutron and gamma-radiation shielding parameters of tellurite vanadio-antimonite glasses with compositions $40TeO_2$-$(60-x)V_2O_5$-xSb_2O_3: $0 \leq xSb_2O_3 \leq$ 10 mol% coded as (TVS0-TVS10) were investigated. The mass attenuation coefficients (MAC) were evaluated using the Monte Carlo simulation code (MCNP-5) and WinXcom program for photon energies in the range of 15 keV to 15 MeV. The SRIM program was used to compute the stopping power and projected range of the charged particles, such as proton and alpha particles, on the investigated glass samples. Based on the theoretically evaluated MAC, some shielding parameters were computed, such as linear attenuation coefficient, electric cross-section, atomic cross-section, effective atomic number, half-value thickness (HVT), and the mean free path. The EXABCal program was applied to predict the level of the photons accumulation in the investigated glass samples (buildup factors). The effective cross-section for fast neutrons was computed theoretically based on the fast neutron effective removal cross-section (Σ_R) for the constituting components. Results revealed that the maximum values of MAC exceed in the range between 28.9-31.3 cm^2/g with increasing the Sb_2O_3 substitution ratio between 0-10 mol %, respectively. In contrast, the HVT values decrease with an increase in the increment of Sb_2O_3 rate. The maximum (Σ_R) was obtained for glass coded TVS0 among the investigated glasses. Results concluded that

the higher Sb_2O_3 concentration in TVS glasses leads to an increase in their capability to apply in several radiation shielding applications.

Keywords: Vanadio-tellurite glasses; Shielding properties, Monte Carlo simulation; SRIM

1. Introduction

Formerly, semiconducting glasses have been extensively studied via two categories: oxide glasses and chalcogenide glasses. The chalcogenide glasses modified with transition metal oxides (TMOs) have unique structure, physical, optical, mechanical, electrical, thermal, semiconducting, and radiation shielding features [1-12].

Recently, glass materials in their different structures have an essential role in most modern applications such as laser medium, optical switching instruments, optoelectronic materials, and space technology [13-15]. Besides, glasses can be applied in medical applications in CT scans, windows, and doors in nuclear medicine. For the characteristics mentioned above, glasses got more attention to be utilized as an alternative radiation protection materials instead of rocks, bricks, concrete, alloys, and polymers materials [9-12, 16-18].

From our best acquaintance that tellurite, phosphate, borate, and silicate-based glass networks are the best glass candidates due to their excellent characteristics, for example (low cost and ease molding, low melting points, high transparency, and good thermal stability) [8-10]. Moreover, TeO_2 based glasses have gained more focusing from many researchers and investigators due to their unique features such as high linear and nonlinear refractive indices and good shield for radiations [11, 15, 19-22]. Therefore, glasses with TeO_2 as a former have many beneficial uses in the solid-state lasers applications, memory switching instruments, and solar cells [23-25].

Commonly, vanadium oxide (V_2O_5) is also an excellent glass former and enhances the magnetic, electric properties of the synthesized glasses [1,3]. Furthermore, modification of the TeO_2 glass with V_2O_5 produces the n-type semiconducting glass samples, which contain V^{+4}/V^{+5} valance states [1,3,9].

The impact of antimony trioxide (Sb_2O_3) on the electrical conduction, optical energy gap, and small polaron transport in TeO_2-V_2O_5 glasses have been reported via Mori et al. [26], Souri and Shomalian [27], and Ghosh [28], respectively.

In this study, neutron and gamma radiation shielding competences, mass stopping power, and projectile range for proton and alpha particles were evaluated for the TeO_2-V_2O_5-Sb_2O_3 (TVS) glass samples to be used in nuclear protection applications.

2. Materials

In the present study, four samples of vanadium–tellurite–antimonite glasses selected from Ref [27] with chemical compotion determined from the formula $40TeO_2$-$(60-x)V_2O_5$-xSb_2O_3; $0 \leq xSb_2O_3 \leq 10$ mol%. The investigated samples coded as:

$40TeO_2$-$60V_2O_5$-$0Sb_2O_3$ (TVS0) for x=0 mol%,

$40TeO_2$-$55V_2O_5$-$5Sb_2O_3$ (TVS5) for x=5 mol%,

$40TeO_2$-$52V_2O_5$-$8Sb_2O_3$ (TVS8) for x=8 mol%,

$40TeO_2$-$50V_2O_5$-$10Sb_2O_3$ (TVS10) for x=10 mol%.

The principle information, such as the density, molecular weight, molar volume, and chemical concentration of the investigated glass samples was listed in **Table 1**.

3. Results and discussion

3.1 Linear and mass attenuation coefficient (LAC and MAC)

The interaction of photons with an absorbing medium, as it propagates in the medium, can be quantified in several parameters. Generally, the transmission of photons of particular energy is governed by the modified Beer-Lambert equation:

$$X = Be^{-\mu t} \quad (1)$$

X is the ratio of a measured photon quantity/quality parameters (such as dose, intensity, energy, and or number flux) of interest at a particular point with an absorber of thickness t to the same parameter without the absorber. The parameters B and μ are called the photon buildup factor and linear attenuation coefficient (LAC) of the absorber. B represents the number of photons scattering and buildup within the material, while μ is the ability of the material to resist the passing of photons

through the studied material. Generally, LAC depends on absorber thickness, photon-energy, and the chemical nature of the glass network.

The mass attenuation coefficient (MAC) defined as:

$$MAC = \frac{\mu}{\rho} = \mu_m \tag{2}$$

With ρ being the mass density of the absorbing medium. However, μ_m does not depend on thickness but on the nature of absorbing material and photon energy only. In equation (1), when μ_m is used, t is given in mass thickness (ρt) to conserve the dimension of the equation. MAC thus measures the level of interaction (absorption) of photons of distinct energy by a material. It is, in fact, an indication of the sum of all possible photon interaction cross-sections (CS) (i.e., photoelectric effect (PE), incoherent scattering (IS), and pair production (PP)) of photons in the material.

The MAC of the four investigated TVS glass samples in this research was simulated MCNP-5 code, and WinXCOM computer code [29, 30] at gamma-photon energies ranged between 0.015-15 MeV. The simulated MAC values for the TVS glasses were illustrated in Fig 1 as a function of the incident photon energy. It was observed that the MAC variation for the TVS glass samples under consideration with photon-energy is similar. The maximum MAC values for TVS glasses were obtained at the lowest photon energy (i.e., 0.015 MeV) among the selected energy range. On the other hand, the maximum MAC values changed between 28.9-31.3 cm^2/g for TVS0 and TVS10, respectively. The recorded MAC values decreased sharply with raising the photon energy to 0.1 MeV for each glass. Above the mentioned energy, the decrease in the MAC slowed down and was almost a constant between 3 MeV and 10 MeV. The least MAC values were obtained at 8 MeV for TVS5 (0.0292 cm^2/g), TVS8 (0.0296 cm^2/g), and TVS10 (0.0299 cm^2/g) and 10 MeV for TVS0 (0.0284). The lower values of the MAC extend from 1 MeV up to the end of the energy spectrum. The behavior of the MACs affected by the different photon partial interaction cross-sections (ICS) and the chemical concentrations of the investigated TVS glasses. Generally, photons with higher energy are more penetrating. This is because the probability of interaction of such energetic photons with the atoms of the interacting medium decreases with an increase in incident photon energy. Such interactions generally reduce the energy of the photons, thus leading to absorption. With the reduction of the different ICS, MAC reduces and hence higher penetration

(transmission) of such photons. Also, at a lower energy region (0.015–0.1 MeV) of the spectrum considered, PE has the highest ICS. Theoretically, the ICS of PE varies inversely with the 3rd-power of the energy [30,31]. This explains the sharp drop in MAC from the maximum value for all glasses. Also, within the lower energy region, the MAC values of all TVS glasses differ in the order of the increase in Sb_2O_3 content. The partial replacement of V_2O_5 in the glass with Sb_2O_3-a denser compound with higher atomic number constituent (Sb) could have increased the effective atomic number of the glass. Since the ICS of PE varies directly with the 4th power of Z of photon absorbing medium, MAC would be higher for the medium with a higher atomic number. It is thus safe to suggest that the addition of a denser Sb_2O_3 to the glass matrix increased the effective atomic number of the glass samples.

Consequently, samples with higher Sb_2O_3 content possess higher MAC values in the low energy region where the photoelectric effect dominates. This explains while the MAC values increase in the order TVS0<TVS5<TVS8<TVS10 at each energy in this region. This is further emphasized in the inset of Fig 1. Furthermore, the increase in the denser Sb_2O_3 content quantitatively manifests in the density of the glass samples. As the molar concentration of Sb_2O_3 was increased from 0 for TVS0 to 10 (mol %) for TVS10, the mass density increased from 3.71 g/cm^3 to 3.922 g/cm^{3,} respectively. The increase in density implies more atoms per unit volume of the absorber are available for interaction with photons. Higher photon interaction per unit volume gives rise to more interactions, higher energy loss for the photons, and ultimately high MAC values as density increased.

For the energy region beyond 0.1 MeV, the IS dominates the MAC values. Generally, the ICS of IS varies inversely with energy and directly with the electron number per unit mass $\left(\approx Z/A\right)$ of the interacting medium. For most elements except H, $\left(Z/A\right)$ is almost a constant [31]. Consequently, for non-hydrogenous mixtures and compounds, such as glass and ceramics, $\left(Z_{eff}/A_{eff}\right)$ is nearly a constant. This explains the roughly constant values of MAC for each glass sample in the energy range of 1 MeV and 6 MeV, where IS interaction mode dominates. Beyond 6 MeV, the PP ICS dominates the MAC values. The PP interaction mode varies the square of the atomic number, thus the slight increase in the MAC values in PP dominated region as the Sb atomic content, and

subsequently, the density is an indication of an increase in the effective atomic (electron) number of the glass samples.

Generally, the MAC variations for TVS glass samples vary smoothly with energy, as depicted in Fig 1, except at gamma-energy around 0.040 MeV, a sharp peak was observed. The observed peak results due to the photon K-absorption edge of Te-atoms, which occurs at the mentioned energy. There is an obvious increase in the MAC values of the glass samples as their density increased in the lower photon energies (less than 1.5 MeV) compared to the energy region above 1.5 MeV. This implies that an increase in Sb content in the investigated TVS glass samples improves the shielding capacity of the glass samples more in the low energy region compared to at energies above 1.5 MeV.

The simulated MAC was compared to the MAC obtained using the WinXCOM computer program, as illustrated in table 2. The difference between the simulated and computed MAC was calculated and also presented in Table 2. The results showed that the difference was ranged between 0.5-10 %.

The variation of the linear attenuation coefficients (LAC) versus the incident photon energy for the glassTVS samples is illustrated in Fig 2. As expected from the equation, the variation of LAC with energy follows a similar pattern as early mentioned in MAC in Fig 1, different only in the magnitude of their values. The trend in which the LAC varies can be attributed to the same reasons as given for MAC. The maximum LAC values of 107, 114, 119, 123 cm^{-1} were obtained at 0.015 MeV for TVS0, TVS5, TVS8, and TVS10. The lowest LAC values are 0.105, 0.111, 0.114, and 0.117 cm^{-1} and obtained at 10 MeV for glasses TVS0, TVS5, TVS8, and TVS10, respectively. Throughout the energy spectrum, the LAC values showed a strong positive linear dependence on the mass density of the glass. However, this linear relationship was more pronounced in the lower energy (E< 1.5 MeV) region than the high energy region.

3.2.2 Half-value layer (HVL) and mean free path (MFP)

The HVL is the thickness of the absorber required to decrease the photon intensity to half its initial value. From equation (1), for good geometry, at HVL value, one can write:

$$X = \frac{1}{2} = Be^{-\mu HVL} \Rightarrow HVL = \frac{\ln 2}{\rho \mu_m} \tag{3}$$

In radiation protection analysis, the HVL is an important parameter when considering the choice of material in radiation shielding application. It is a quantity that can be used to relatively compare the photon shielding capacity of different materials when faced with different choices. **Fig 3** shows the variation of HVL of the glass materials with photon energy. The inset shows the variation for energies between 30 keV and 80 keV. The HVL variation shows a reverse trend when compared to those of MAC and LAC. The HVL generally increased in values for all the glass systems as the photon energy increased. At all energies, the HVL of TVS0 was highest while those of TVS10 were at least. At 0.1 MeV, the HVL of TVS0, TVS5, TVS8, and TVS10 were 0.29, 0.252, 0.232, and 0.218 cm respectively. These are lower when compared to 0.417 cm, the value of that of heavy (steel magnetite) concrete [32] at the same energy. This is an interesting result since the density of the heavy concrete of 5.11 g/cm^3 is higher than those of the glass samples. Using the HVL data, the photon shielding efficacy of TVS10 was almost twice that of heavy concrete despite being more than 20 % less dense.

The mfp of photons of specific energy, as defined in equation (4), is another quantity that compares the shielding effectiveness of materials.

$$MFP = \frac{1}{LAC} \tag{4}$$

The variation of MFP (cm) as a function of photon energy is shown in Fig 4. The inset as well indicates the interpretation for the energy range of 30-80 keV. The trend of MFP is similar to that of HVL; consequently, the MFP has a negative linear relationship with the density of the glass samples. The difference in density of the glass samples under consideration was strongly influenced by their relative shielding capacity.

3.2.3 Effective Atomic Number (Z_{eff})

Many photon interaction modes depend on the effective atomic number (Z_{eff}) of the interacting medium. Unlike the atomic number of pure elements, Z_{eff} is not a constant concerning photon energies. Still, it depends on the comparative importance of photon interaction processes at the energy of interest and the chemical composition of the material. Z_{eff} can be an essential quantity in radiation dose measurement and shielding calculation. The effective atomic number can be estimated using Equation (5) [33]:

$$Z_{eff} = \frac{\sum_i f_i A_i (\mu_m)_i}{\sum_j f_j \frac{A_j}{Z_j} (\mu_m)_j} \quad (5)$$

f_i, A_i and Z_i refer to fractional abundance, atomic mass, and the atomic number of the elements constituting the TVS glass samples . The relative variations of Z_{eff} versus photon energy for the glasses are depicted in **Fig 5**. The Fig shows the trends for the four sampled glasses between energies of 15 keV and 15 keV. Throughout the energy spectrum, the Z_{eff} increased in the order of increasing Sb_2O_3 concentration in the glass. Thus, Z_{eff} of TVS0<TVS5<TVS8<TVS10. This trend follows similarly with the density. This confirms the hypothesis that the addition of high atomic number Sb increased the Z_{eff} of the glasses. From this result, one can conclude that glasses with higher Z_{eff} have higher MAC and are thus better photon shield comparatively. Generally, the Z_{eff} increased with energy up to 0.06 MeV before they begin to decrease afterward until the energy of 5 MeV is attained. After 5 MeV, the $Z_{eff\ begins}$ to rise again. This trend is due to the dependence of the different photon interaction modes on Z_{eff} and their relative dominance at different photon energy range. A similar trend has been reported for other types of glasses [34]. The mean Z_{eff} of the glasses for the considered energy spectrum was 18.81, 19.79, 20.37, and 20.75 for TVS0, TVS5, TVS8, and TVS10, respectively.

3.2.4 Fast neutron effective removal cross-section (FNRCS)

The probability that a fast neutron will undergo its first collision with the nucleus of an interactive medium, which could lead to its slowing down and subsequent removal from un-colliding ones, may be referred to as fast neutron effective removal cross-section (FNRCS)- Σ_R. Σ_R has been developed to accommodate neutron scattering and buildup. For the glass samples, Σ_R was estimated via the next equation (6) [34]:

$$\sum_R = \sum w_i \left(\frac{\sum_R}{\rho} \right)_i \quad (6)$$

where w_i and $\left(\Sigma_R/\rho\right)_i$ The partial density and the fast neutron mass removal cross-section of the ith component of the composite glass, respectively. Table 3 presents the calculated Σ_R/ρ of the

glasses. The values of Σ_R/ρ are: 0.0954 and 0.0257; 0.094 and 0.0249; 0.0939 and 0.0244; and 0.0945 cm^{-1} and 0.0241 cm^2g^{-1} for TVS0, TVS5, TVS8, and TVS10 correspondingly. The maximum value of the Σ_R/ρ was obtained for TVS0 while the least value is0.0241 cm^2g^{-1} and for 0btained for TVS10. The variation of the chemical constituents of the glasses is mainly responsible for the difference in their neutron removal cross-sections. The increase in the atomic concentration of Sb is largely responsible for decreasing the Σ_R/ρ values since it has higher fast neutron removal cross-sections compared to V.[35,36]

3.2.5 Buildup factors

The buildup factors measure the accumulation of photons during passing the energetic photons thought the investigated TVS glass samples. The energy absorption buildup factor (EABF) and exposure buildup factor (EBF) of the TVS glasses evaluated utilizing the EXABCal [37,38]. The calculation was runout along the energy range varied between 0.015 and 15 MeV and for penetration depth extended to 40 mfp. Generally, the variation of the buildup factors (EABF and EBF) as a function of the gamma-photon energy and the absorber penetration depth are illustrated in **Figs 6-9** for the investigated TVS glasses.

The mentioned figures showed that the calculated values of the buildup factors are virtually affected by the penetration depth of the utilized glass and the gamma-photon energies. Along with the gamma-energy range, the lowest accumulation of photons recorded in the photoelectric (PE) region, where the photon energy ranged 0.015-0.2 MeV. In the previously mentioned energy zone, one boundary electron absorbs the incident photon energy. Thus, the number of photons inside the glass is almost eradicated, and the buildup factor dropped to minimum values. Like the MAC and LAC, an unexpected increase in the EABF and EBF values around 0.04 MeV due to the K edges of Te, representing one of the former glass elements in the current study. Above gamma energy of 0.2 MeV, the PE interaction became weaker while the Compton Scattering (CS) interaction gradually increased. In the mentioned interaction, the energy of the incident photon is partially absorbed by the glass electrons and the photons with the rest of the energy accumulated inside the investigated glass samples. Thus, the buildup factors gradually increased with increasing the incident gamma photon energies. The buildup factors for all studied TVS glass samples touch maximum values around 0.8 MeV, where the CS is the primary interaction in the fabricated glass

samples. After that, the CS began to decreased gradually, associated with reducing the buildup factors. For high gamma energy above several MeV, the Pair production interaction (PP) become stronger, and the incident gamma photon in this energy range was annihilated and produced electron-positron pairs. Thus, the accumulation of photons decreased associated with reducing the buildup factors.

The variation of the buildup factors as a function of the glass chemical composition and the penetration depth was illustrated in Figs 10-12. It is clear that the absorbed penetration depth has a significant effect on the accumulation of photons in the studied glass material. The mentioned figures depict that the thicker layers of the studied materials can accumulate photons higher than the thinner once. The reason for this phenomenon is that the thicker glass layers required more time to be penetrated by photons. Thus, the photons can make more interaction along there path length in the glass samples, and this causes more scattering for photons from their path length. Therefore, the result is the accumulation of the photons in the thicker thickness more than, the thinner once. The chemical composition of the studied glass samples also plays an essential role in the accumulation of the incoming photons. Figures 10-12 showed that increasing the insertion ratio of the Sb_2O_3, causing a diminished in the photon accumulation in the fabricated glass samples at low and mid- energy photons (0.15 and 1.5 MeV). It is clear that the buildup factors for TVS0>TVS5>TVS8>TVS10. In contrast, for high gamma photon energy (i.e., 15 MeV), increasing the substitution ratio of Sb_2O_3 causing an increase in the buildup factors of the studied glass samples where the values of the buildup factors in the mentioned energy are in order of TV10> TVL8>TVL5>TVL0. The way in which the buildup factors varied with the material chemical composition is related to the Zeff of the studied glass samples.

3.2.6 The charged particles stopping power and projected range

In the present study, the SRIM program was utilized to predict stopping power (Ψ) and projected range (Φ) for some charged ions, such as (^4_2He) Alpha particle and (^1H) proton in the energy range between 0.01-10 MeV [39,40]. The stopping power is used to describe the amount of energy lost by the charged particles (alpha and proton) along their path length in the studied glasses. This loss in energy is due to the collision of the incident charged particles with the electrons and atoms constituting the glass network. The projected range is a term used to show the distance in which

the charged particle lost all of its energy and transferred to a rest state. The predicted results were presented in Figs 13 and 14. The mentioned figures showed that both Ψ and Φ are affected by the same parameters chemical composition and the kinetic energy of the incident particle. Fig 13a and 14a showed that the Ψ of proton and alpha particles have the same variation with the kinetic energy of the incident charged particle where the Ψ for proton and alpha particles began small at low kinetic energy and increased gradually with increase the kinetic energy of the incident particle. The mass stopping power for protons reaches maximum values at kinetic energy around 0.1 MeV, while for alpha particle, it reaches maximum values at higher energy around 0.8 MeV. This can be related to the mass and speed of particles where the mass of alpha particles is high, so it creeps and lost a high amount of energy in a small path distance. In contrast, protons have a small mass and high speed. Thus, the mass storing power of the alpha particle is higher than that of the proton.

Figures 13b and 14b showed that the Φ of protons and alpha particles increases with an increase in the incident kinetic energy of the incident particle. The Φ of protons is several hundred μm while the Φ of alpha is lower and in the range of several μm only. This high gape between the Φ of proton and alpha particles related to their speed. The alpha particles have a slow speed, so it loses a considerable amount of energy in a small range along its path length. In contrast, protons have a high speed to travel a longe distance associated with losing a small part of their energies.

The Φ of protons and alpha particles was also affected by the Sb_2O_3 substitution ratio, where the Φ decreased with increasing the Sb_2O_3 insertion ratio for both proton and alpha particles.

4. Conclusion

The main objective of this study is to investigate the effects of antimony trioxide (Sb_2O_3) on neutron and gamma radiation shielding parameters of ternary tellurite vanadio-antimonite glasses with compositions $40TeO_2$-$(60-x)V_2O_5$-xSb_2O_3: $0 \leq xSb_2O_3 \leq 10$ mol% coded as (TVS0-TVS10). The (MAC), (LAC), (HVL), (mfp), and (Z_{eff}) were evaluated using WinXcom program for photon energies in the range of 15 keV to 15 MeV. Photon energy absorption (EABF) and exposure (EBF) buildup factors were evaluated via the use of EXABCal program. Results revealed that:

1- The HVL values decrease with the increment of Sb_2O_3 content in the order TVS0>TVS5>TVS8>TVS10.

2- The maximum values of fast neutron mass (Σ_R/ρ) and effective removal (Σ_R) cross-sections were obtained for TVS0.

3- The (EABF) and (EBF) values were in the order TVS0>TVS5>TVS8>TVS10.

4- For proton (p^+) and alpha (α) particles, the mass stopping power (MSP) is maximum for TVS0 and least for TVS10 samples.

5- The range (R) of p^+ in all the glasses were all greater than those of α- particles for all energies.

Results concluded that the higher Sb_2O_3 concentration in TVS glasses leads to an increase in their capability to apply in several radiation shielding applications.

Acknowledgment:

This work was support of King Khalid University, the Ministry of Education, and Kingdom of Saudi Arabia for this research through a grant (RCAMS/KKU/005/20) under the research center for advanced material science.

References

[1] U. Gökhan Işsever, Gökhan Kilic, Mehmet Peker, Tevfik Ünaldi, A. Şenol Aybek, Effect of low ratio V^{5+} doping on structural and optical properties of borotellurite semiconducting oxide glasses, Journal of Materials Science: Materials in Electronics 30 (2019) 15156–15167.

[2] B. Aktas, S. Yalcin, K. Dogru, Z. Uzunoglu, D. Yilmaz, Structural and radiation shielding properties of chromium oxide doped borosilicate glass, Radiat. Phys. Chem. 156 (2019) 144–149.

[3] YS. Rammah, Gökhan Kilic, R. El-Mallawany, U. Gökhan Issever, F.I. El-Agawany, Investigation of optical, physical, and gamma-ray shielding features of novel vanadyl boro-phosphate glasses. Journal of Non-Crystalline Solids 533 (2020) 119905.

[4] EE Assem, I. Elmehasseb, Structure, magnetic, and electrical studies on vanadium phosphate glasses containing different oxides, Journal of Materials Science, 46(7) (2011) 2071-2076.

[5] GD Khattak, A. Mekki, Structure and electrical properties of SrO-borovanadate $(V_2O_5)_{0.5}(SrO)_{0.5-y}(B_2O_3)_y$ glasses. J. Phys. Chem. Solids 70 (2009) 1330–1336.

[6] YS. Rammah, M.I. Sayyed, A.S. Abohaswa, H.O. Tekin, FTIR, electronic polarizability and shielding parameters of B_2O_3 glasses doped with SnO_2. Applied Physics A 124 (2018) 650.

[7] N. Elkhoshkhany, Eslam Syala, El Sayed Yousef, Kinetics characterization and visible photoluminescence spectroscopy of an erbium-doped tellurite glass, Results in Physics 14 (2019) 102370.

[8] N. Elkhoshkhany, Eslam Syala, El Sayed Yousef, Concentration dependence of the elastic moduli, thermal properties, and non-isothermal kinetic parameters of Yb^{3+} doped multicomponent tellurite glass system, Results in Physics 16 (2020) 102876.

[9] Y. S. Rammah, F. I. El-Agawany, K. A. Mahmoud, R. El-Mallawany, Erkan Ilik, Gokhan Kilic, FTIR, UV–Vis–NIR spectroscopy, and gamma rays shielding competence of novel ZnO-doped vanadium borophosphate glasses, Journal of Materials Science: Materials in Electronics (2020), https://doi.org/10.1007/s10854-020-03440-5.

[10] YS. Rammah, A.S. Abouhaswa, M.I. Sayyed, HO Tekin, R. El-Mallawany. Structural, UV and shielding properties of ZBPC glasses. Journal of Non-Crystalline Solids 509 (2019) 99–105.

[11] R. El-Mallawany, M.I. Sayyed, M.G. Dong, Y.S. Rammah, Simulation of radiation shielding properties of glasses contain PbO, Radiation Physics and Chemistry 161 (2019) 55–59.

[12] E. Kavaz, An experimental study on gamma ray shielding features of lithium borate glasses doped with dolomite, hematite and goethite minerals, Radiation Physics and Chemistry 160 (2019) 112–123.

[13] V.B. Sreedhar, D. Ramachari, C.K. Jayasankar, Optical properties of zincfluorophosphate glasses doped with Dy^{3+} ions. Physica B Condens. Matter 408 (2013) 158–163**.**

[14] P. Pascuta, G. Borodi, E. Culea, Influence of europium ions on structure and crystallization properties of bismuth borate glasses and glass ceramics. J. Non-Cryst. Solids 354 (2008) 5475–5479.

[15] A.A. Ali, Y.S. Rammah, M.H. Shaaban, The influence of TiO_2 on structural, physical and optical properties of B_2O_3 –TeO_2 – Na_2O – CaO glasses. Journal of Non-Crystalline Solids 514 (2019) 52–59.

[16] M. Kurudirek, Heavy metal borate glasses: Potential use for radiation shielding, Journal of Alloys and Compounds 727 (2017) 1227-1236.

[17] Y.S Rammah, M. S. Al-Buriahi, A. S. Abouhaswa. "B_2O_3–$BaCO_3$–Li_2O_3 glass system doped with Co_3O_4: Structure, optical, and radiation shielding properties. Physica B: Condensed Matter (2019) 411717.

[18] Y. Al-Hadeethi, M. S. Al-Buriahi, M. I. Sayyed, Bioactive glasses and the impact of Si3N4 doping on the photon attenuation up to radiotherapy energies, Ceramics International 46 (2020) 5306-5314.

[19] H.M.M. Moawad, H. Jain, R. El-Mallawany, DC conductivity of silver vanadium tellurite glasses, J. Phys. Chem. Solids 70 (2009) 224–233.

[20] N. Narasimha Rao, I.V. Kityk, V. Ravi Kumar, Ch. Srinivasa Rao, M. Piasecki, P. Bragiel, N. Veeraiah, Dc field induced optical effects in ZnF_2 –PbO–TeO_2: TiO_2 glass ceramics, Ceram. Int. 38 (2012) 2551–2562.

[21] Shams A.M. Issa, A.M.A., Mostafa, effect of Bi_2O_3 in borate-tellurite-silicate glass system for development of gamma-rays shielding materials, J. Alloys Compd. 695 (2017) 302–310.

[22] A. Aşkın, M.I. Sayyed, Amandeep Sharma, M. Dal, R. El-Mallawany, M.R. Kaçal, Investigation of the gamma ray shielding parameters of (100-x)[0.5Li_2O–0.1B_2O_3–0.4P_2O_5]-xTeO_2 glasses using Geant4 and FLUKA codes, J. Non-Crys. Solids 521 (2019) 119489.

[23] D. Sushama, P. Predeep, Thermal and optical studies of rare earth doped tungsten–tellurite glasses. Int. J. Appl. Phys. Math. 4 (2014) 139–143.

[24] R. El-Mallawany, The optical properties of tellurite glasses, J. Appl. Phys. 72 (1992) 1774–1777.

[25] R. El-Mallawany, Introduction to tellurite glasses, in: V.A.G. Rivera, D. Manzani (Eds.), Technological Advances in Tellurite Glasses: Properties, Processing, and Applications, Springer, Switzerland (2017) 1–13.

[26] H. Mori, T. Kitami, H. Sakata, Electrical conductivity of V_2O_5-Sb_2O_3-TeO_2 glasses, J. Non-Cryst. Solids 168 (1994) 157-166.

[27] D. Souri, K. Shomalian, Band gap determination by absorption spectrum fitting method (ASF) and structural properties of different compositions of (60 –x) V_2O_5–40TeO–xSb_2O_3 glasses, Journal of Non-Crystalline Solids 355 (2009) 1597–1601.

[28] Ghosh A, Hopping transport in vanadium tellurite glasses containing antimony oxide, J. Phys.: Condens. Matter 5 (1993) 4485.

[29] Briesmeister J, MCNP – a general Monte Carlo code for neutron and photon transport. Report LA13709-M, version 4C, National Laboratory, Los Alamos, 2000

[30] Gerward, L., Guilbert, N., Jensen, K.B., Levring, H., 2004. WinXCom - a program for calculating X-ray attenuation coefficients. Radiat. Phys. Chem. 71, 653–654.

[31] Khan, F.M., Gibbons, J.P. (2014). The physics of radiation therapy. Lippincott Williams &Wilkin, London, 67.

[32] Brar, G.S., Singh, K., Singh, M., Mudahar, G.S. (1994). Energy absorption buildup factor studies In water, air and concrete up to 100 mfp using GP fitting formula. Radiation Physics and Chemistry, 43(6), 623-627.

[33] YS. Rammah, M.I. Sayyed, A.A. Ali, Tekin, HO, R. El-Mallawany. (2018). Optical properties and gamma shielding features of bismuth borate glasses. Applied Physics A, 124:824-832.

[34] MI Sayyed, Investigation of gamma ray and fast neutron shielding properties of tellurite glasses with different oxide oxide compositions, Can. J. Phys. 94 (2016) 1133-1137.

[35] O. Olarinoye, C. Oche, Gamma-rays and fast neutrons shielding parameters of two new Ti-based bulk metallic glasses. Iranian Journal of Medical Physics (2020). https://dx.doi.org/10.22038/ijmp.2020.42684.1635

.[36] I.I. Bashter, Calculation of radiation attenuation coefficients for shielding concretes. Annals of nuclear Energy, 24(17) (1997) 1389-1401.

[37] I. O. Olarinoye, R.I. Odiaga, S. Paul, EXABCal: A program for calculating photon exposure and energy absorption buildup factors. Heliyon, 5(7) (2019) e02017.

[38] U. Kara, S.A. Issa, G. Susoy, M. Rashad, E. Kavaz, N.Y. Yorgun, H.O. Tekin, Synergistic effect of serpentine mineral on Li2B4O7 glasses: optical, structural and nuclear radiation shielding properties, Applied Physics A126 (3) (2020) 1-19.

[39] J.F. Ziegler, J.P. Biersack, The Stopping and Range of Ions in Matter, Treatise on Heavy-Ion Science. Springer (1985) 93–129.

[40] J.F. Ziegler, M.D. Ziegler, J.P. Biersack, SRIM - the stopping and range of ions in matter (2010). Nucl. Instrum. Methods B 268 (2010) 1818–1823.

Figures

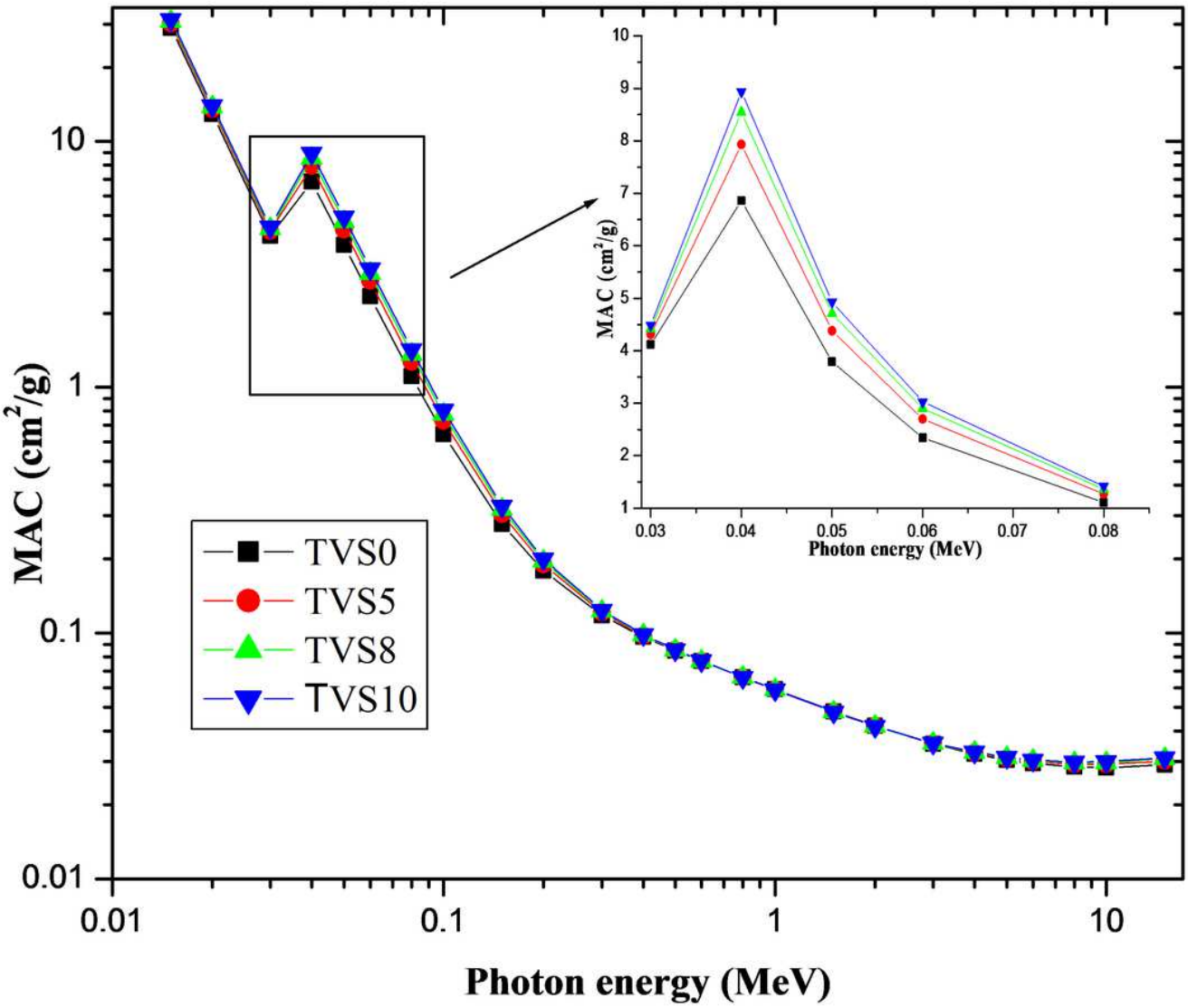

Figure 1

Mass attenuation coefficient of TVS glass samples (inset, magnified for 30-80 keV).

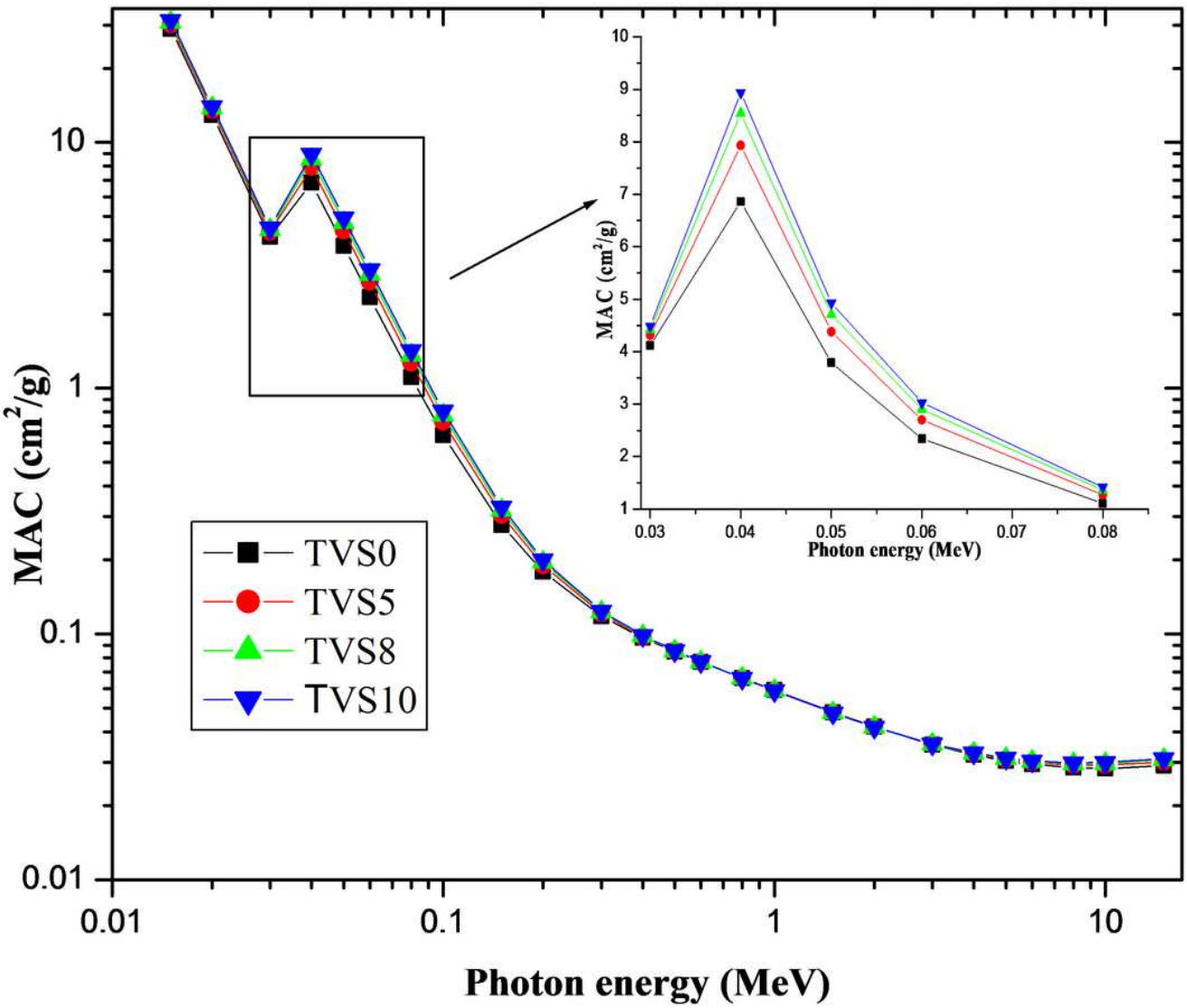

Figure 1

Mass attenuation coefficient of TVS glass samples (inset, magnified for 30-80 keV).

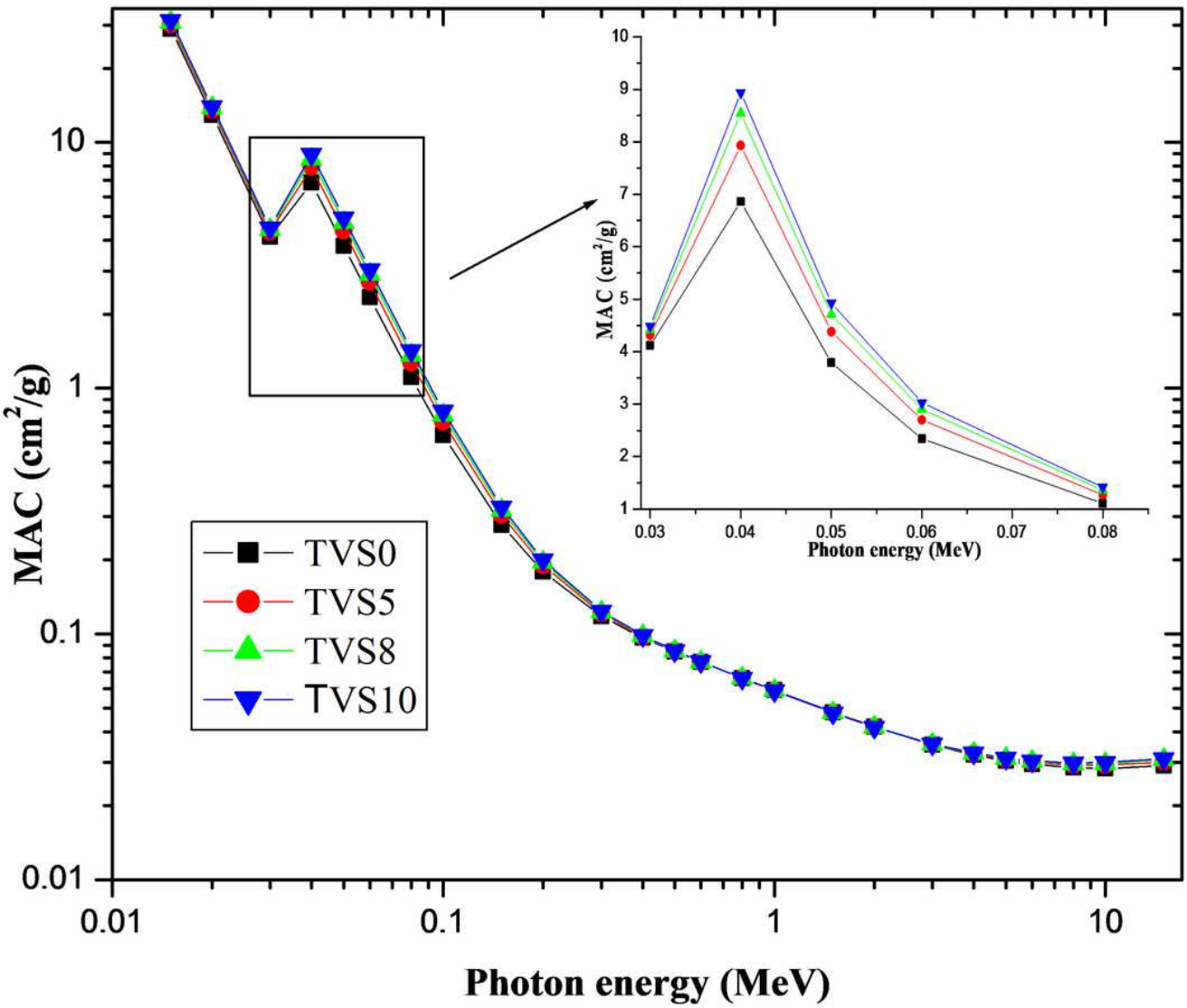

Figure 1

Mass attenuation coefficient of TVS glass samples (inset, magnified for 30-80 keV).

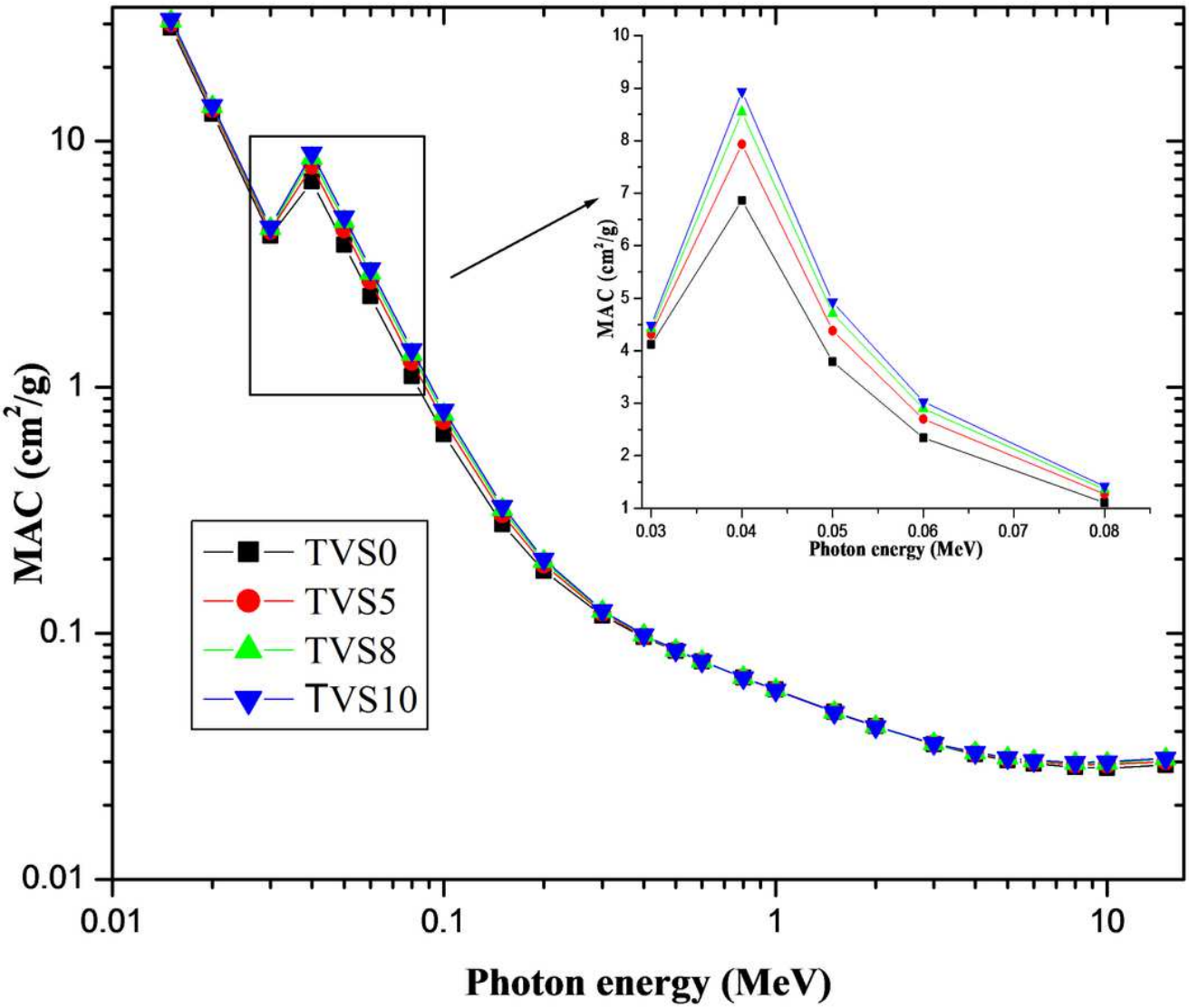

Figure 1

Mass attenuation coefficient of TVS glass samples (inset, magnified for 30-80 keV).

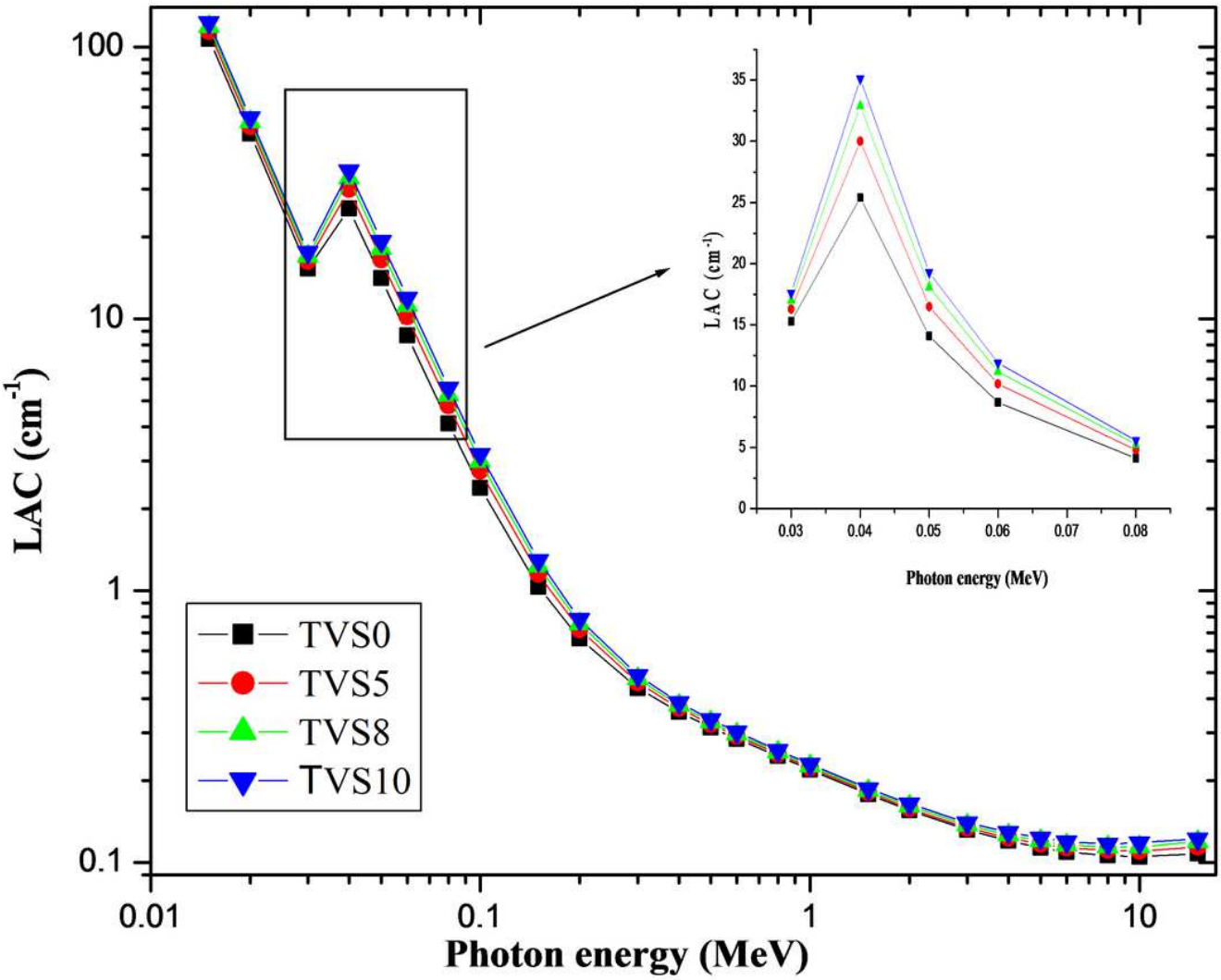

Figure 2

Linear attenuation coefficient of TVS glass samples (inset, magnified for 30-80 keV).

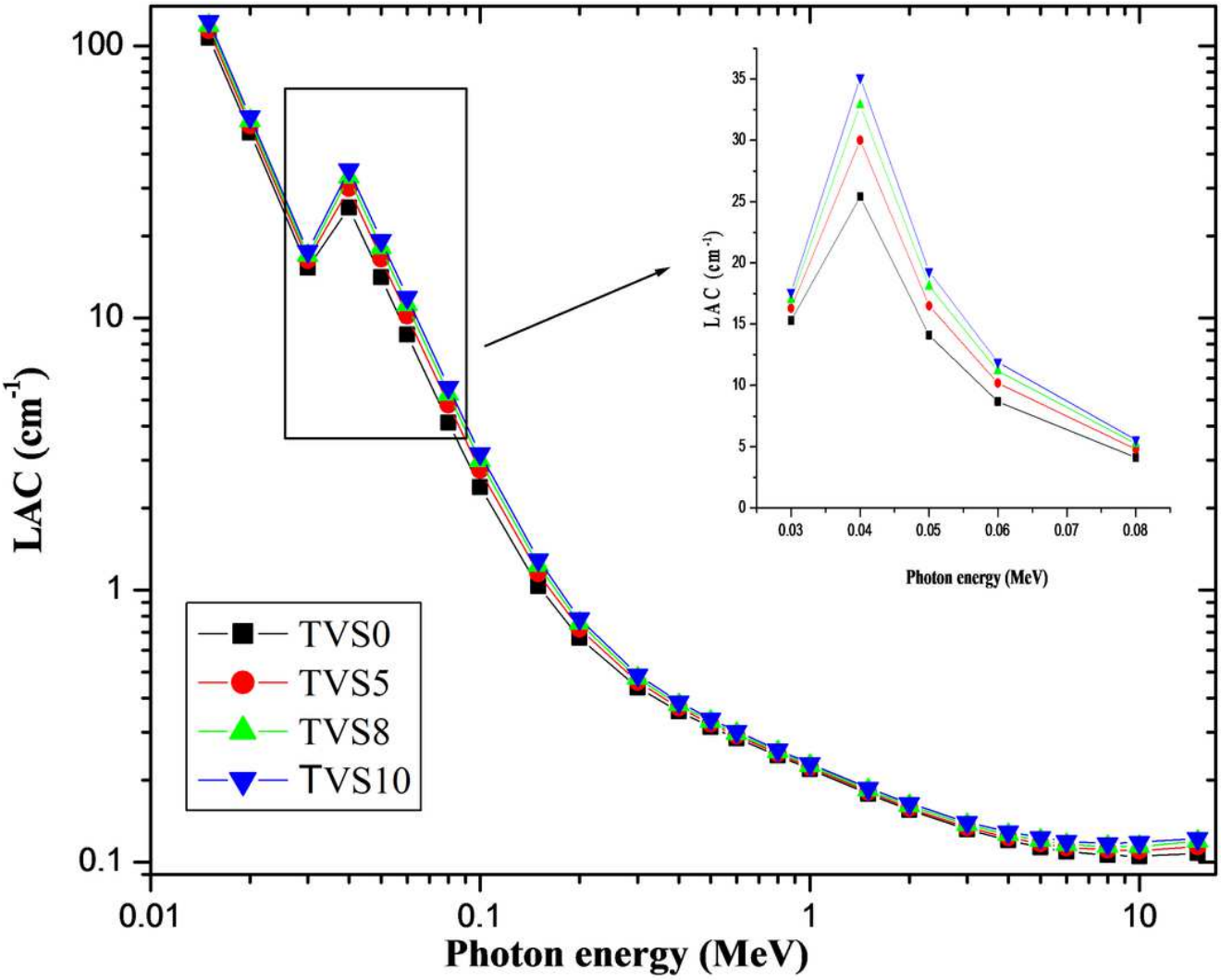

Figure 2

Linear attenuation coefficient of TVS glass samples (inset, magnified for 30-80 keV).

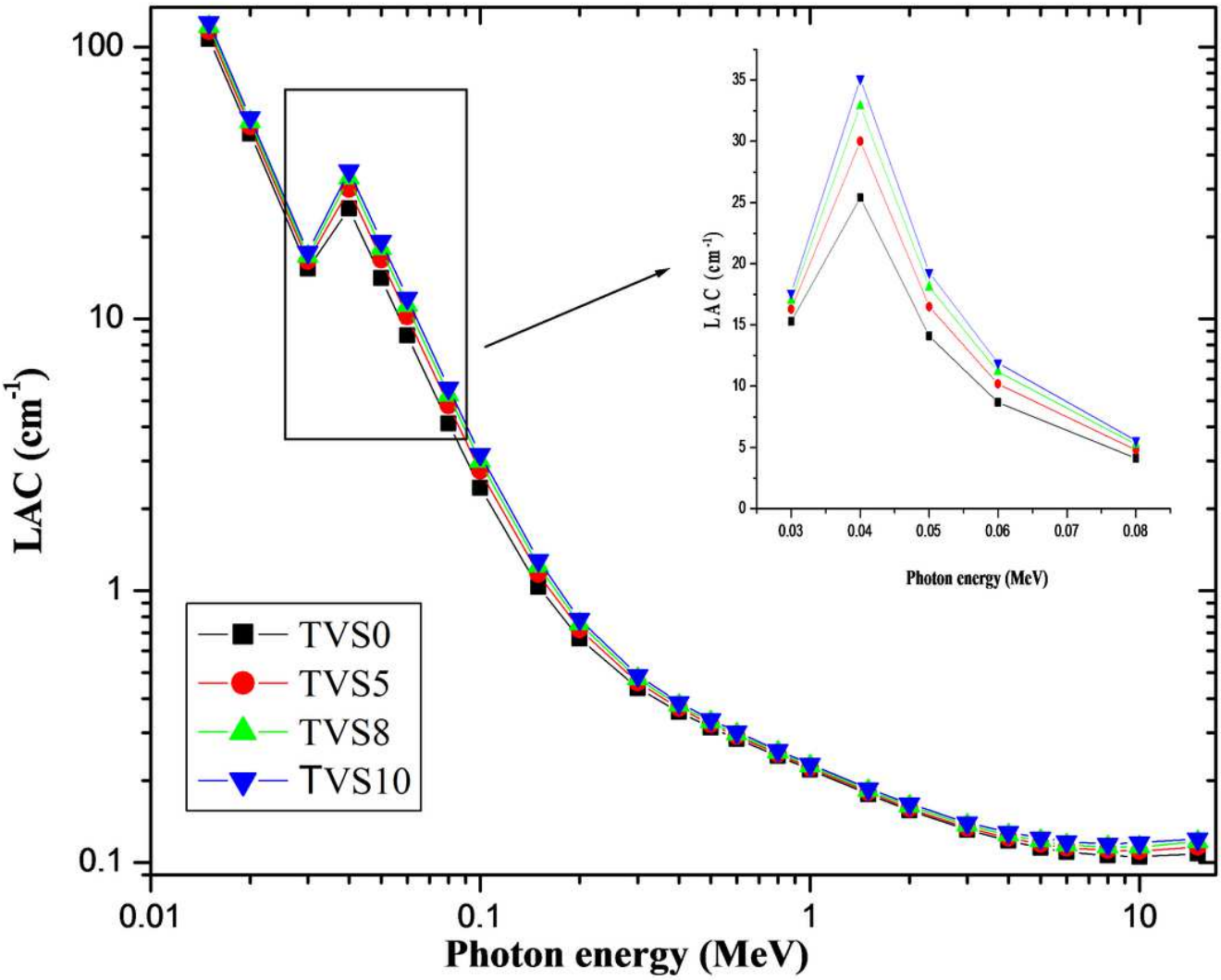

Figure 2

Linear attenuation coefficient of TVS glass samples (inset, magnified for 30-80 keV).

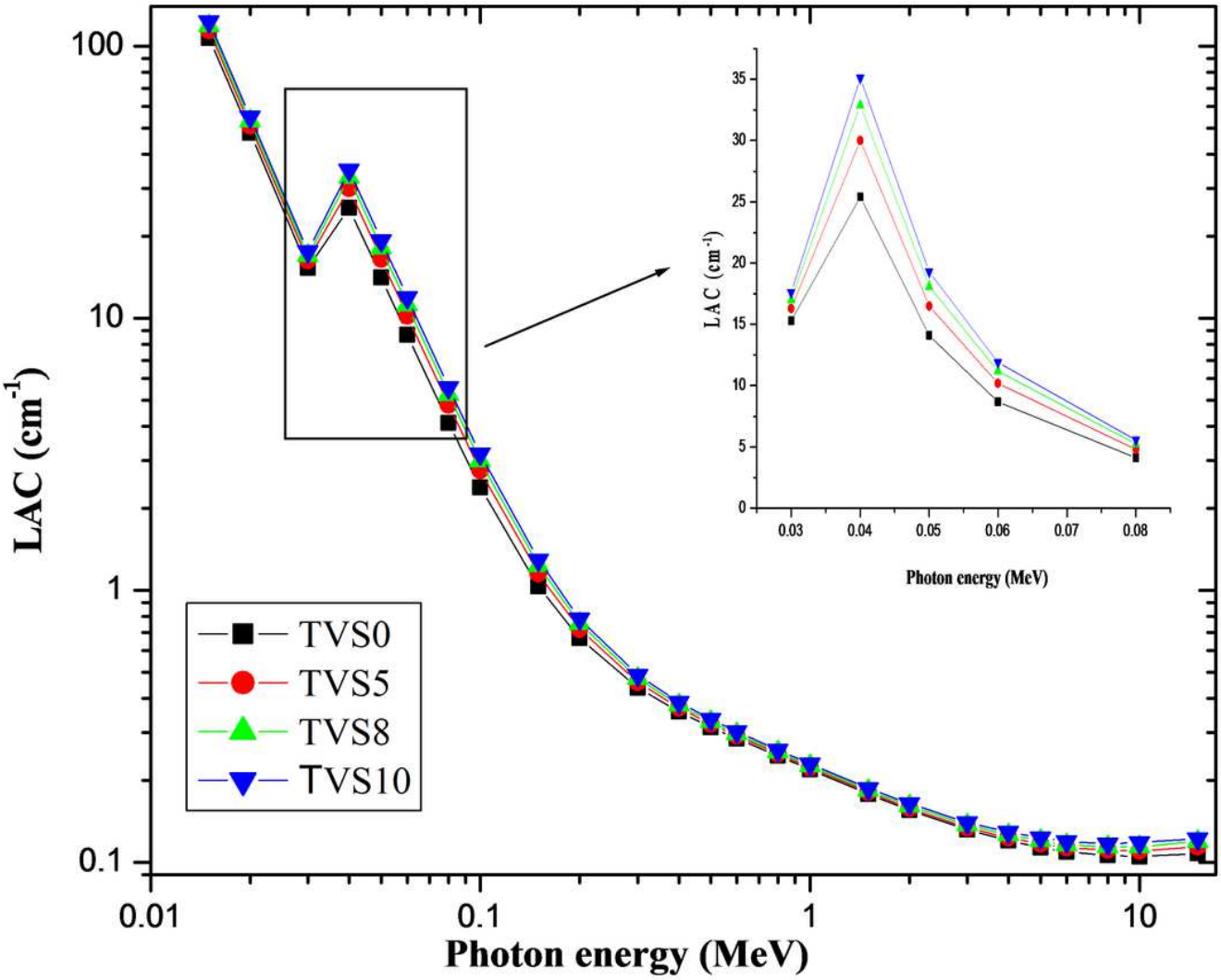

Figure 2

Linear attenuation coefficient of TVS glass samples (inset, magnified for 30-80 keV).

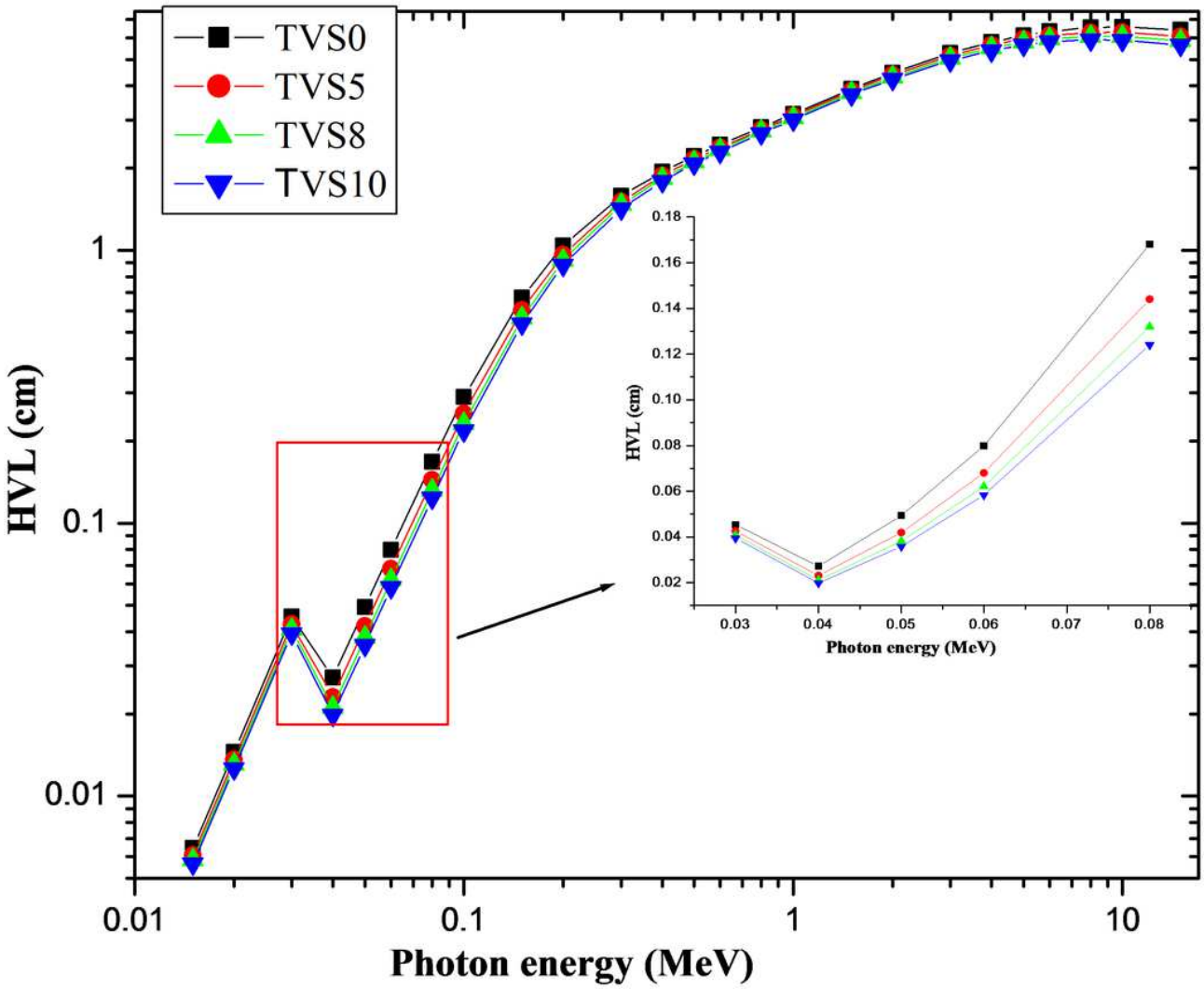

Figure 3

HVL as a function of energy for TVS glass samples (inset, magnified for 30-80 keV).

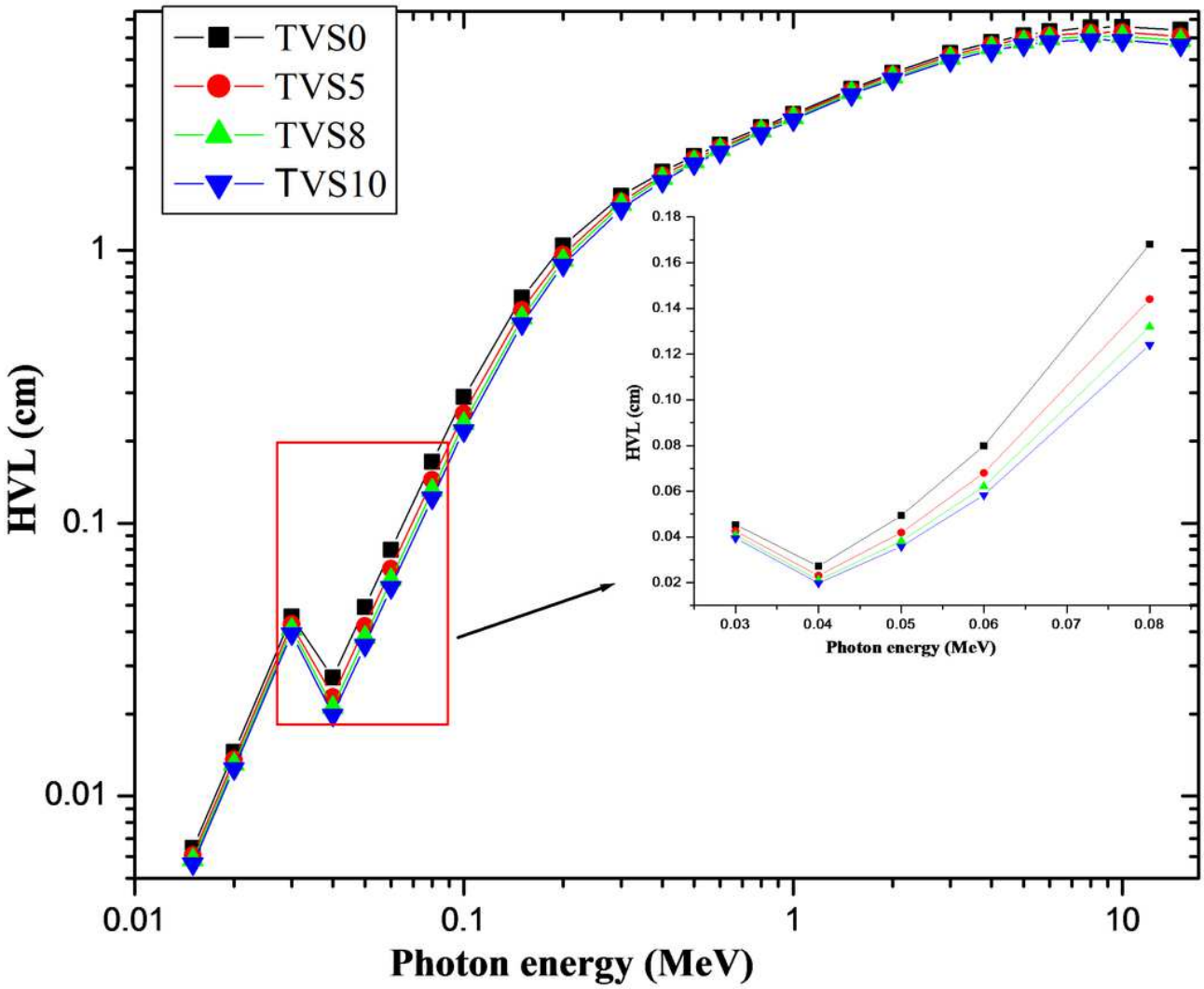

Figure 3

HVL as a function of energy for TVS glass samples (inset, magnified for 30-80 keV).

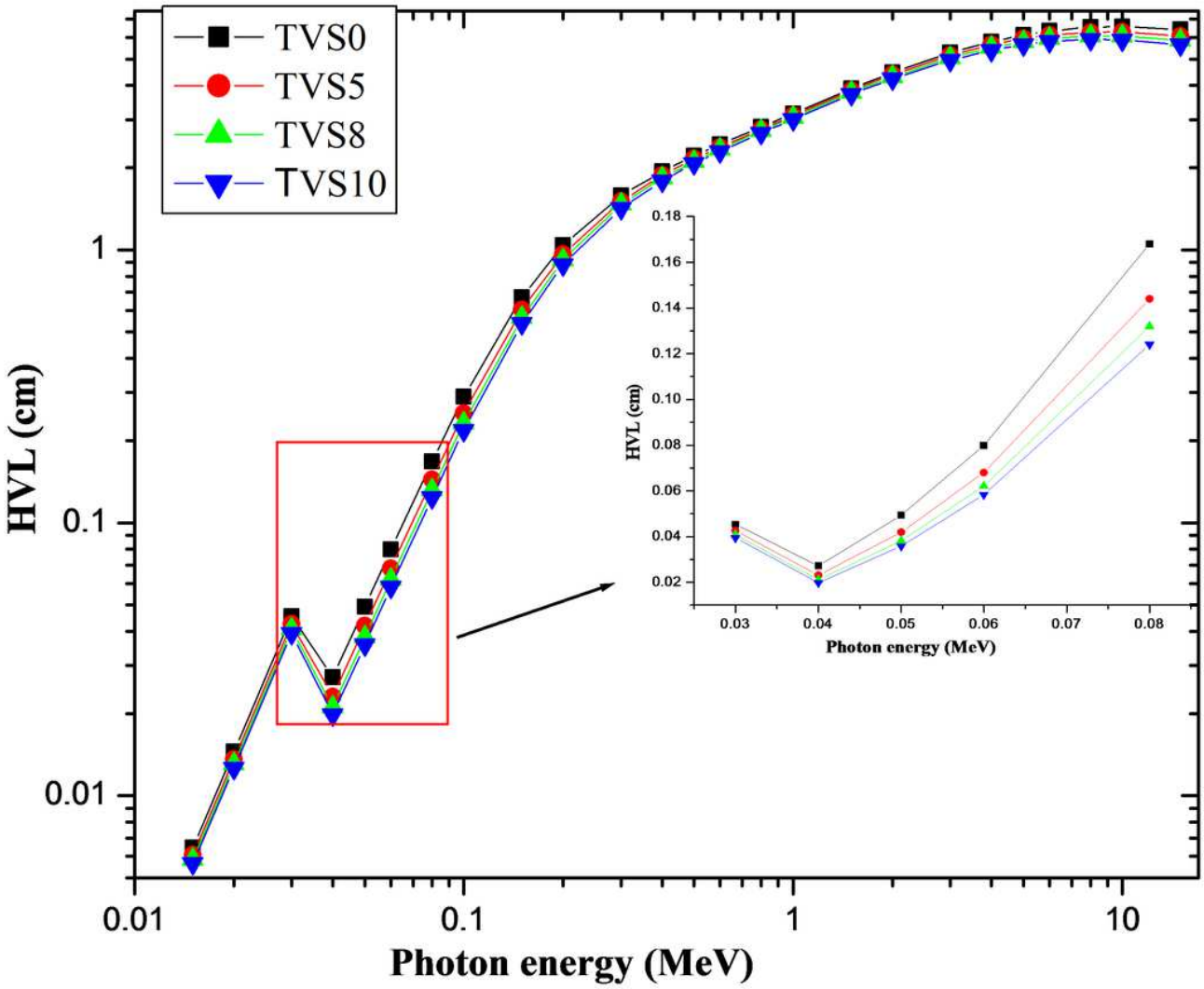

Figure 3

HVL as a function of energy for TVS glass samples (inset, magnified for 30-80 keV).

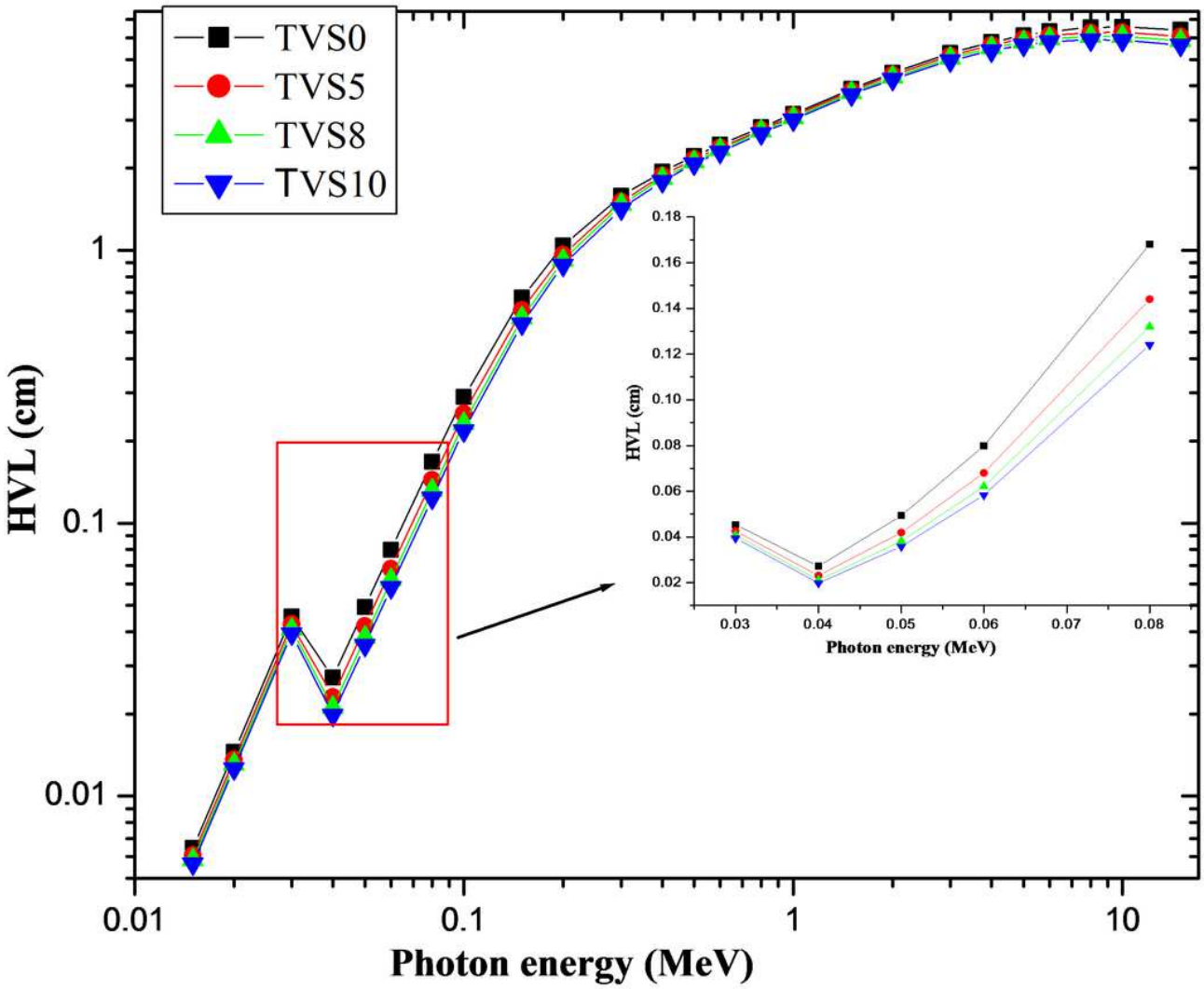

Figure 3

HVL as a function of energy for TVS glass samples (inset, magnified for 30-80 keV).

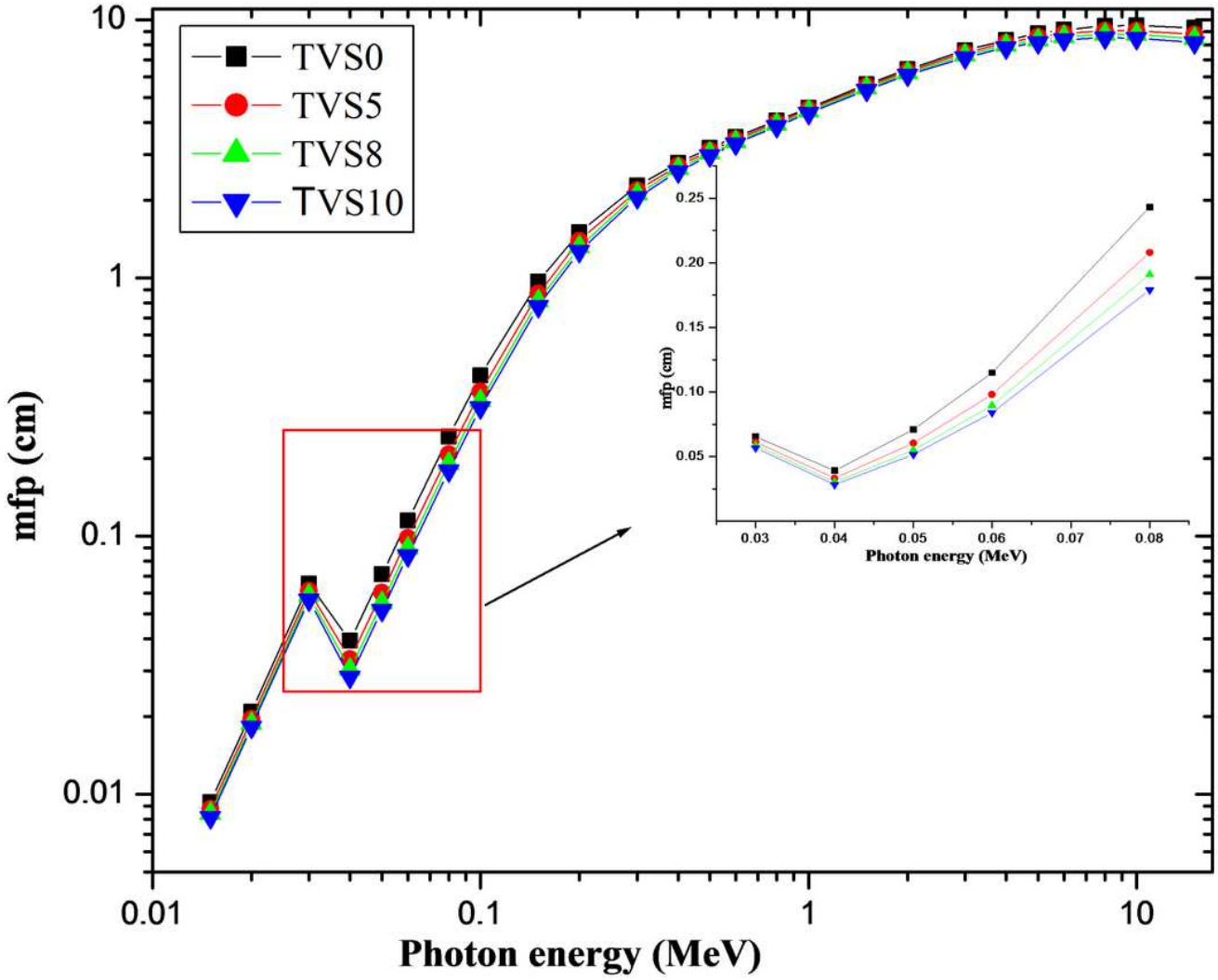

Figure 4

mfp as a function of energy for TVS glass samples (inset, magnified for 30-80 keV).

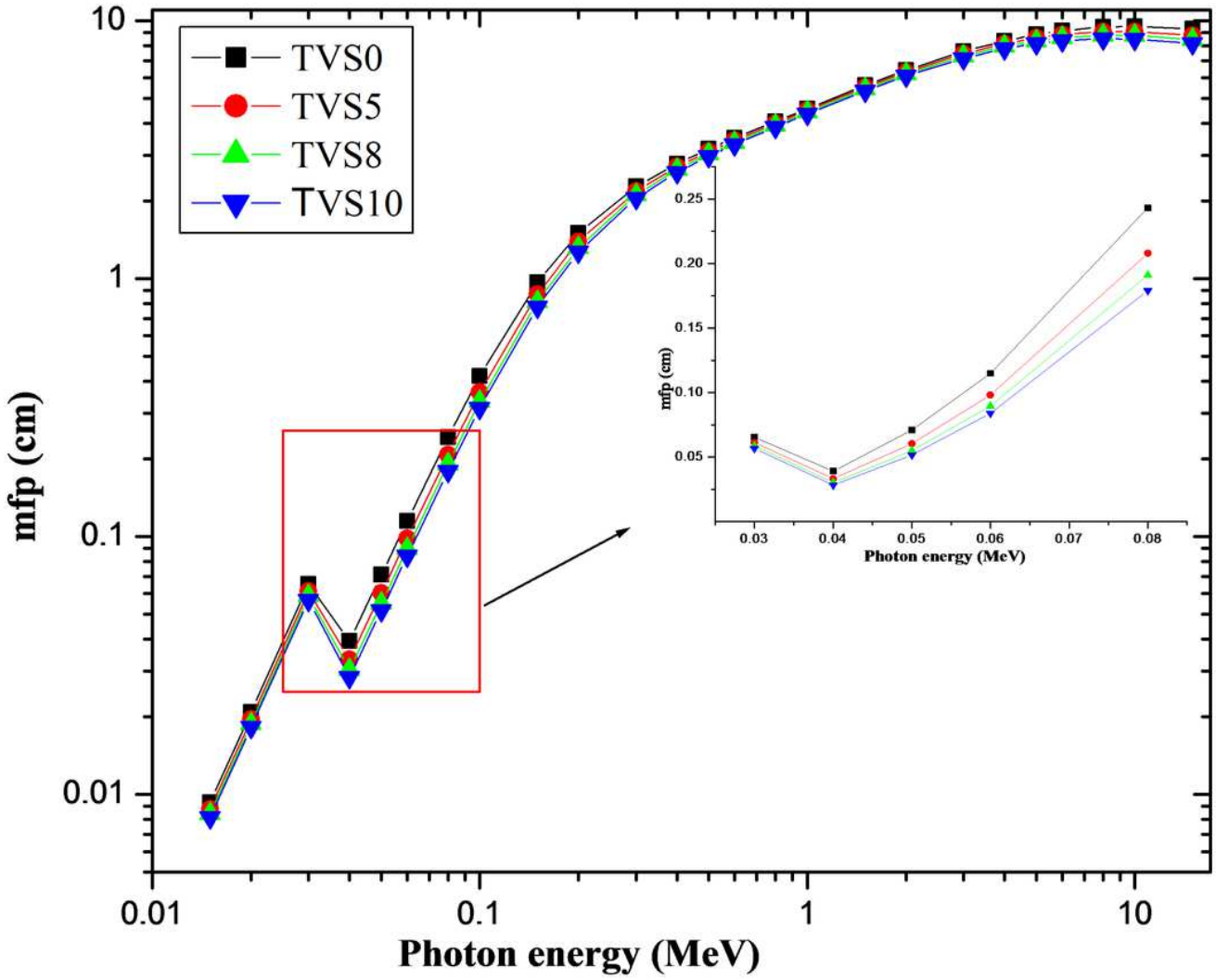

Figure 4

mfp as a function of energy for TVS glass samples (inset, magnified for 30-80 keV).

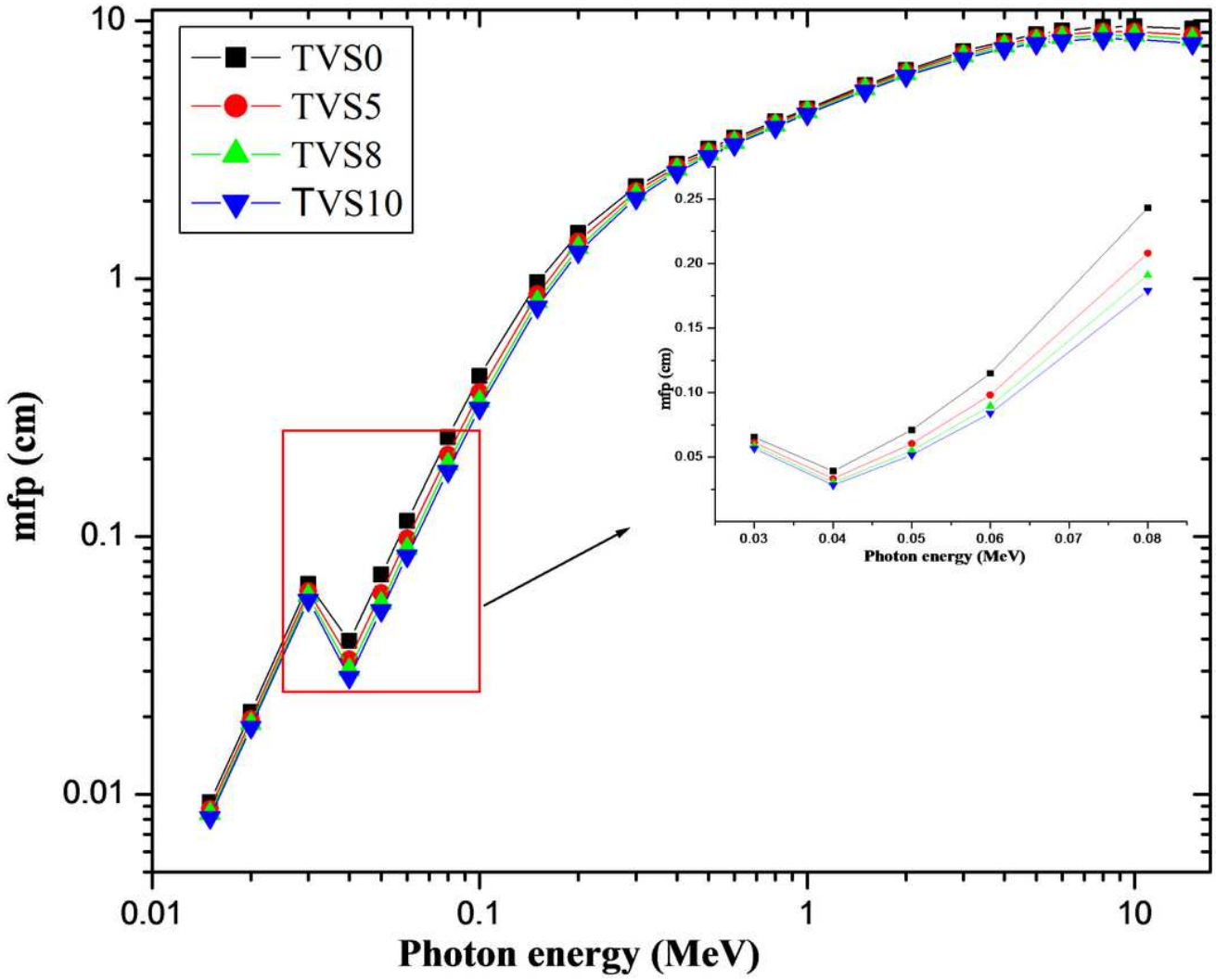

Figure 4

mfp as a function of energy for TVS glass samples (inset, magnified for 30-80 keV).

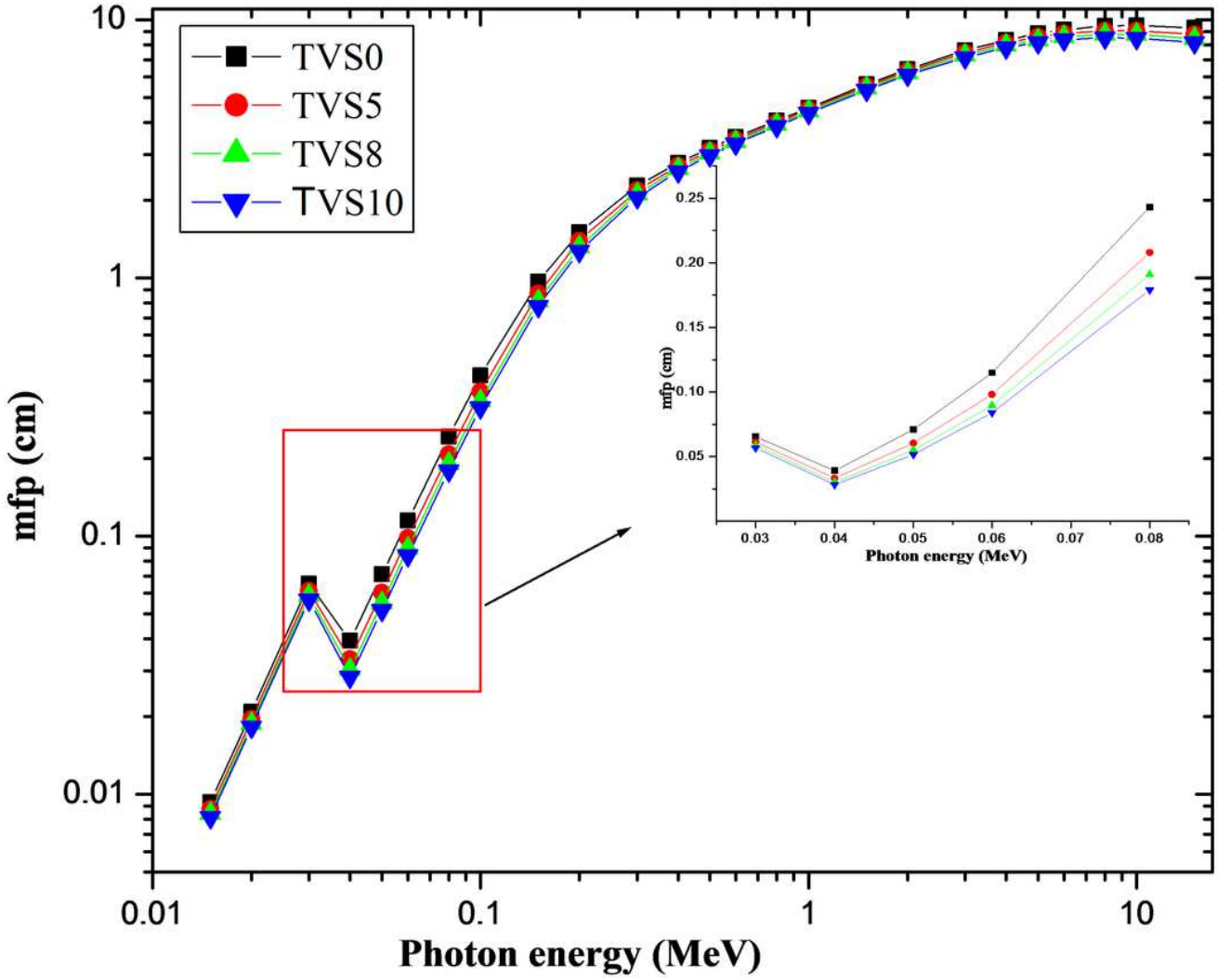

Figure 4

mfp as a function of energy for TVS glass samples (inset, magnified for 30-80 keV).

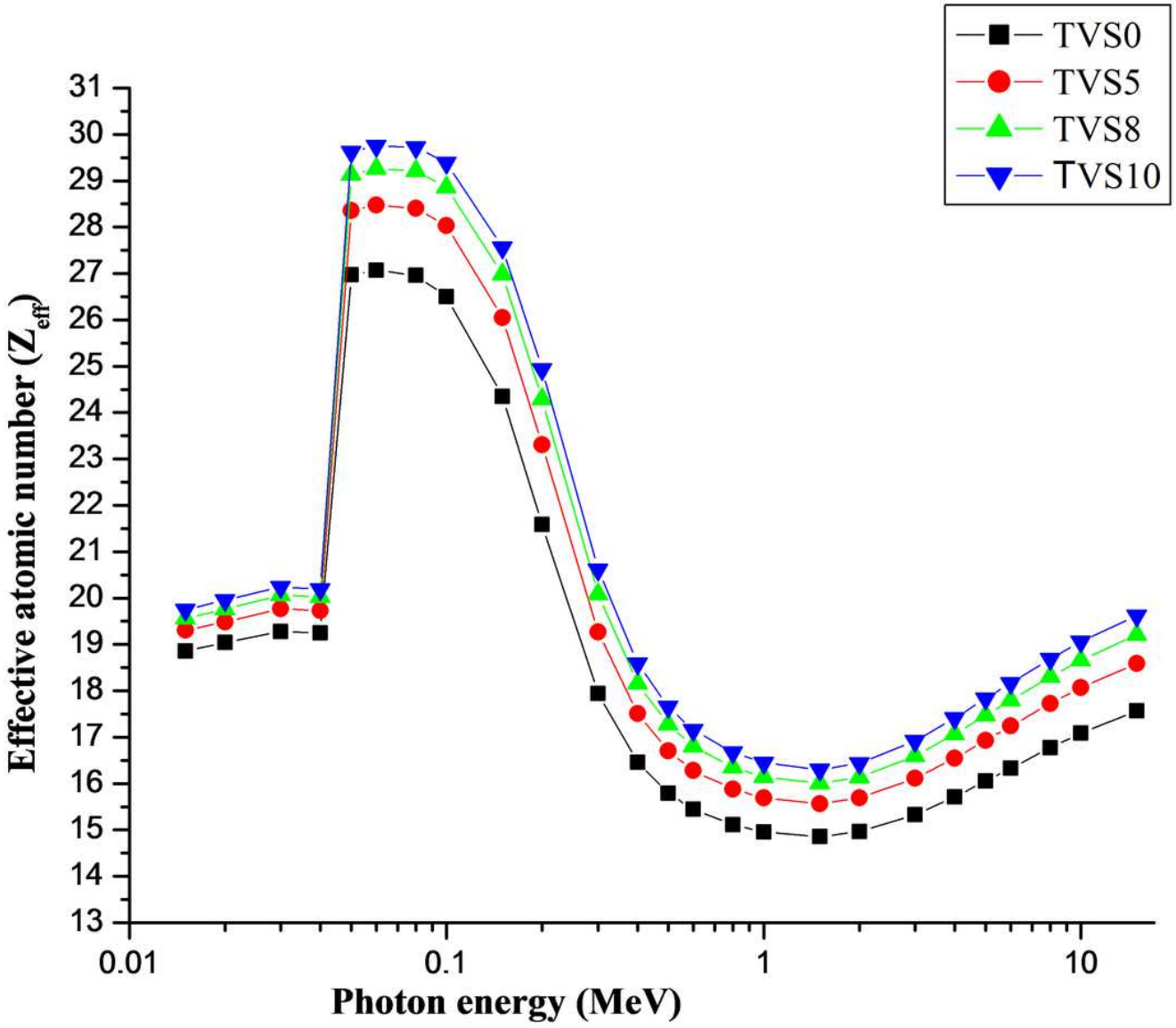

Figure 5

Variation of Zeff as a function energy for the investigated TVS glasses

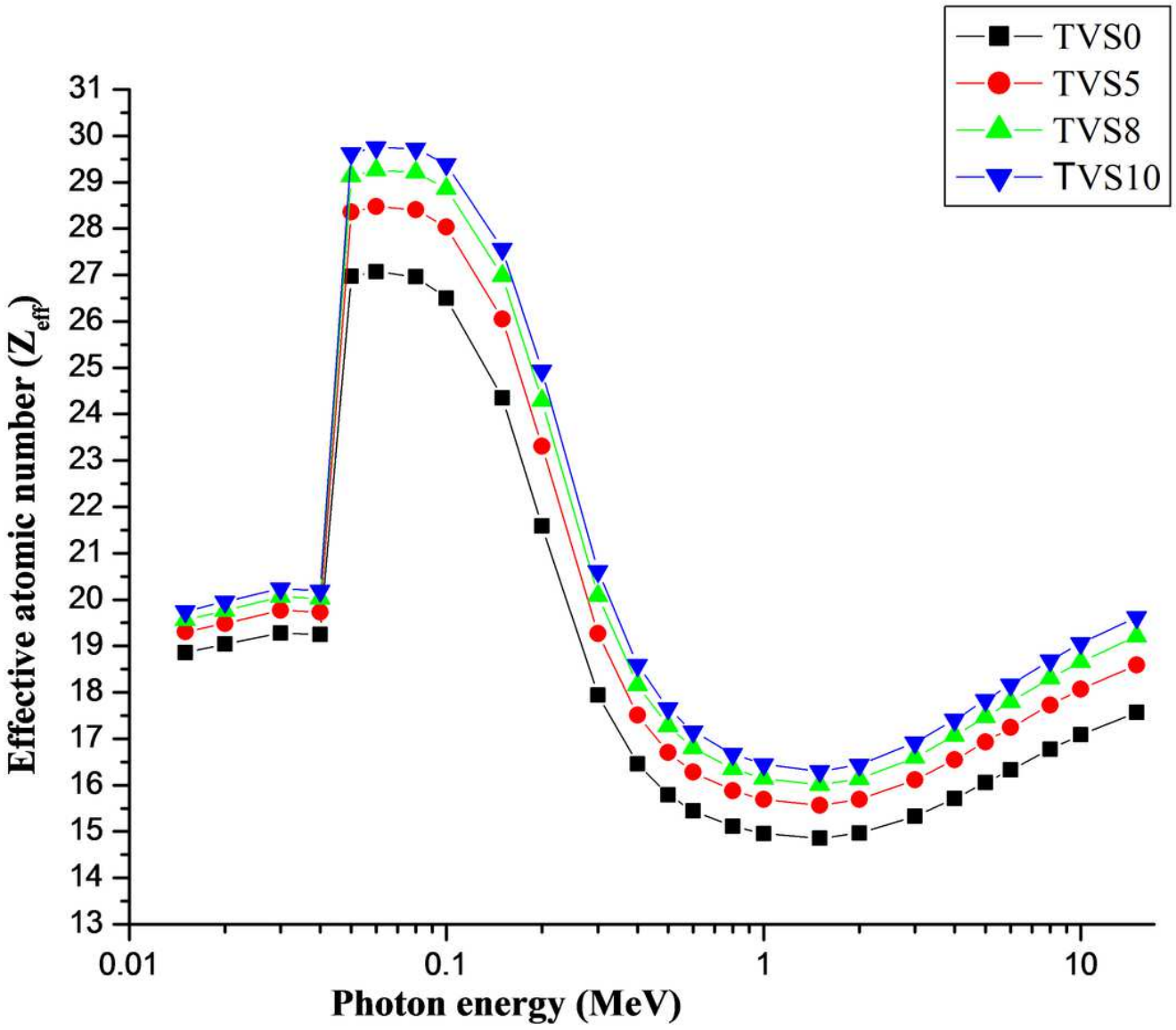

Figure 5

Variation of Zeff as a function energy for the investigated TVS glasses

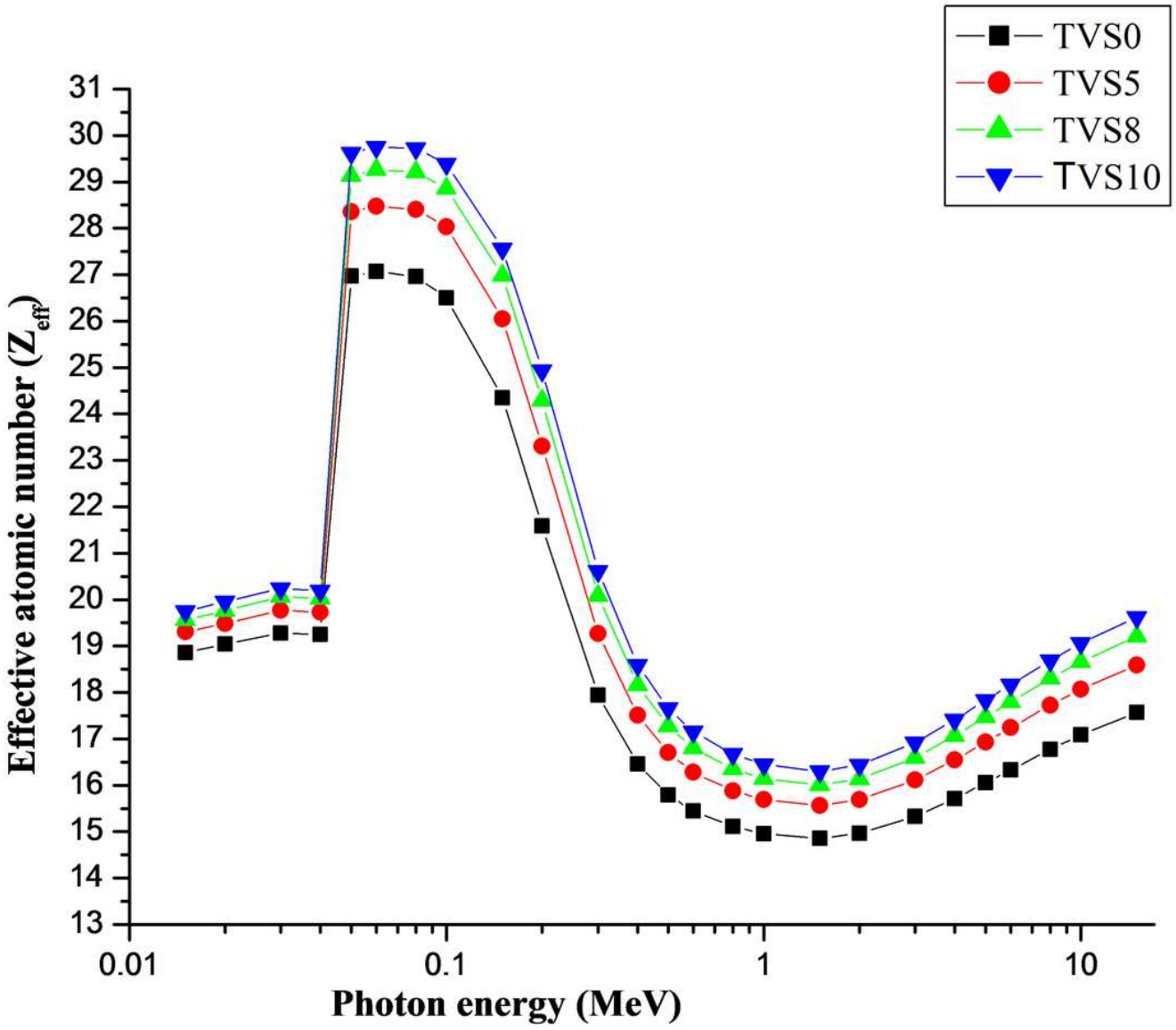

Figure 5

Variation of Zeff as a function energy for the investigated TVS glasses

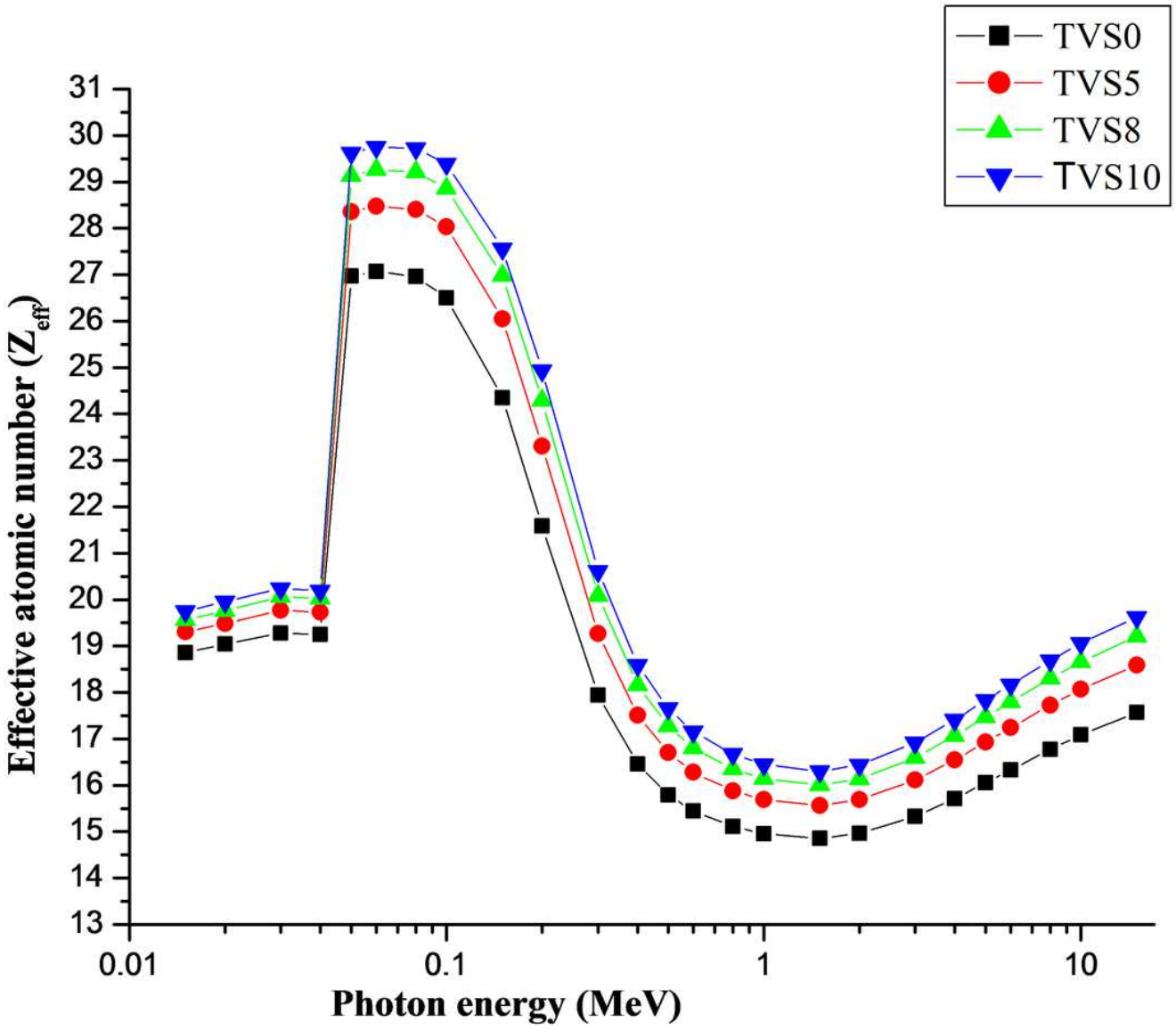

Figure 5

Variation of Zeff as a function energy for the investigated TVS glasses

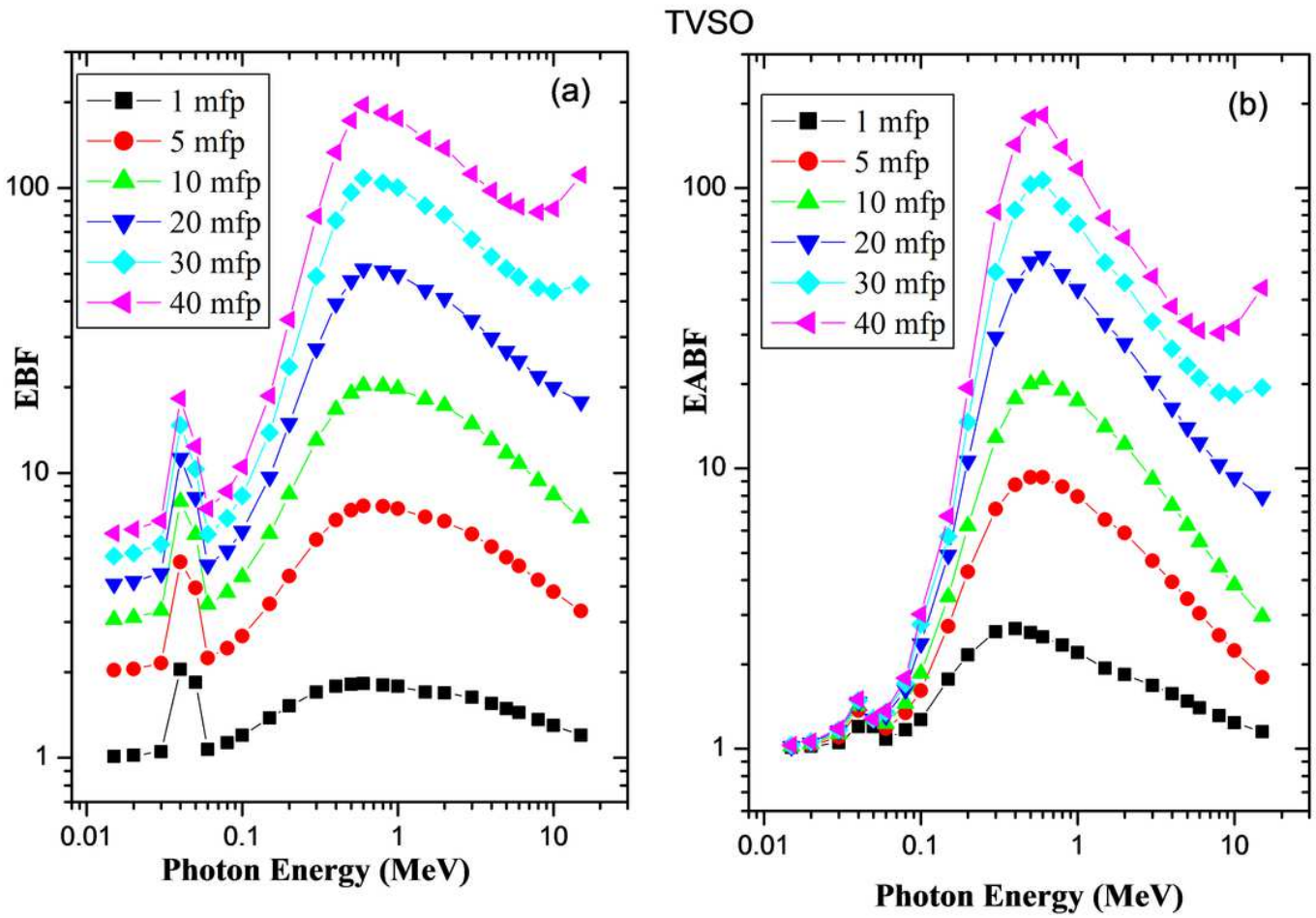

Figure 6

EBF (a) and EABF (b) as a function photon energy for TVS0 glass at different mfp values.

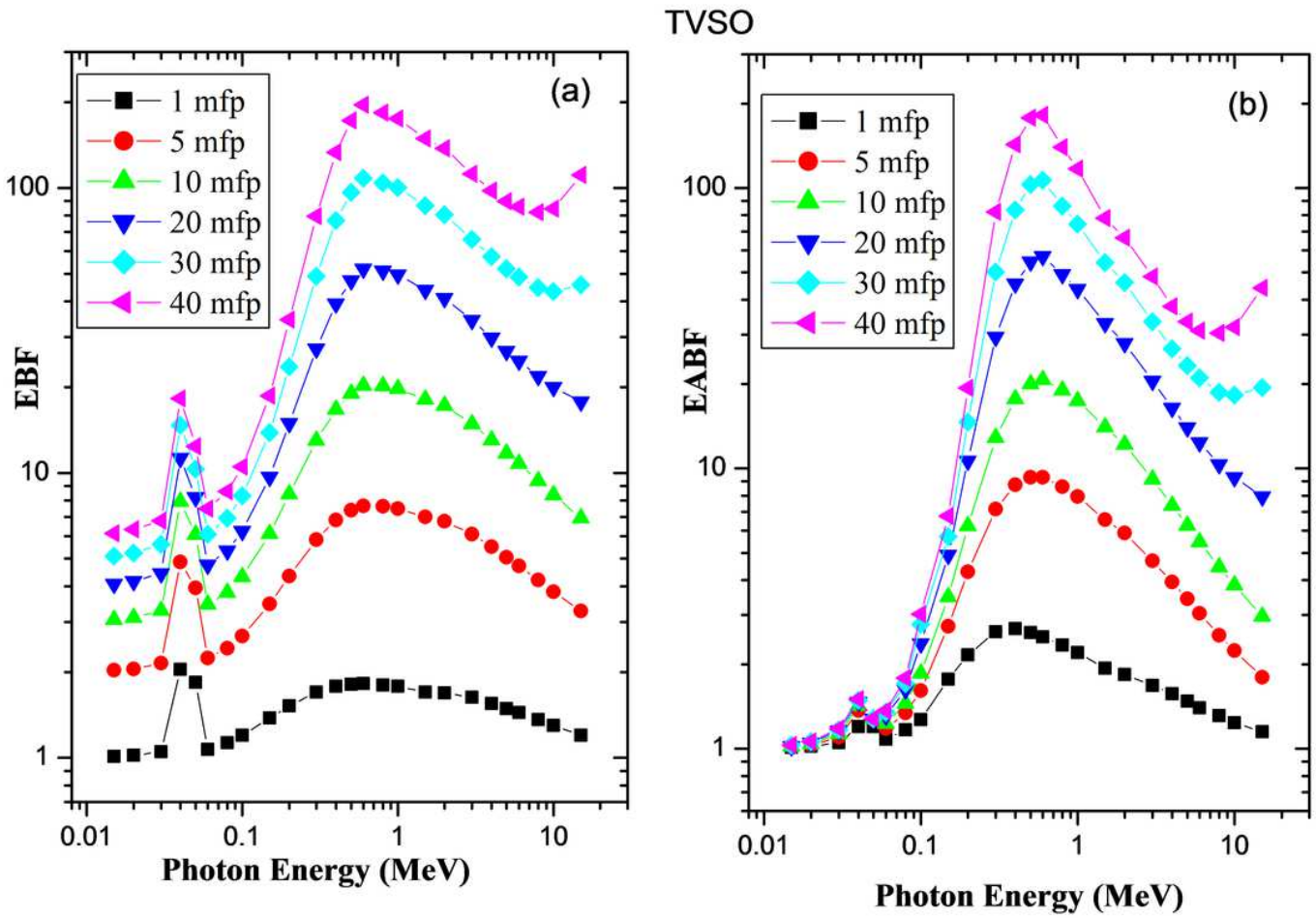

Figure 6

EBF (a) and EABF (b) as a function photon energy for TVS0 glass at different mfp values.

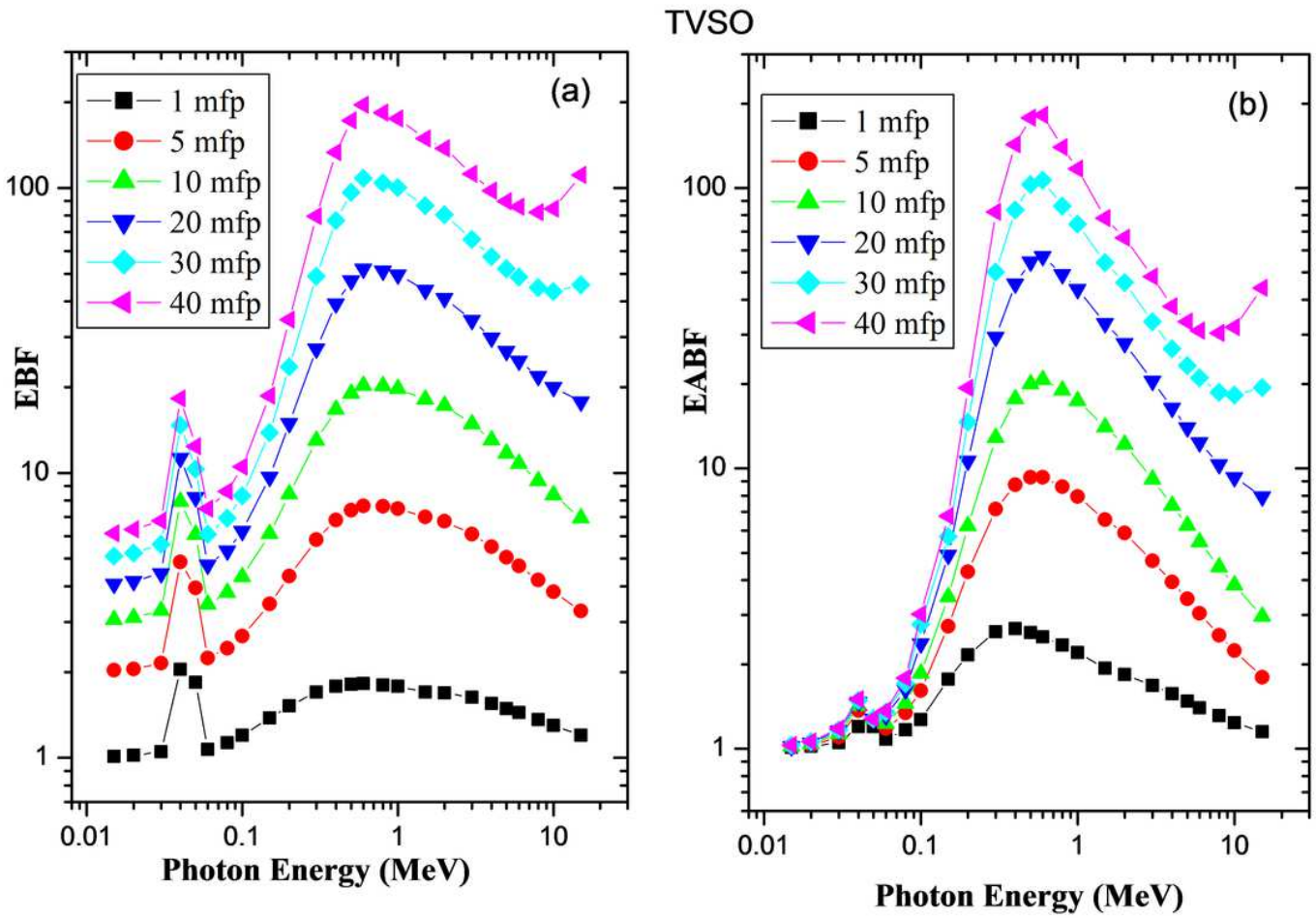

Figure 6

EBF (a) and EABF (b) as a function photon energy for TVS0 glass at different mfp values.

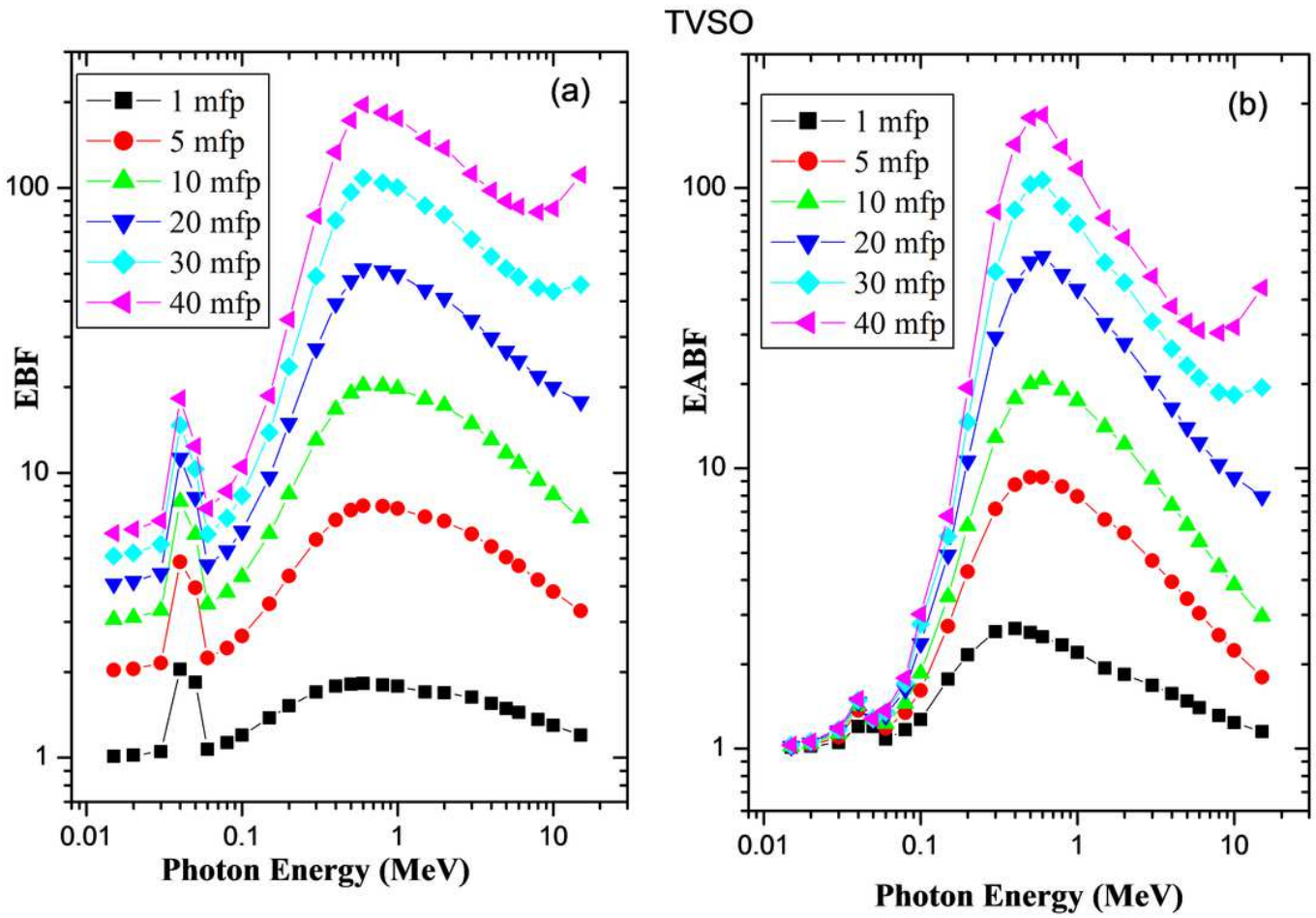

Figure 6

EBF (a) and EABF (b) as a function photon energy for TVS0 glass at different mfp values.

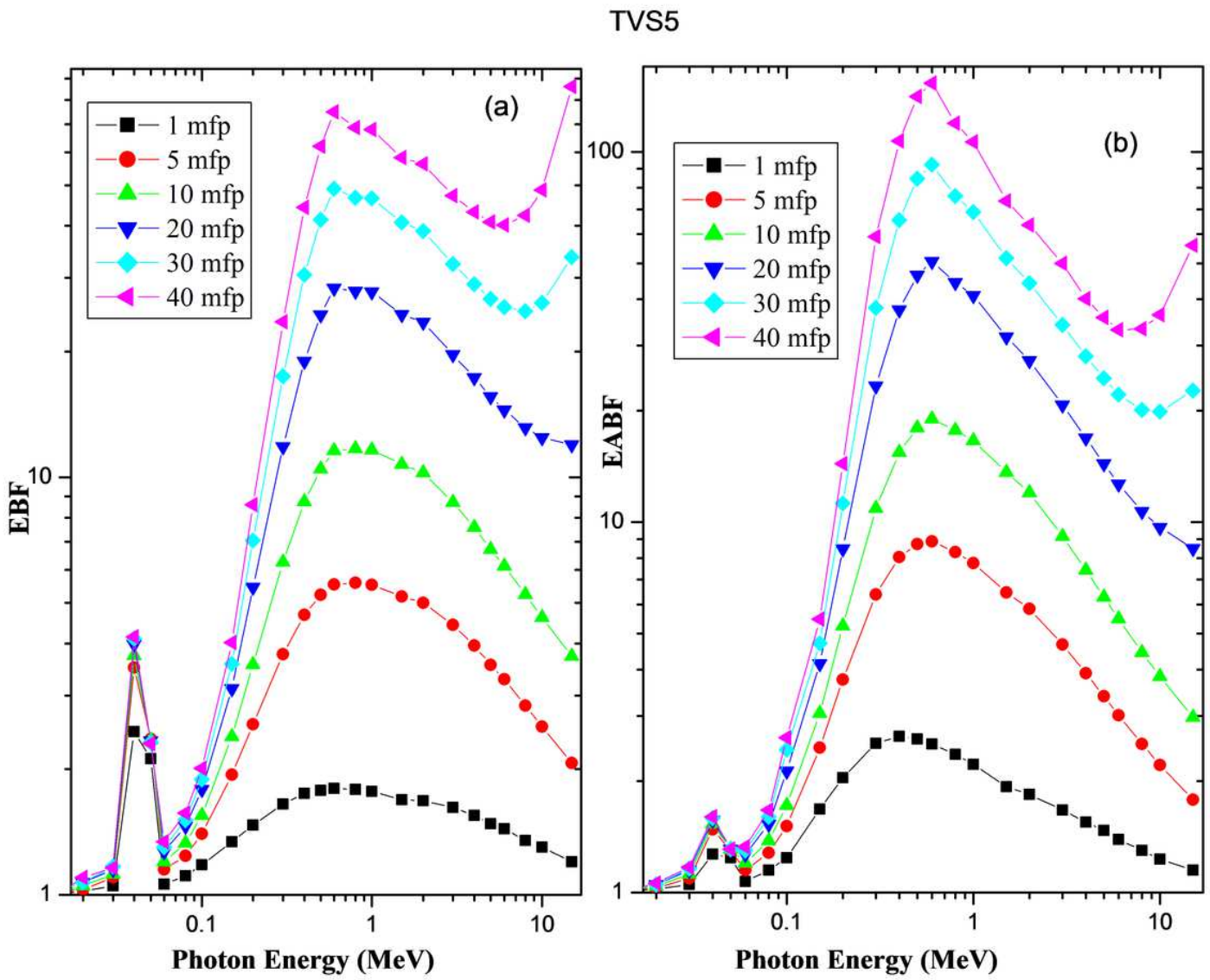

Figure 7

EBF (a) and EABF (b) as a function photon energy for TVS5 glass at different mfp values.

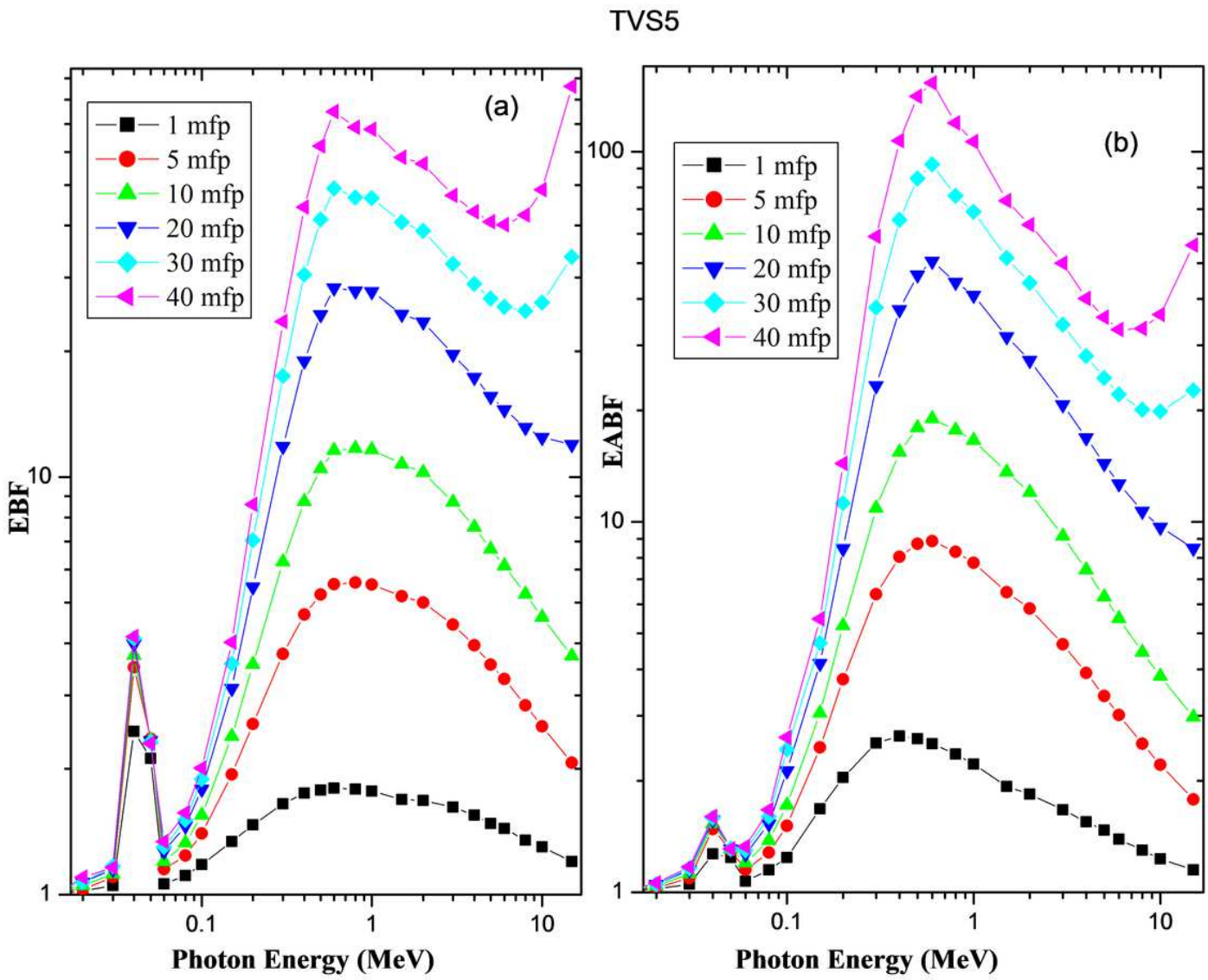

Figure 7

EBF (a) and EABF (b) as a function photon energy for TVS5 glass at different mfp values.

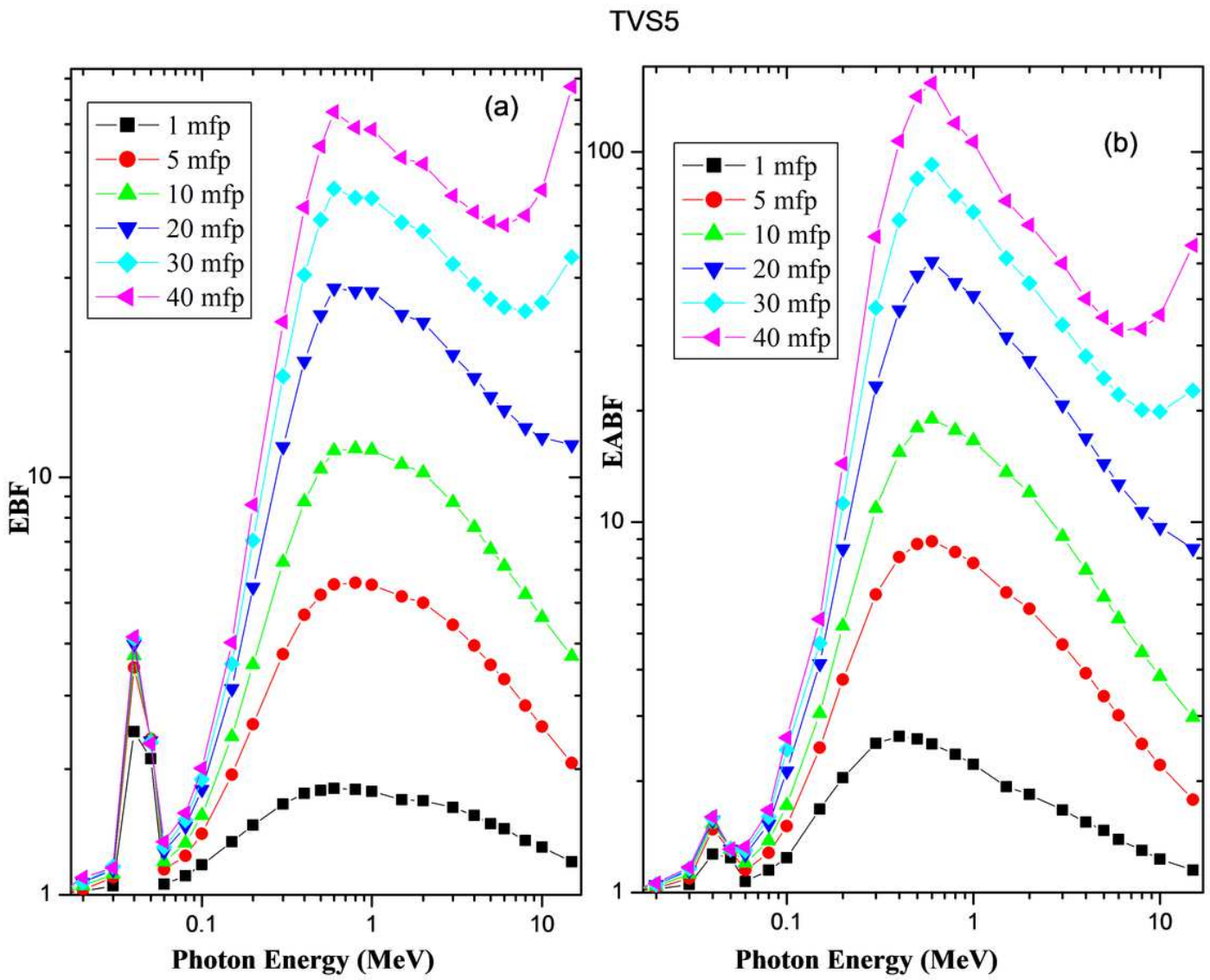

Figure 7

EBF (a) and EABF (b) as a function photon energy for TVS5 glass at different mfp values.

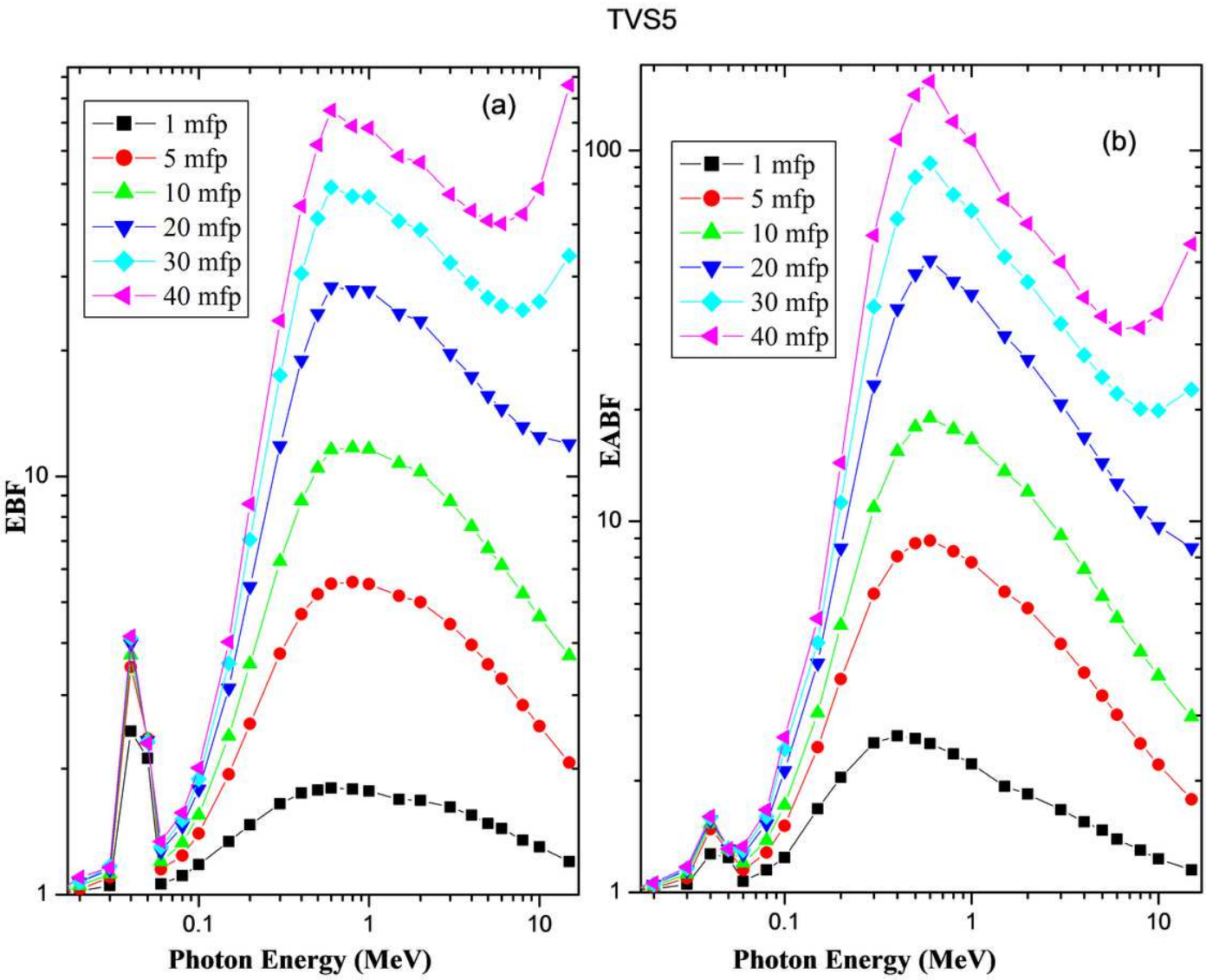

Figure 7

EBF (a) and EABF (b) as a function photon energy for TVS5 glass at different mfp values.

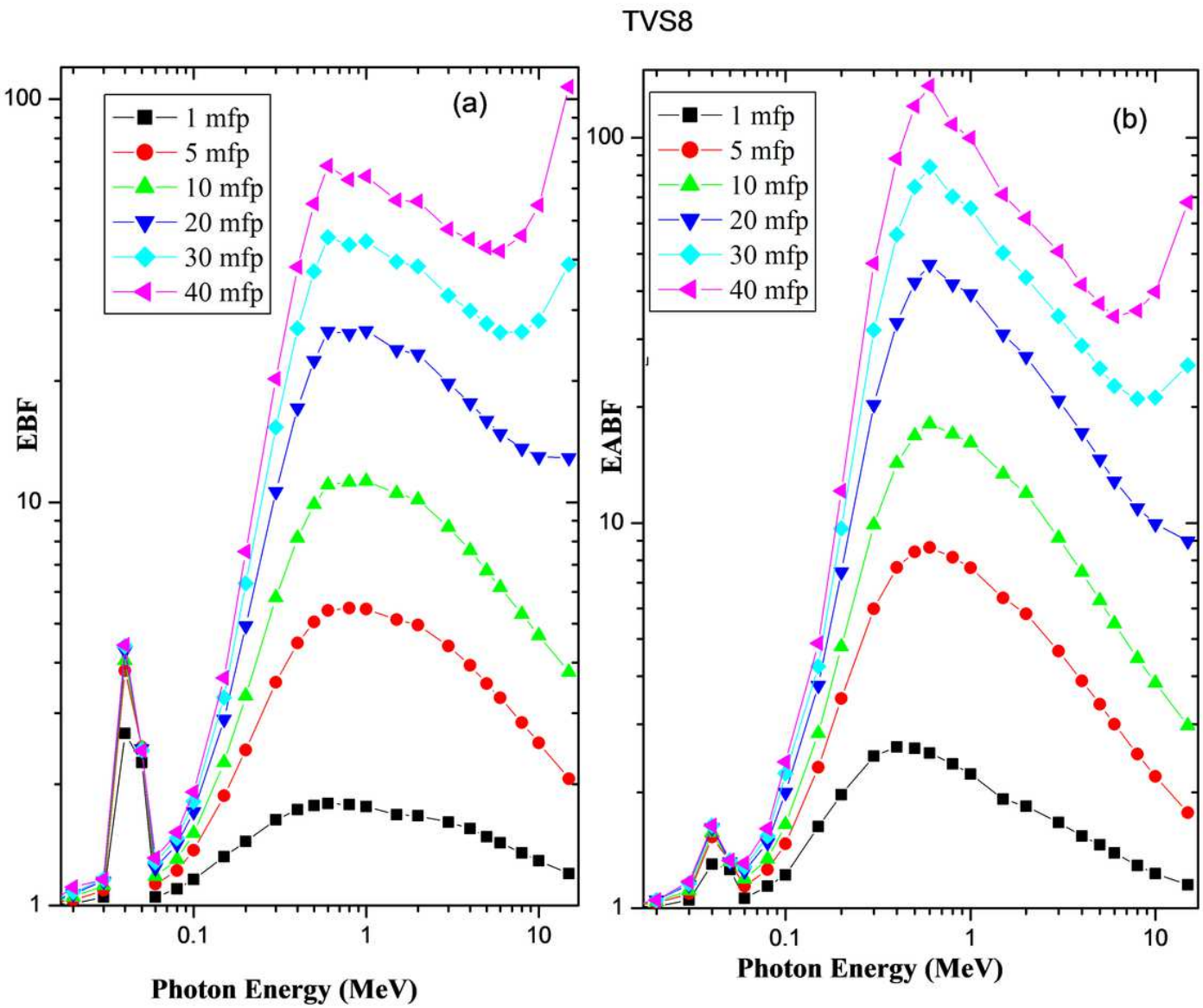

Figure 8

EBF (a) and EABF (b) as a function photon energy for TVS5 glass at different mfp values.

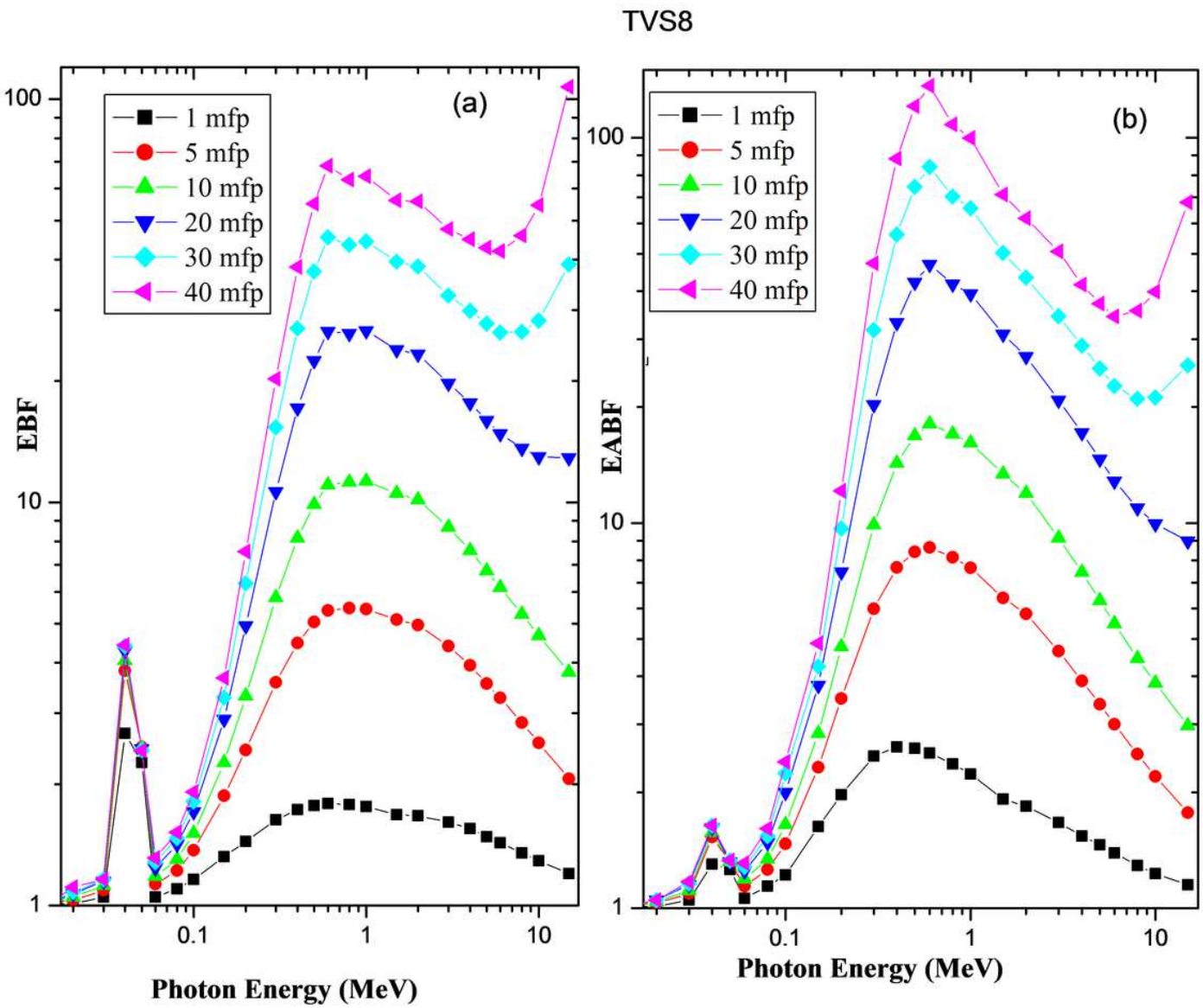

Figure 8

EBF (a) and EABF (b) as a function photon energy for TVS5 glass at different mfp values.

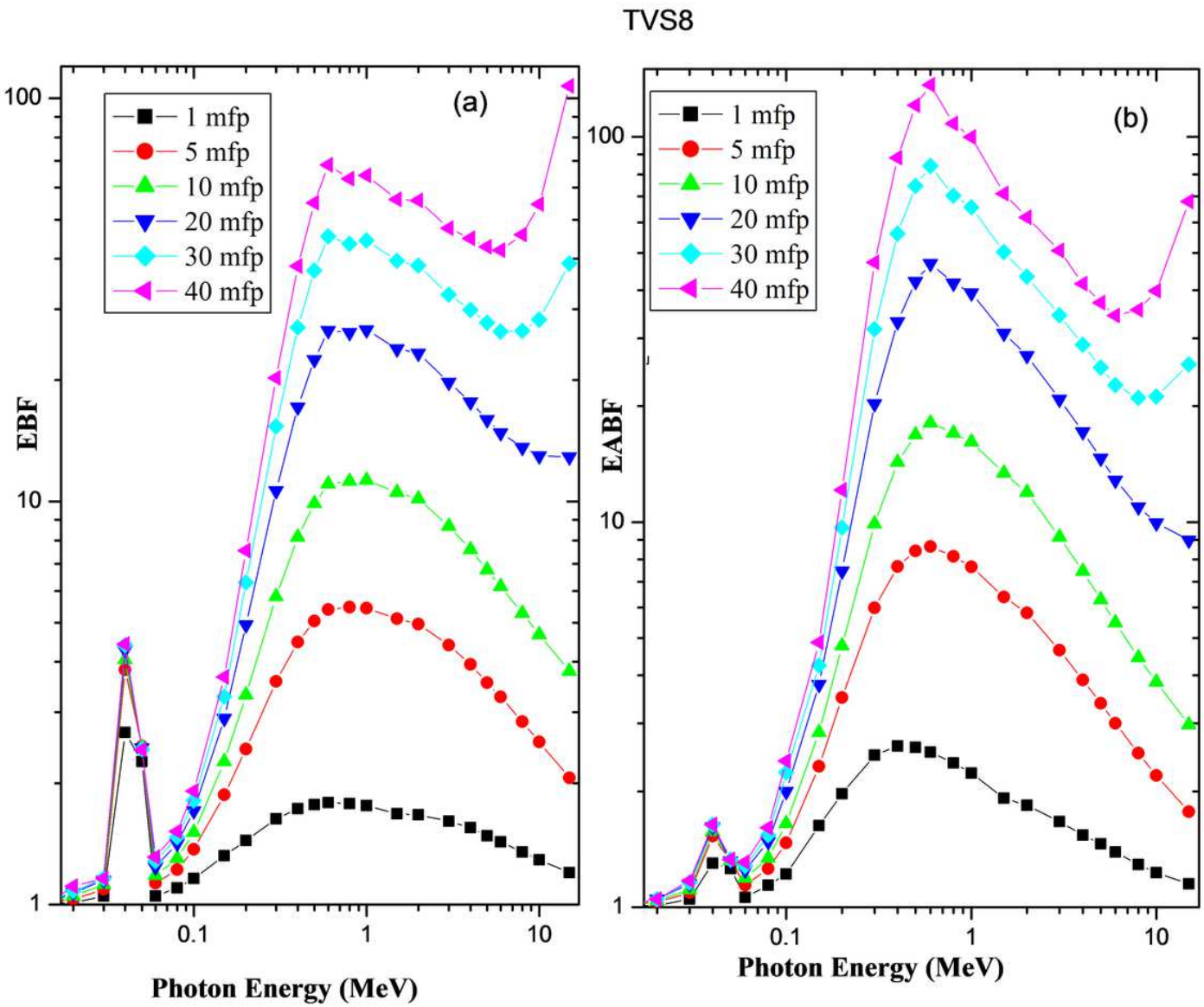

Figure 8

EBF (a) and EABF (b) as a function photon energy for TVS5 glass at different mfp values.

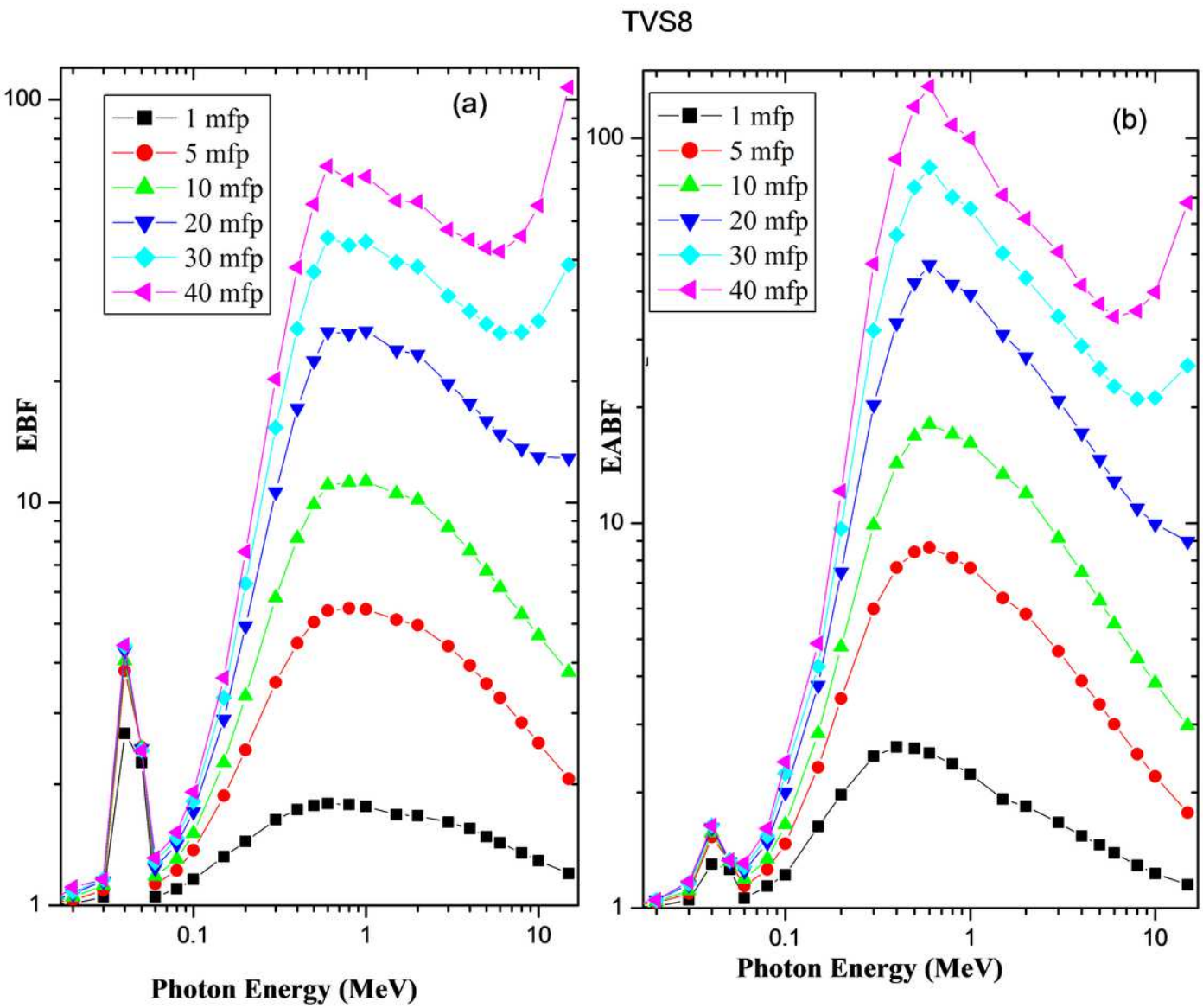

Figure 8

EBF (a) and EABF (b) as a function photon energy for TVS5 glass at different mfp values.

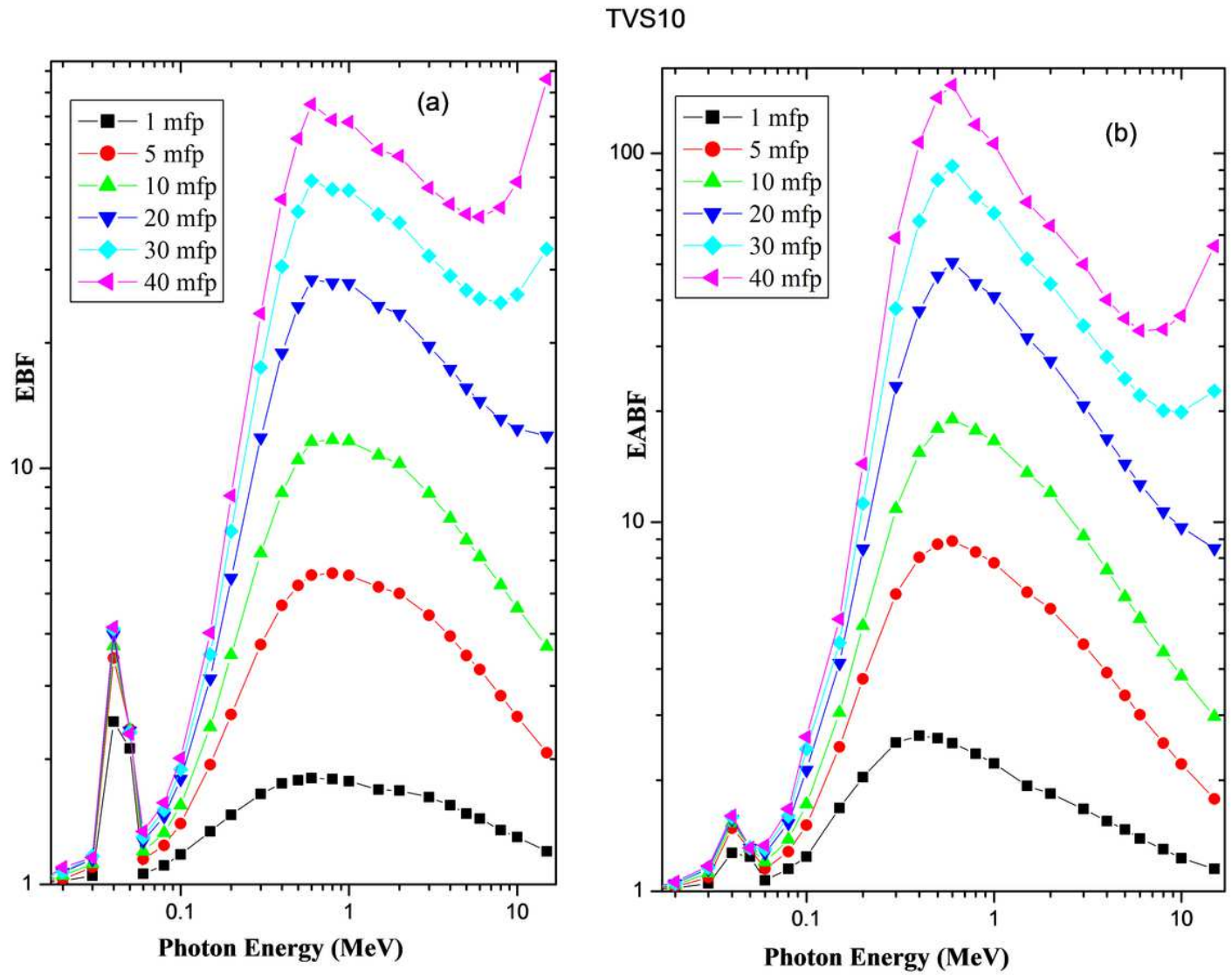

Figure 9

EBF (a) and EABF (b) as a function photon energy for TVS10 glass at different mfp values.

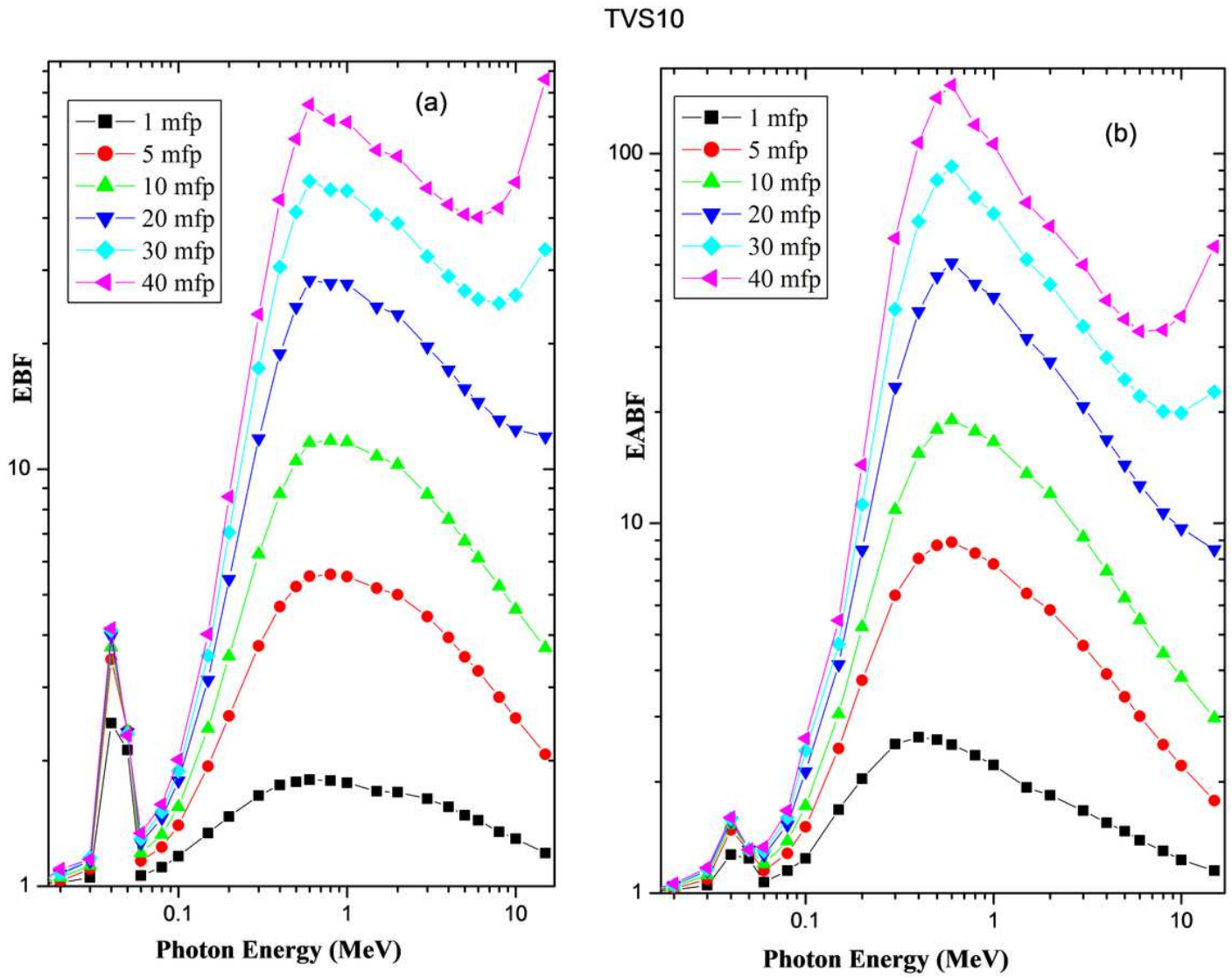

Figure 9

EBF (a) and EABF (b) as a function photon energy for TVS10 glass at different mfp values.

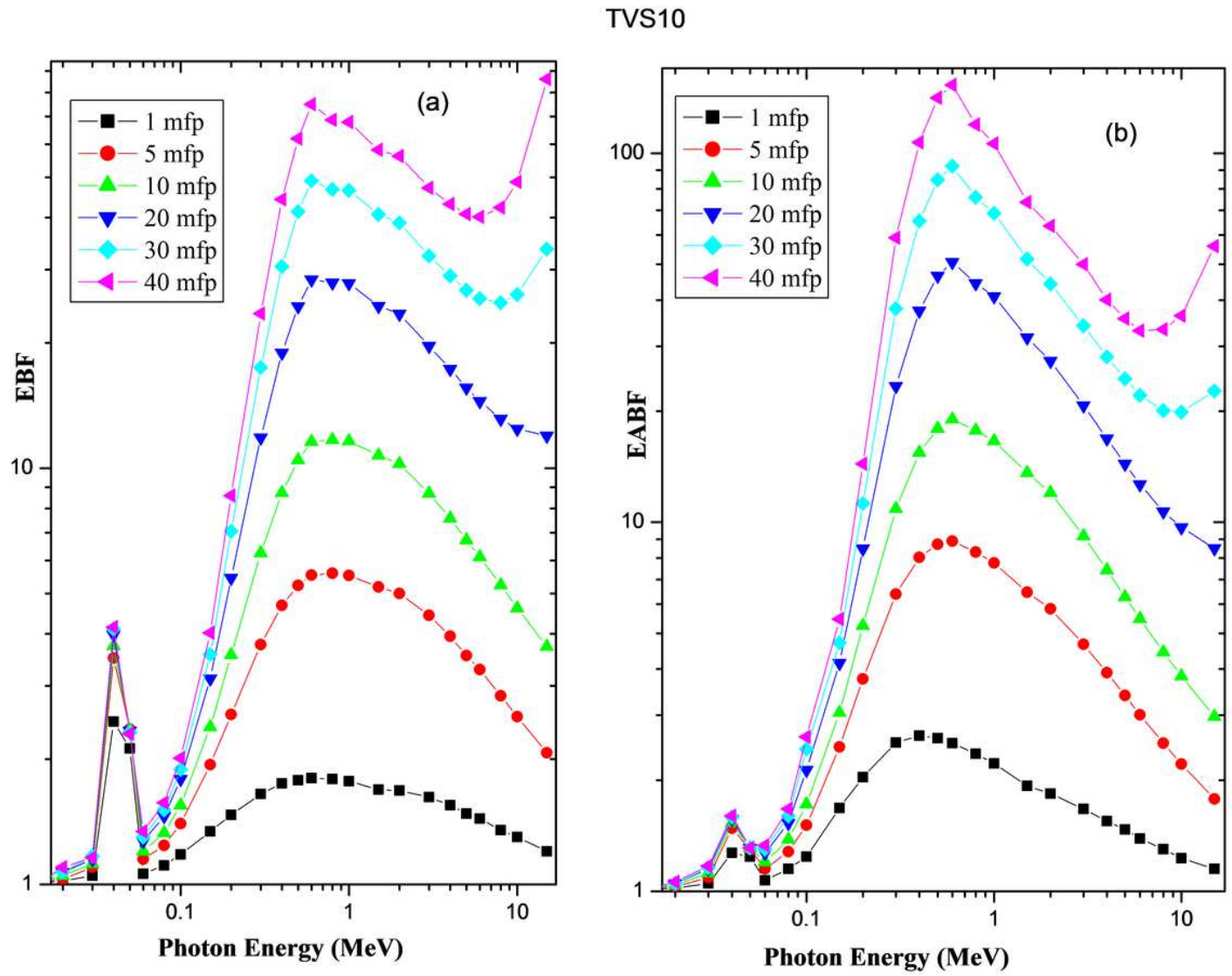

Figure 9

EBF (a) and EABF (b) as a function photon energy for TVS10 glass at different mfp values.

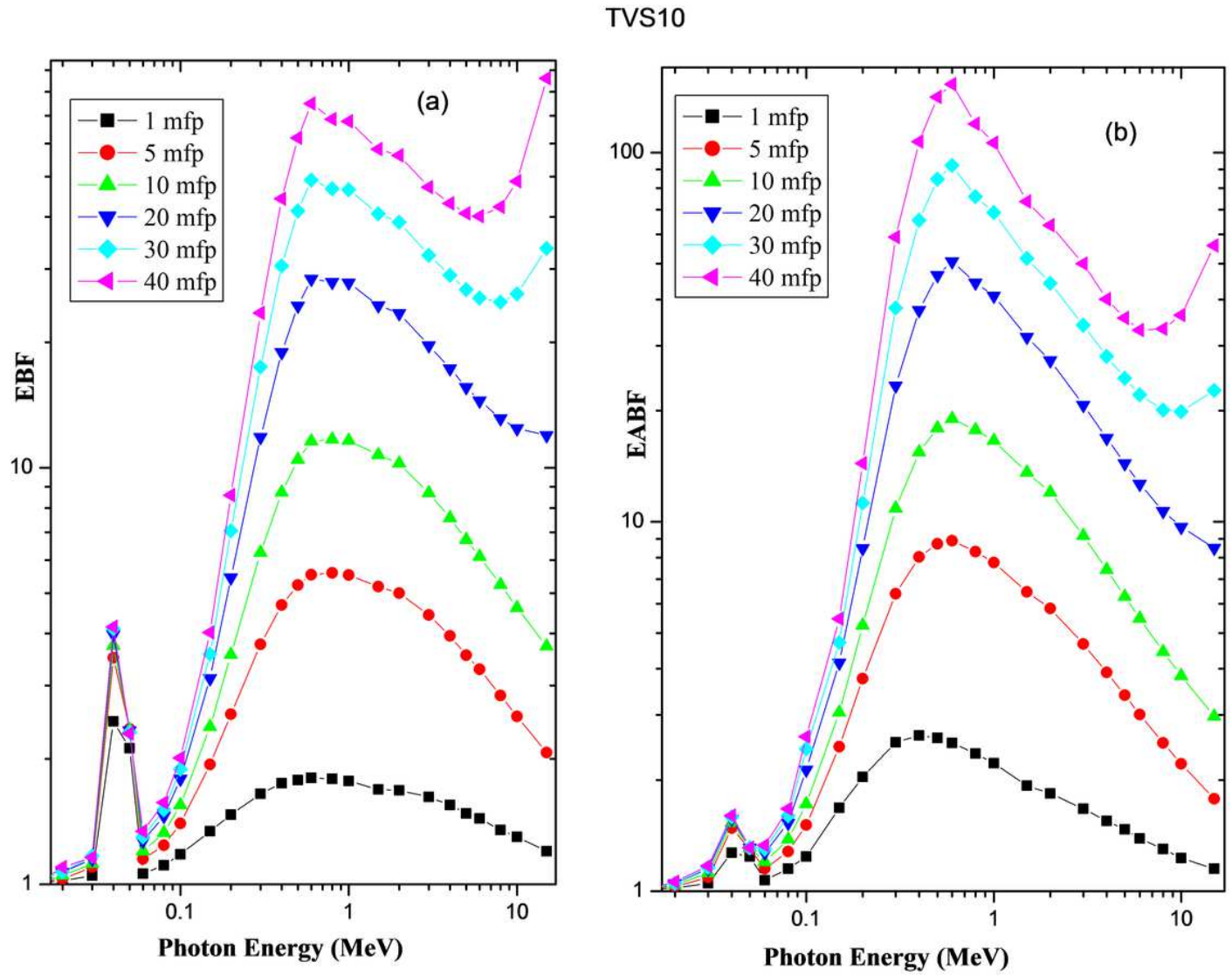

Figure 9

EBF (a) and EABF (b) as a function photon energy for TVS10 glass at different mfp values.

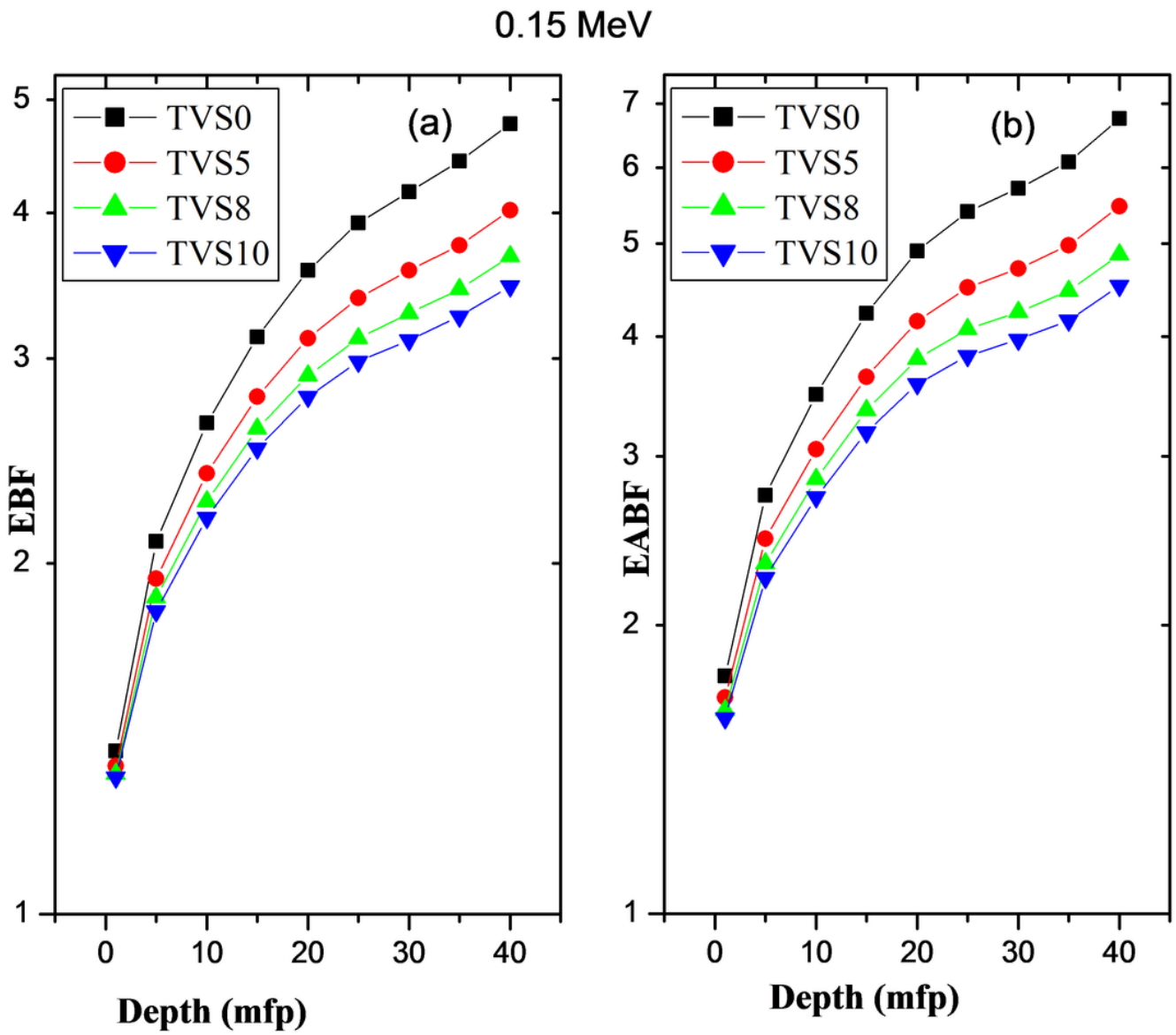

Figure 10

EBF (a) and EABF (b) as a function of penetration depth for TVS glasses at energy 0.15 MeV.

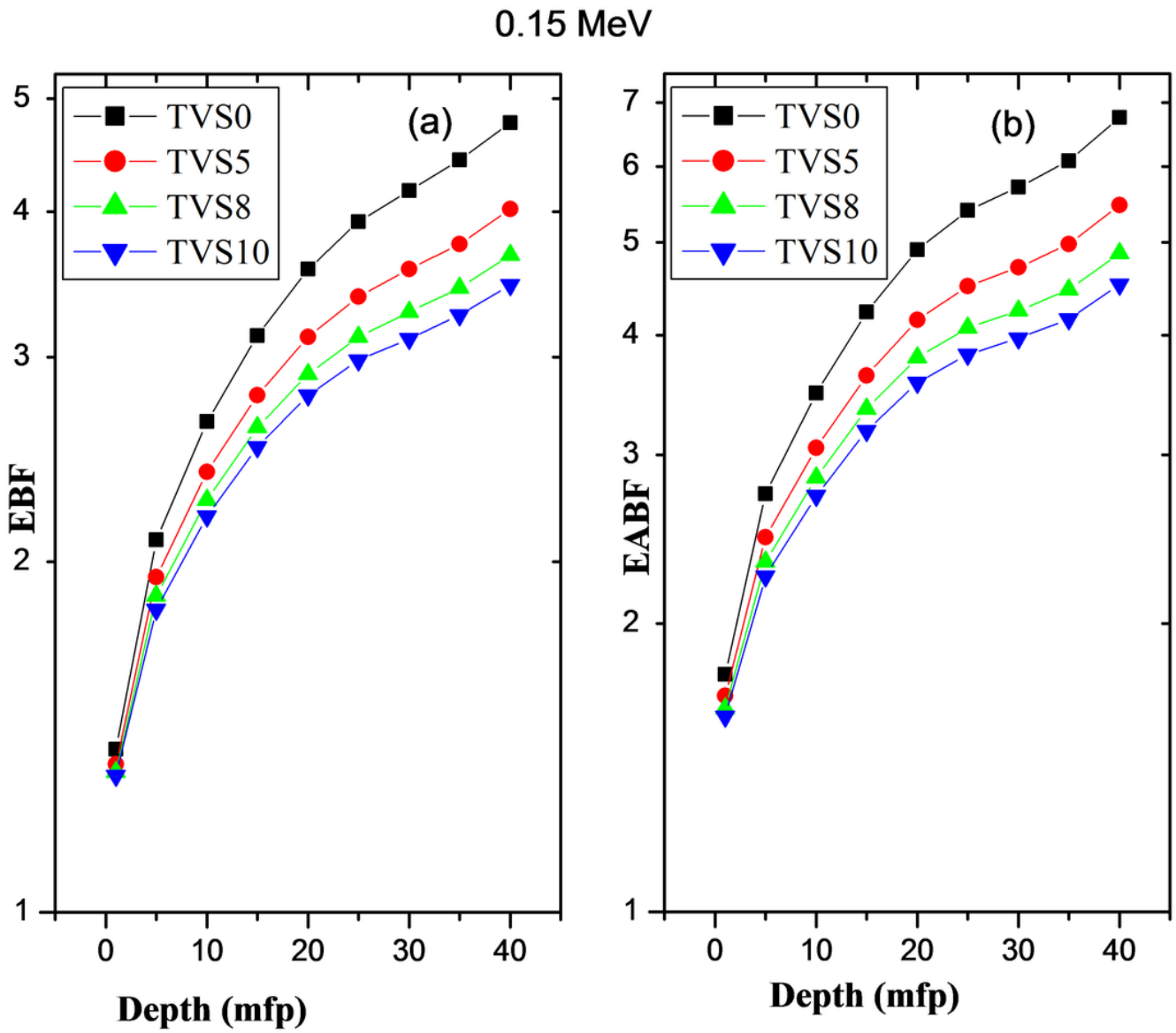

Figure 10

EBF (a) and EABF (b) as a function of penetration depth for TVS glasses at energy 0.15 MeV.

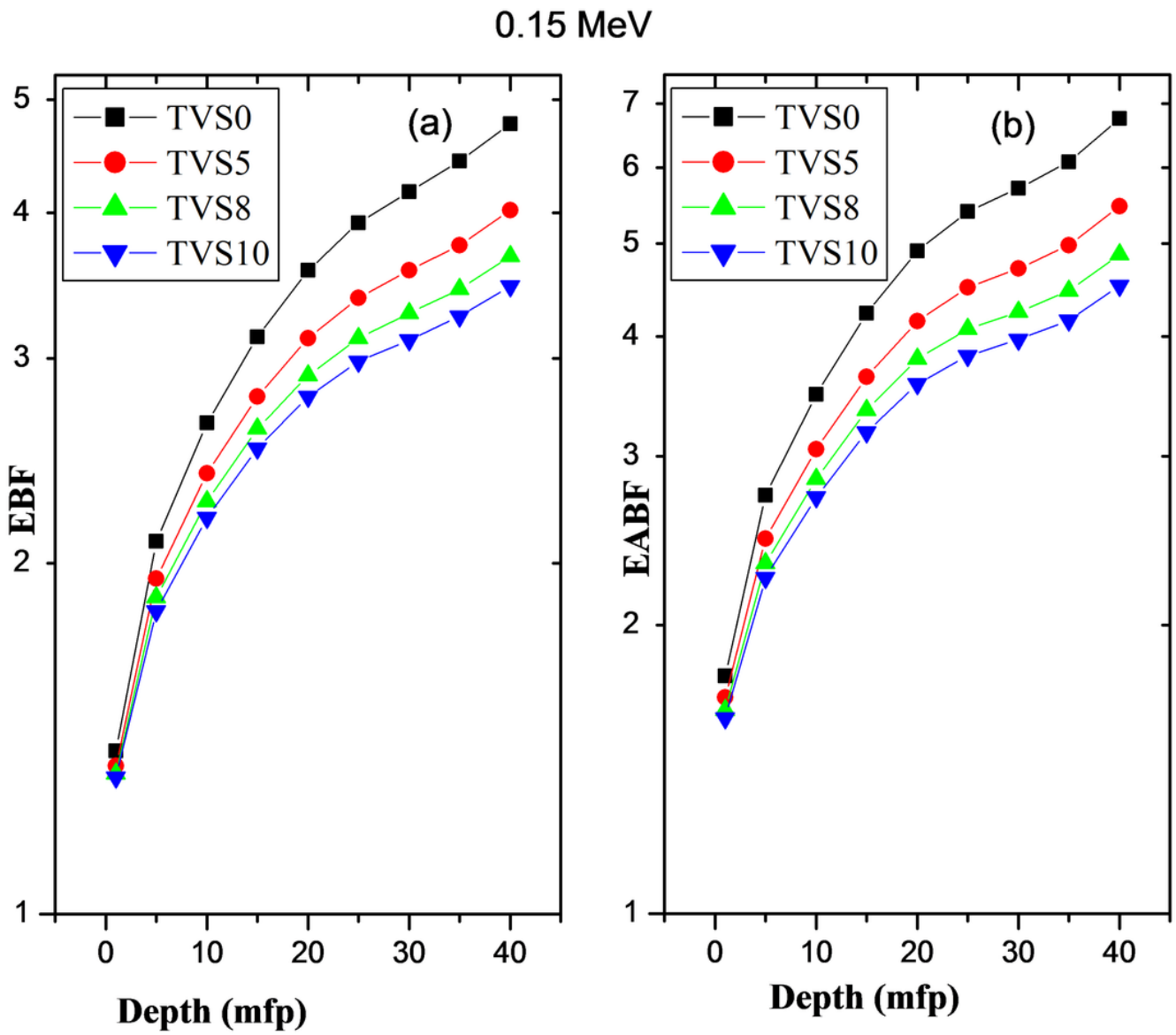

Figure 10

EBF (a) and EABF (b) as a function of penetration depth for TVS glasses at energy 0.15 MeV.

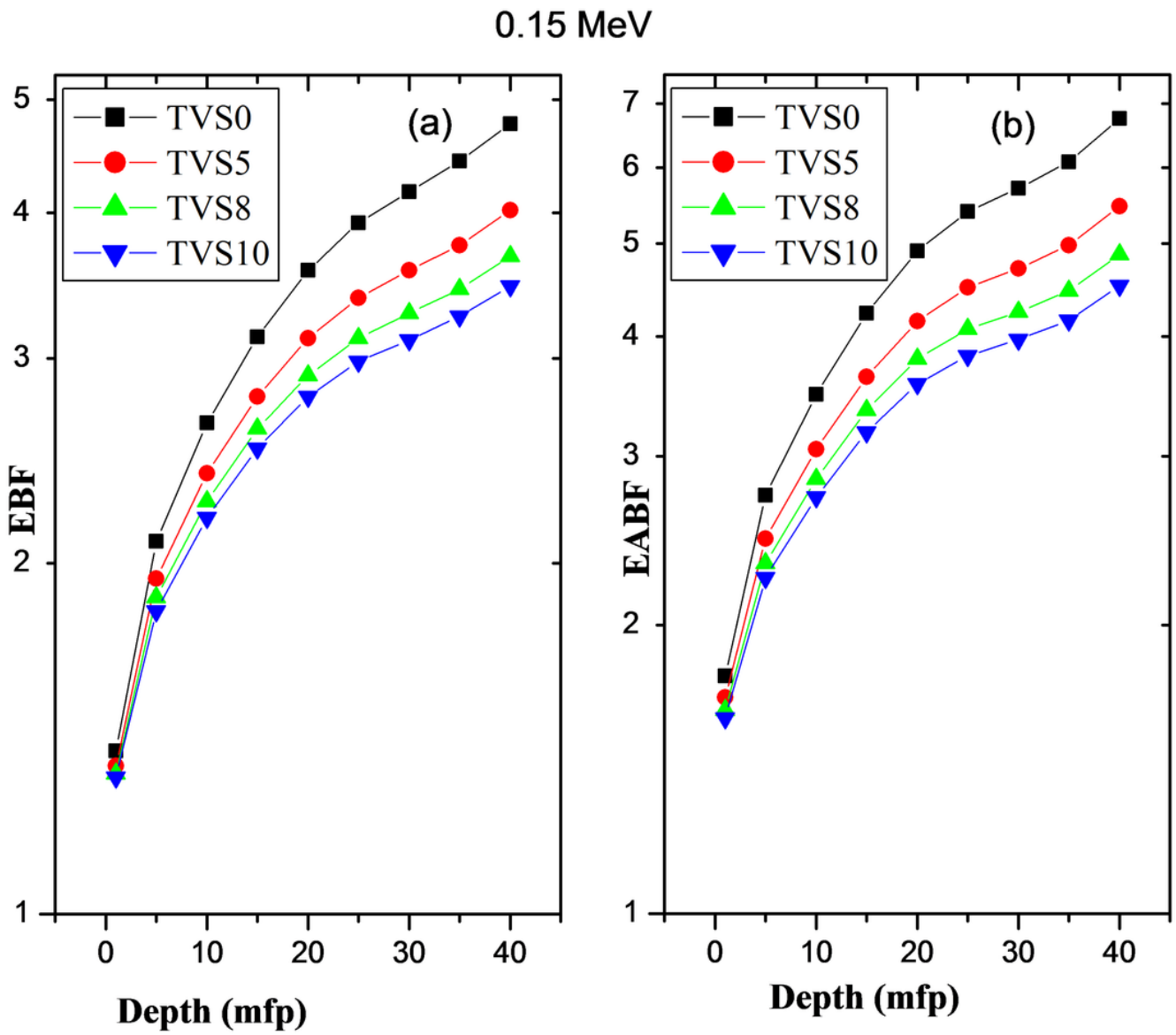

Figure 10

EBF (a) and EABF (b) as a function of penetration depth for TVS glasses at energy 0.15 MeV.

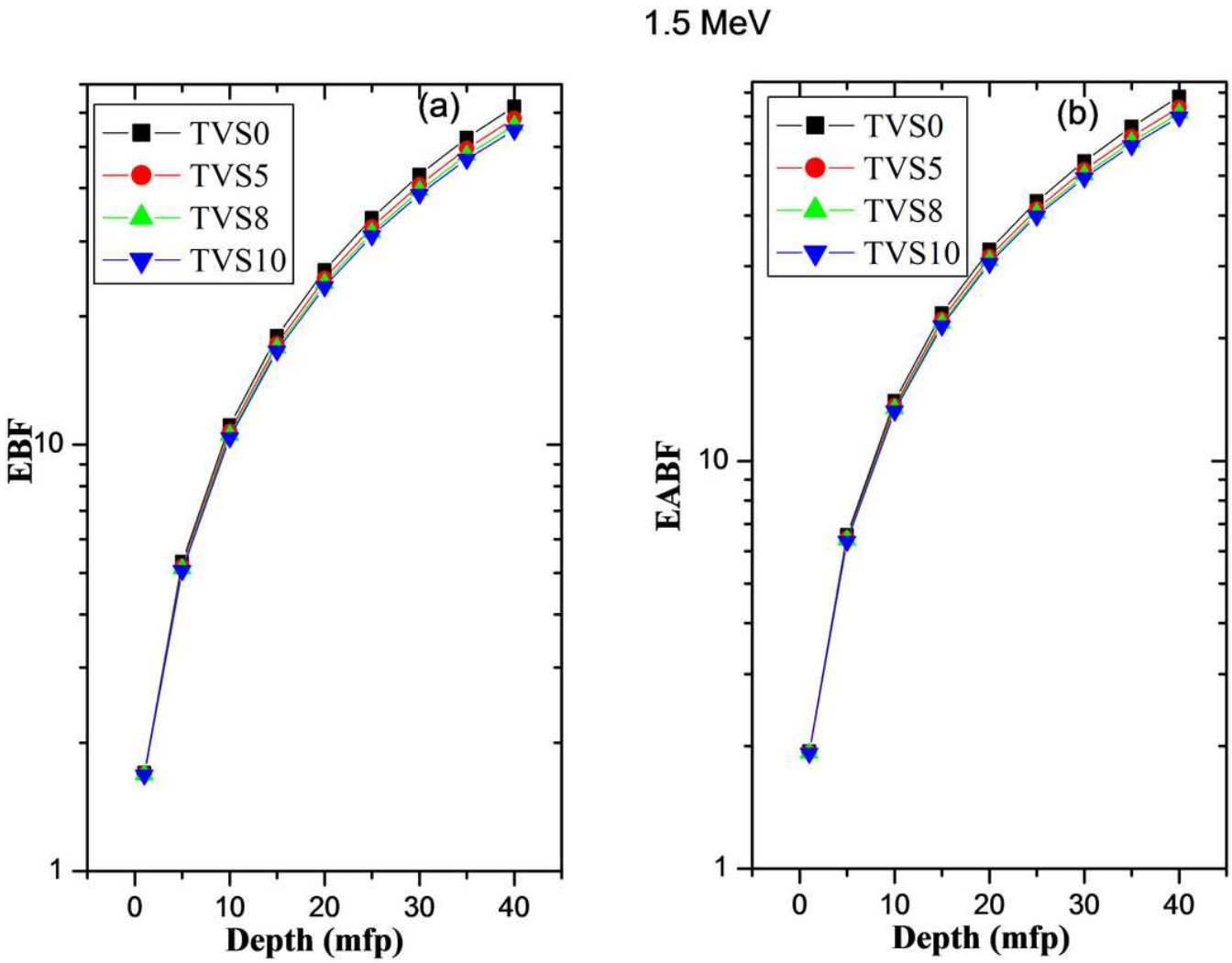

Figure 11

EBF (a) and EABF (b) as a function of penetration depth for TVS glasses at energy 1.5 MeV.

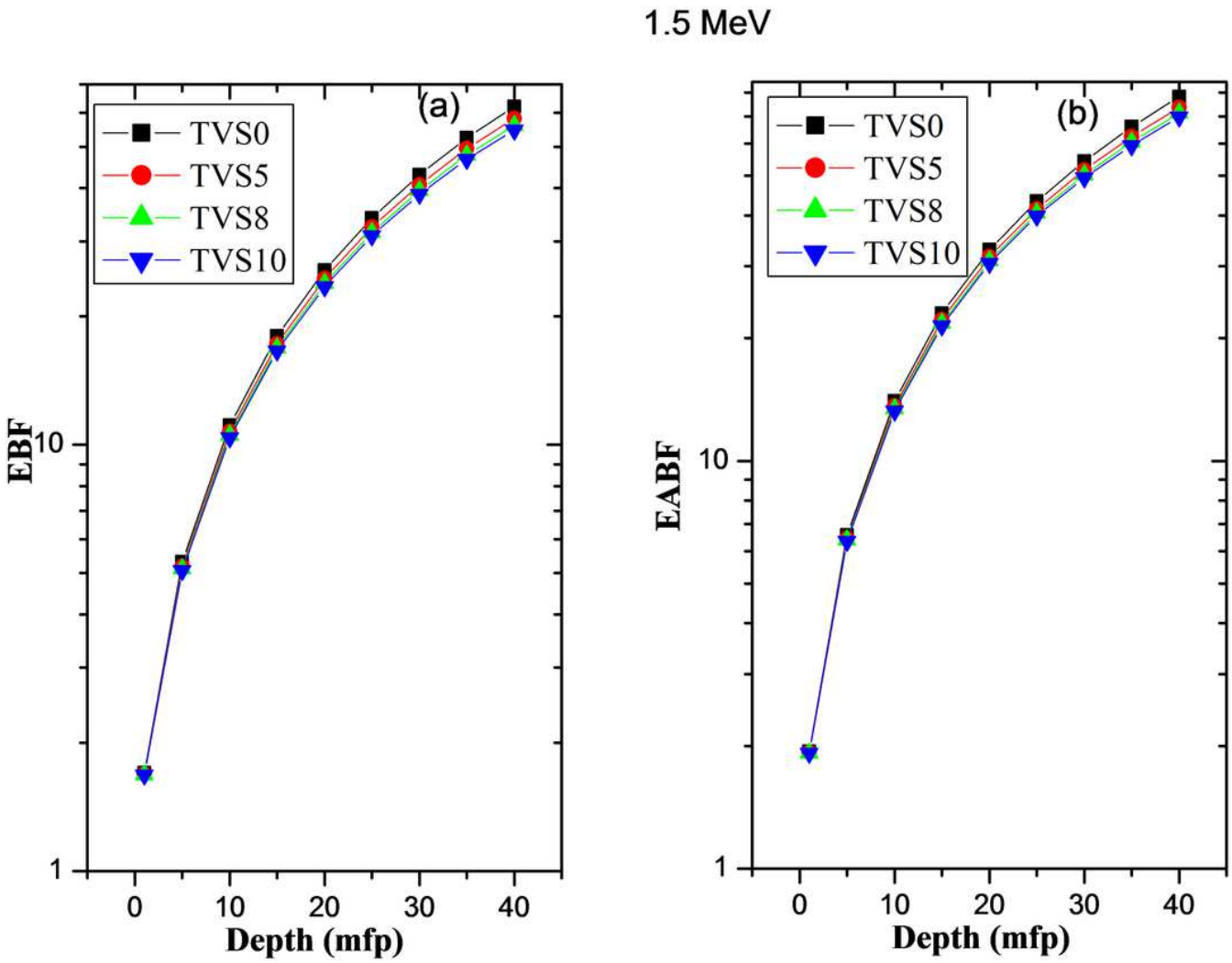

Figure 11

EBF (a) and EABF (b) as a function of penetration depth for TVS glasses at energy 1.5 MeV.

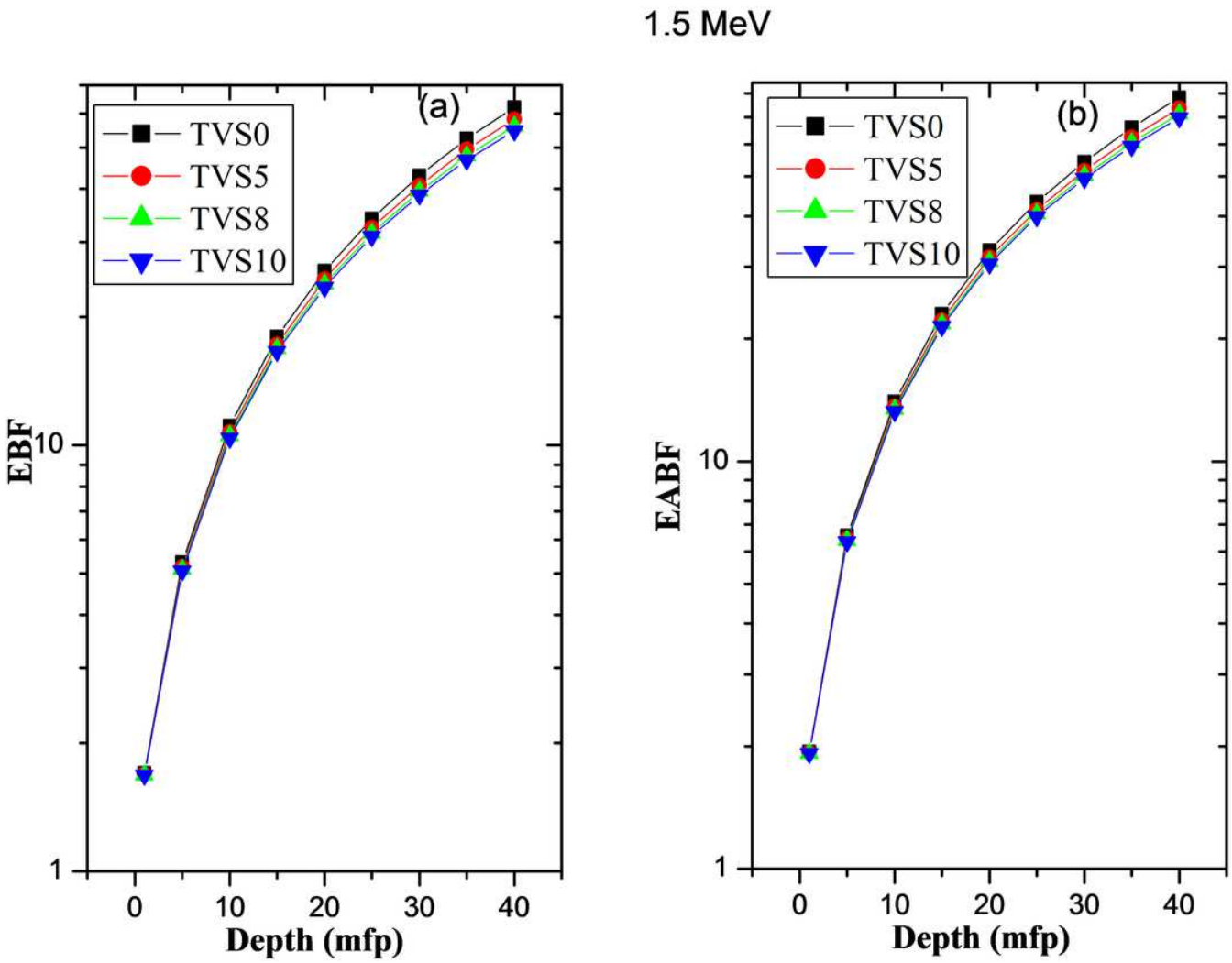

Figure 11

EBF (a) and EABF (b) as a function of penetration depth for TVS glasses at energy 1.5 MeV.

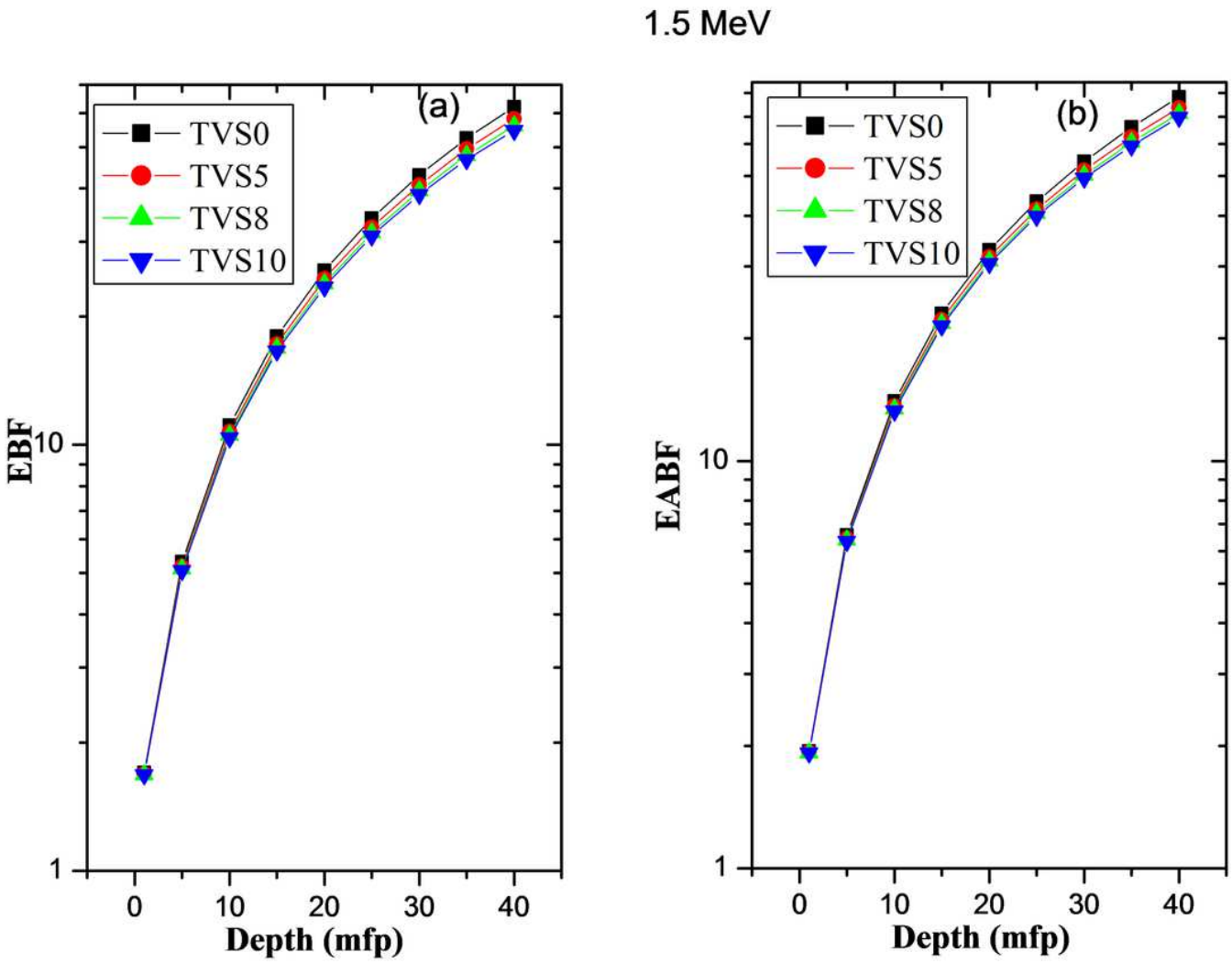

Figure 11

EBF (a) and EABF (b) as a function of penetration depth for TVS glasses at energy 1.5 MeV.

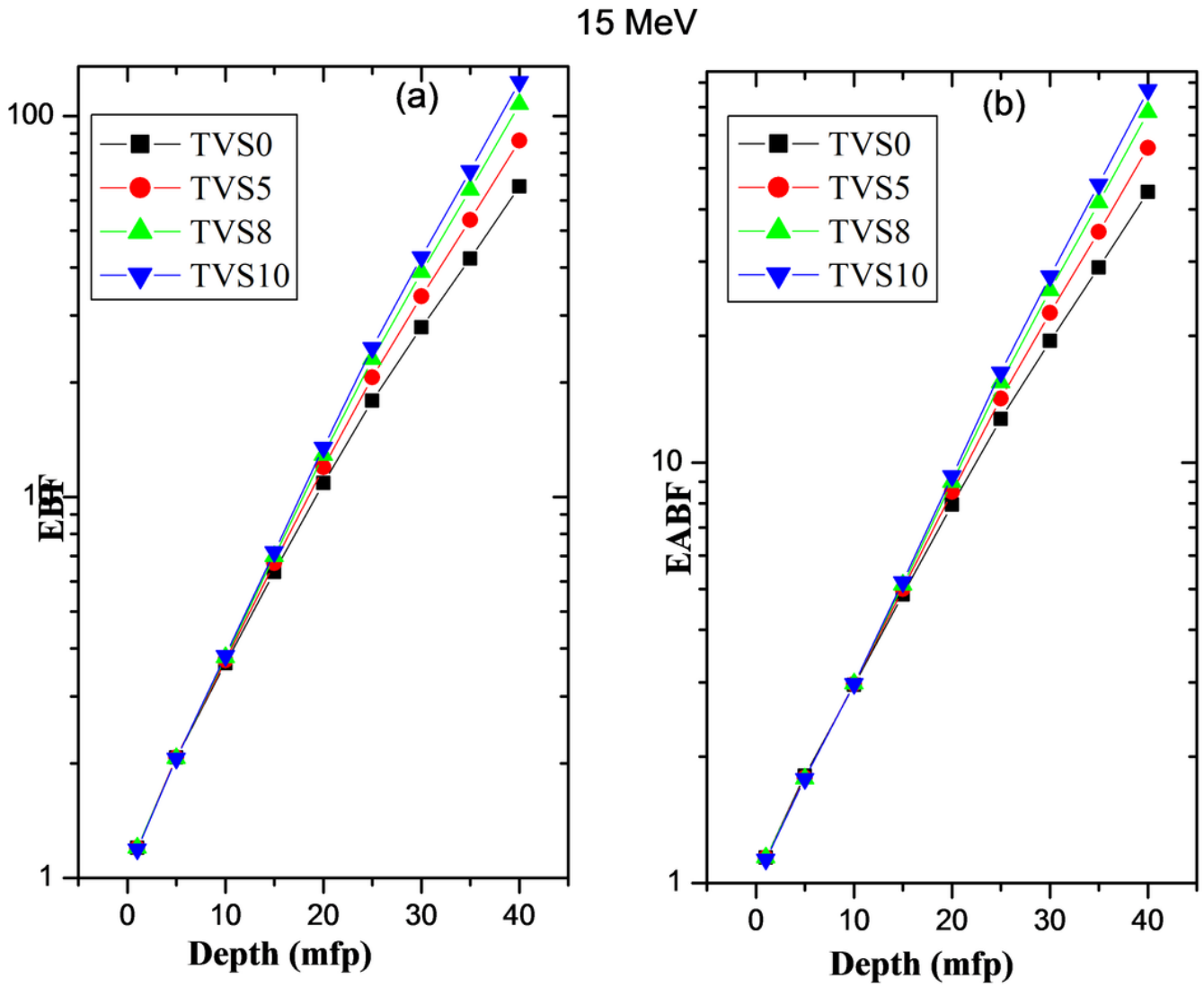

Figure 12

EBF (a) and EABF (b) as a function of penetration depth for TVS glasses at energy 15 MeV.

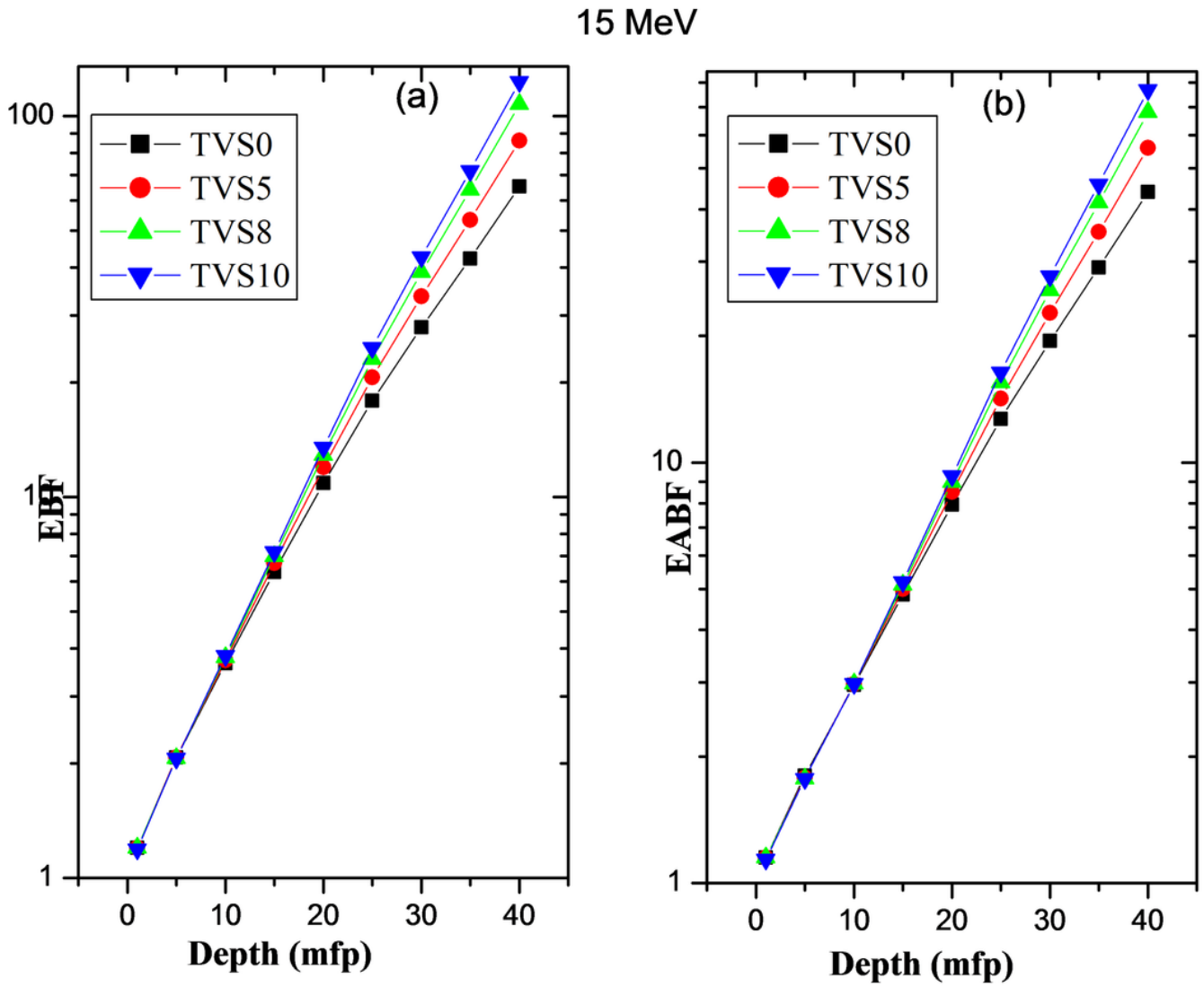

Figure 12

EBF (a) and EABF (b) as a function of penetration depth for TVS glasses at energy 15 MeV.

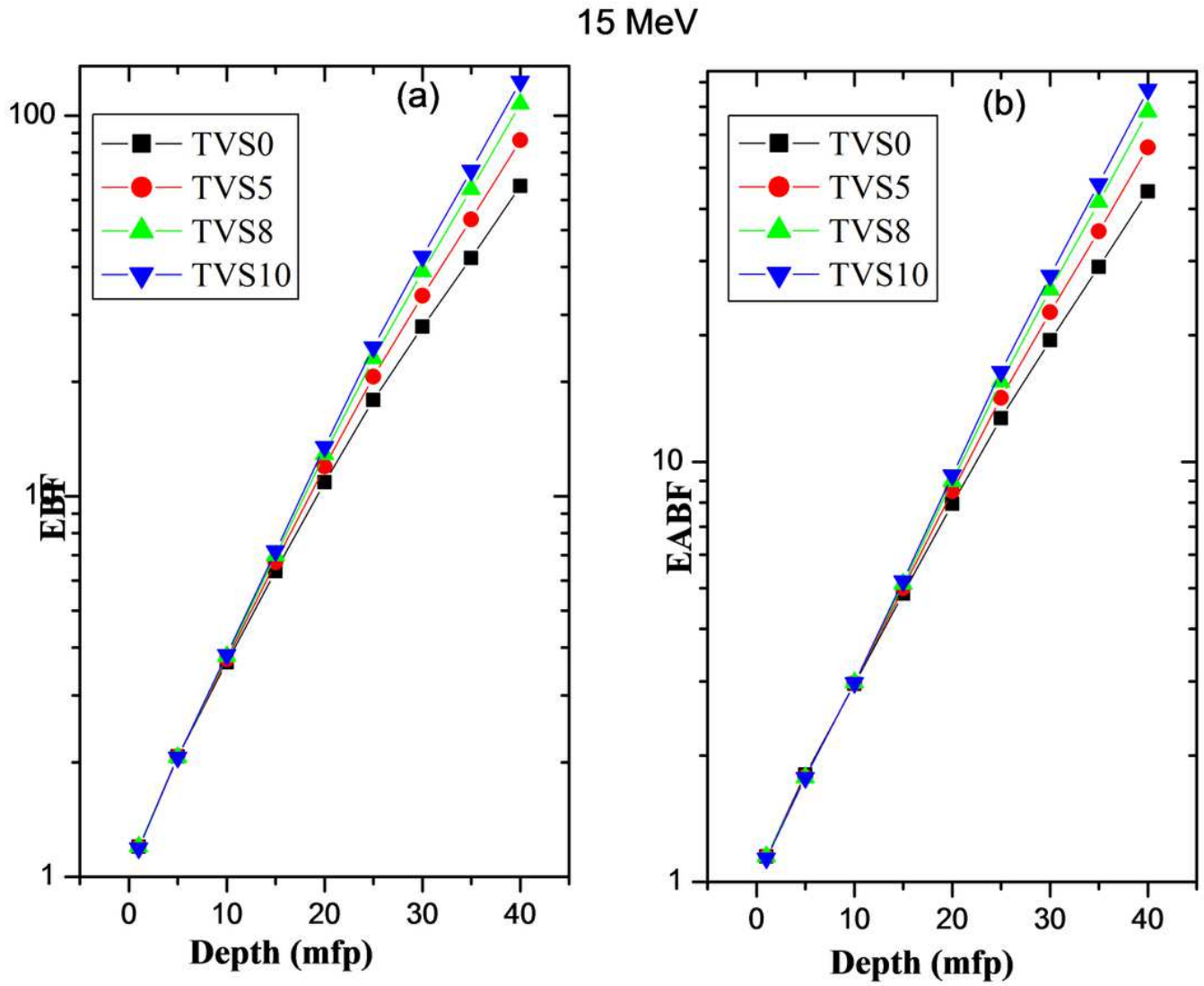

Figure 12

EBF (a) and EABF (b) as a function of penetration depth for TVS glasses at energy 15 MeV.

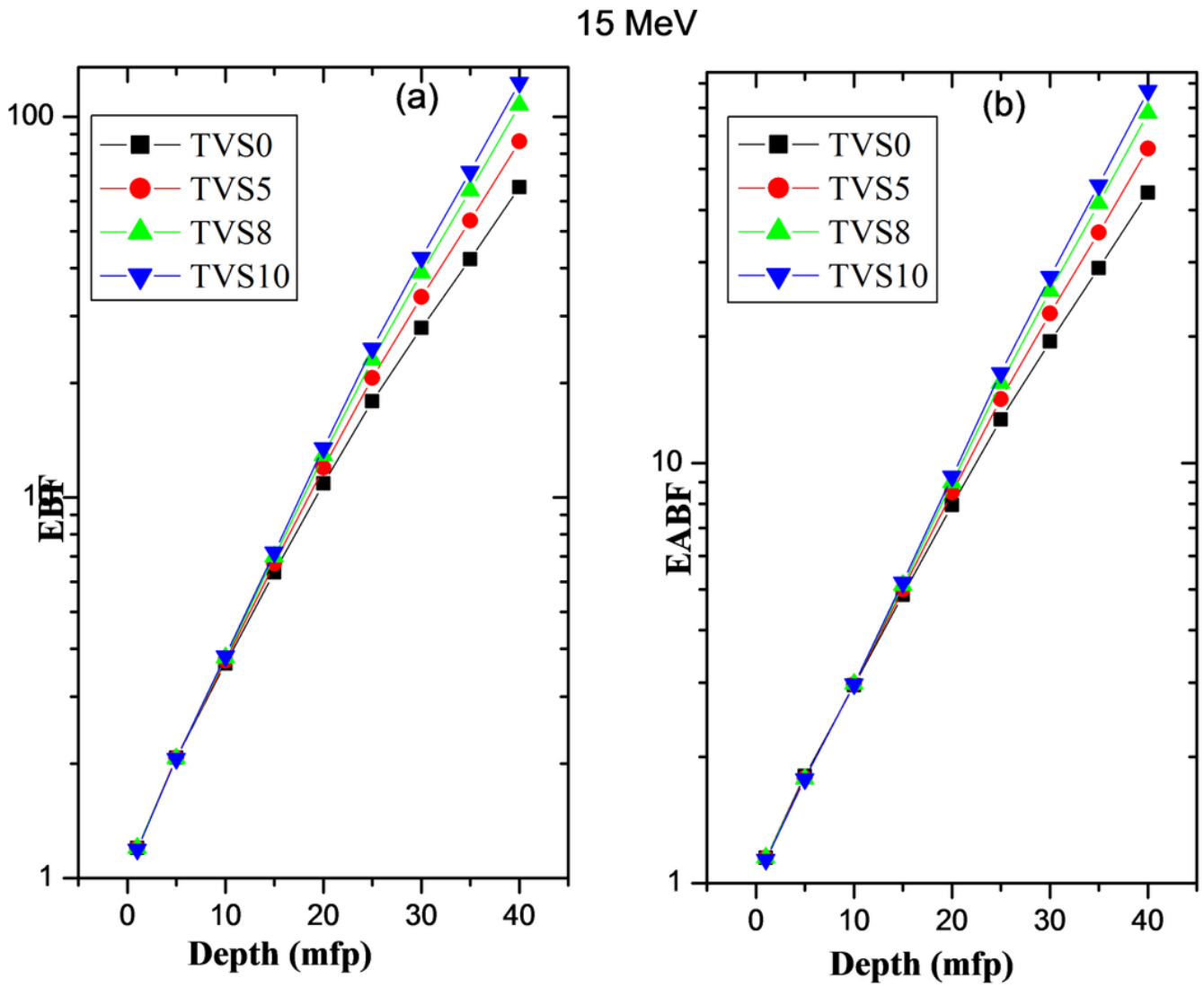

Figure 12

EBF (a) and EABF (b) as a function of penetration depth for TVS glasses at energy 15 MeV.

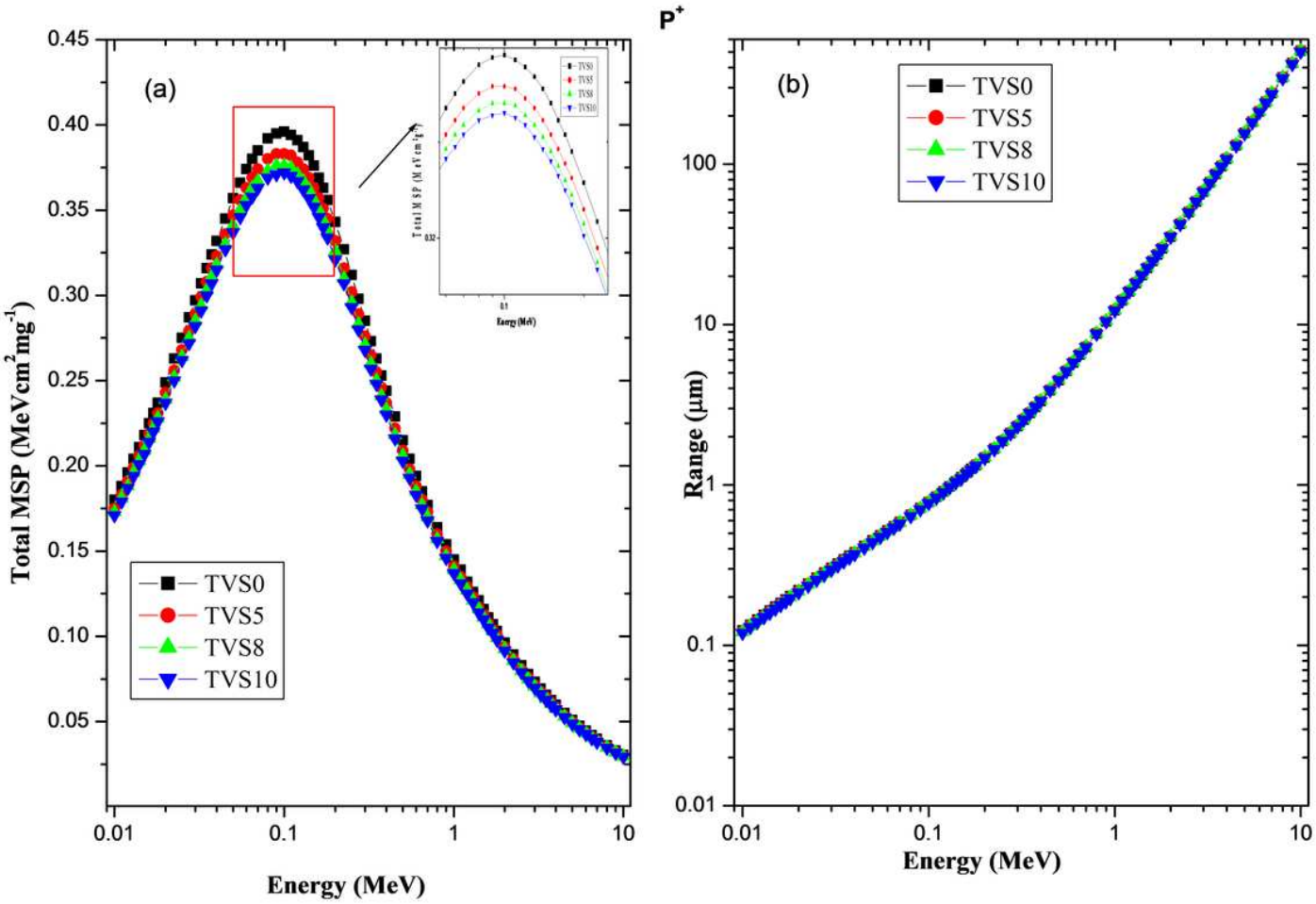

Figure 13

Total MSP (a) and range (b) of proton as a function of proton energy for TVS glasses.

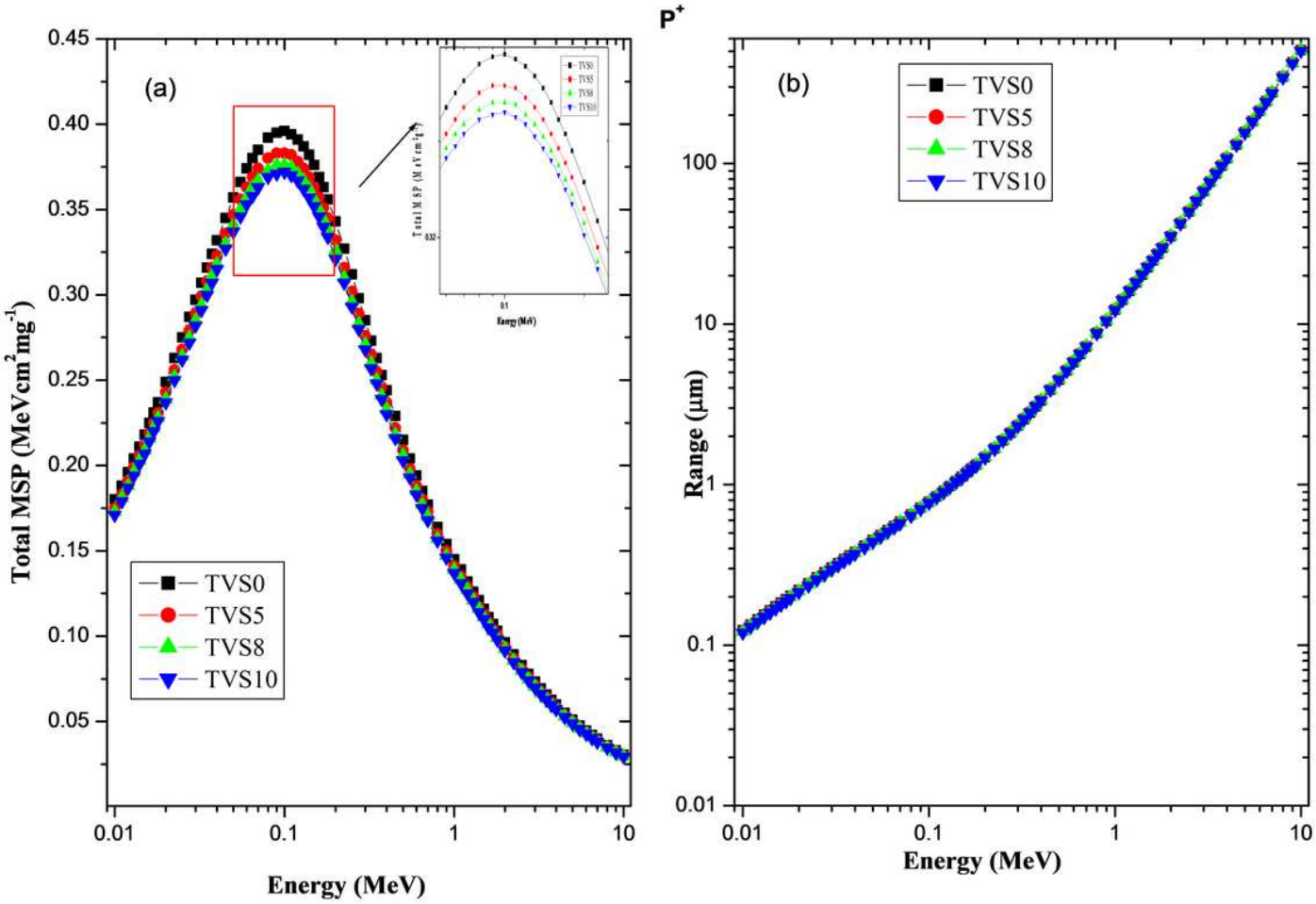

Figure 13

Total MSP (a) and range (b) of proton as a function of proton energy for TVS glasses.

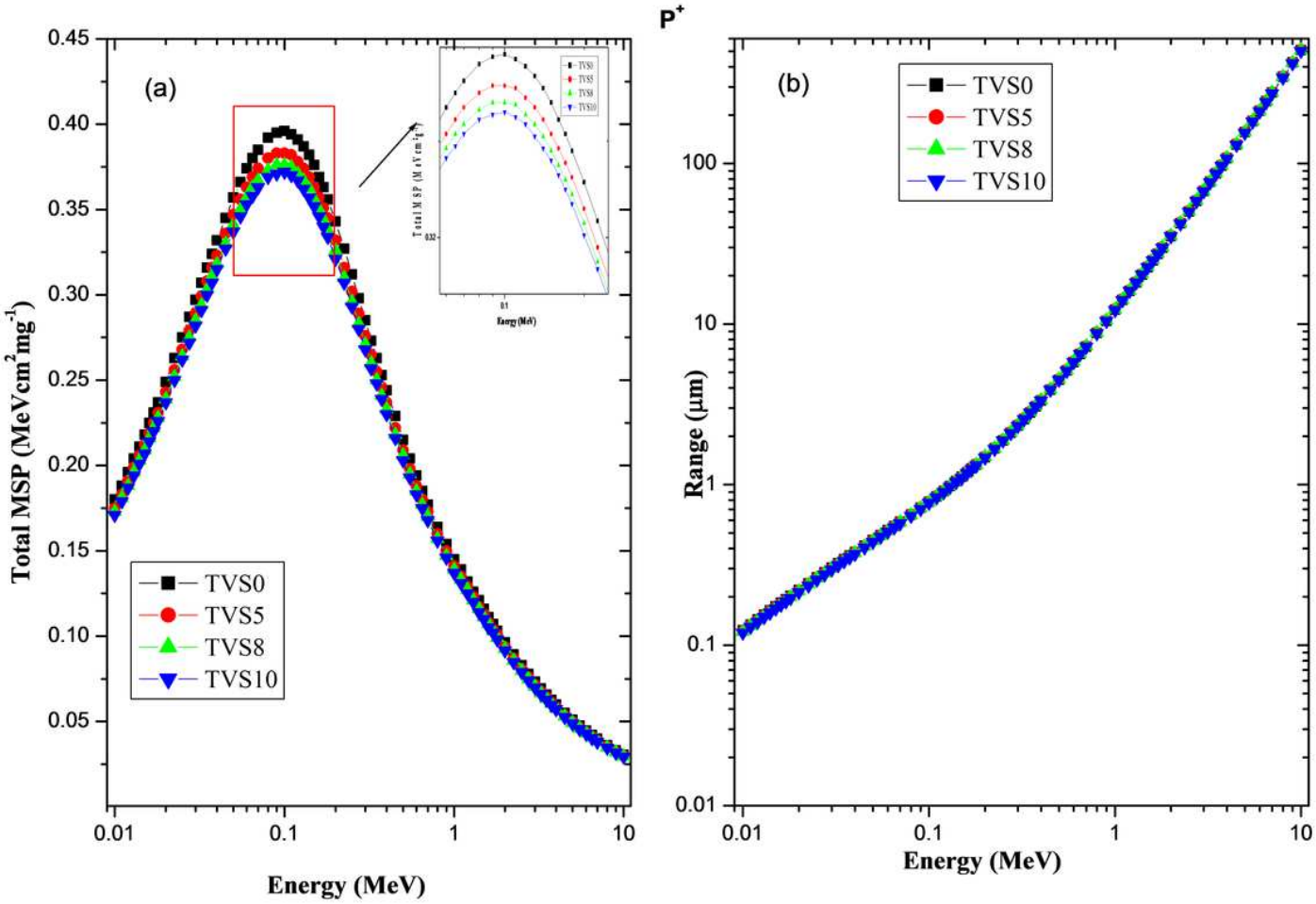

Figure 13

Total MSP (a) and range (b) of proton as a function of proton energy for TVS glasses.

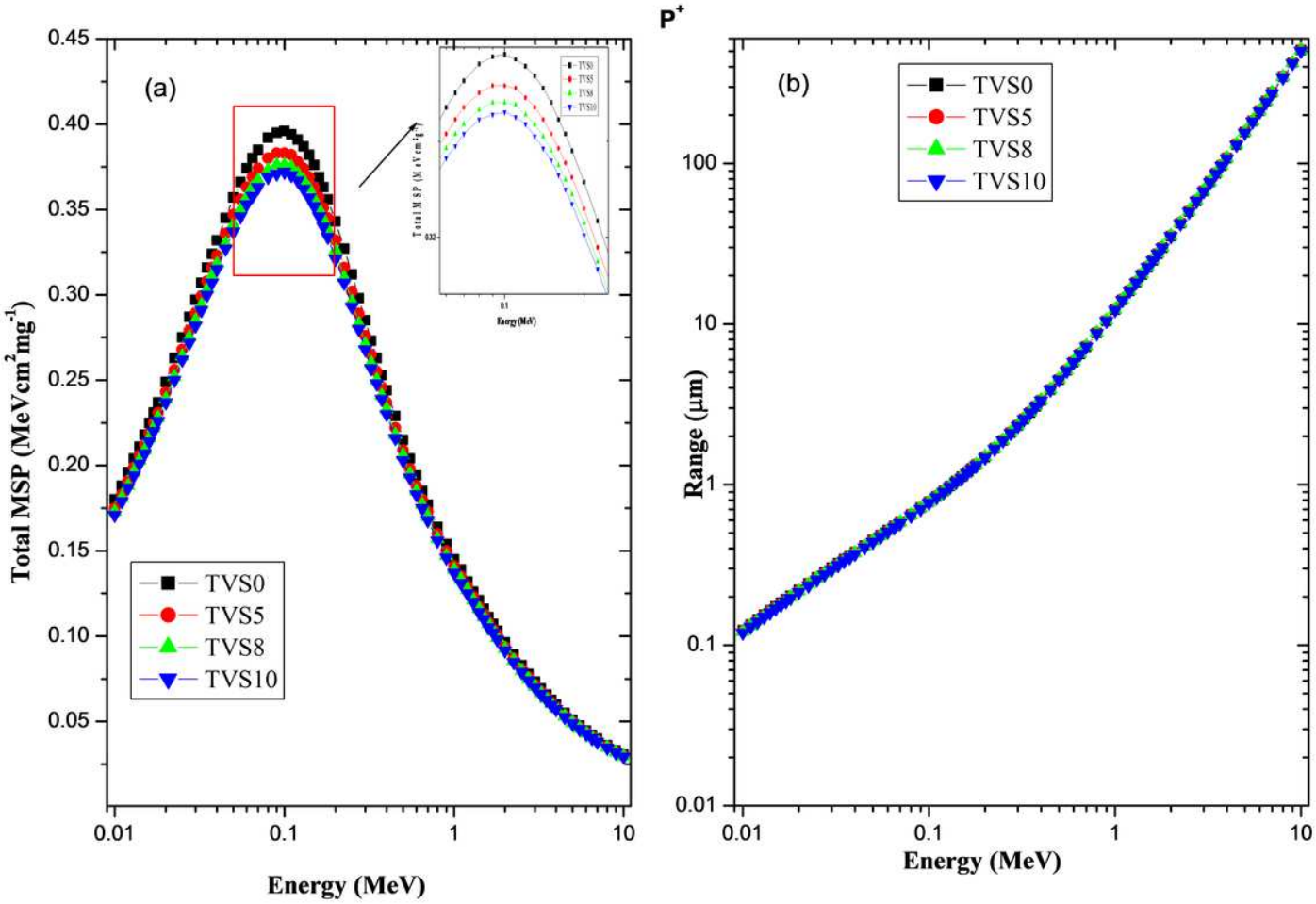

Figure 13

Total MSP (a) and range (b) of proton as a function of proton energy for TVS glasses.

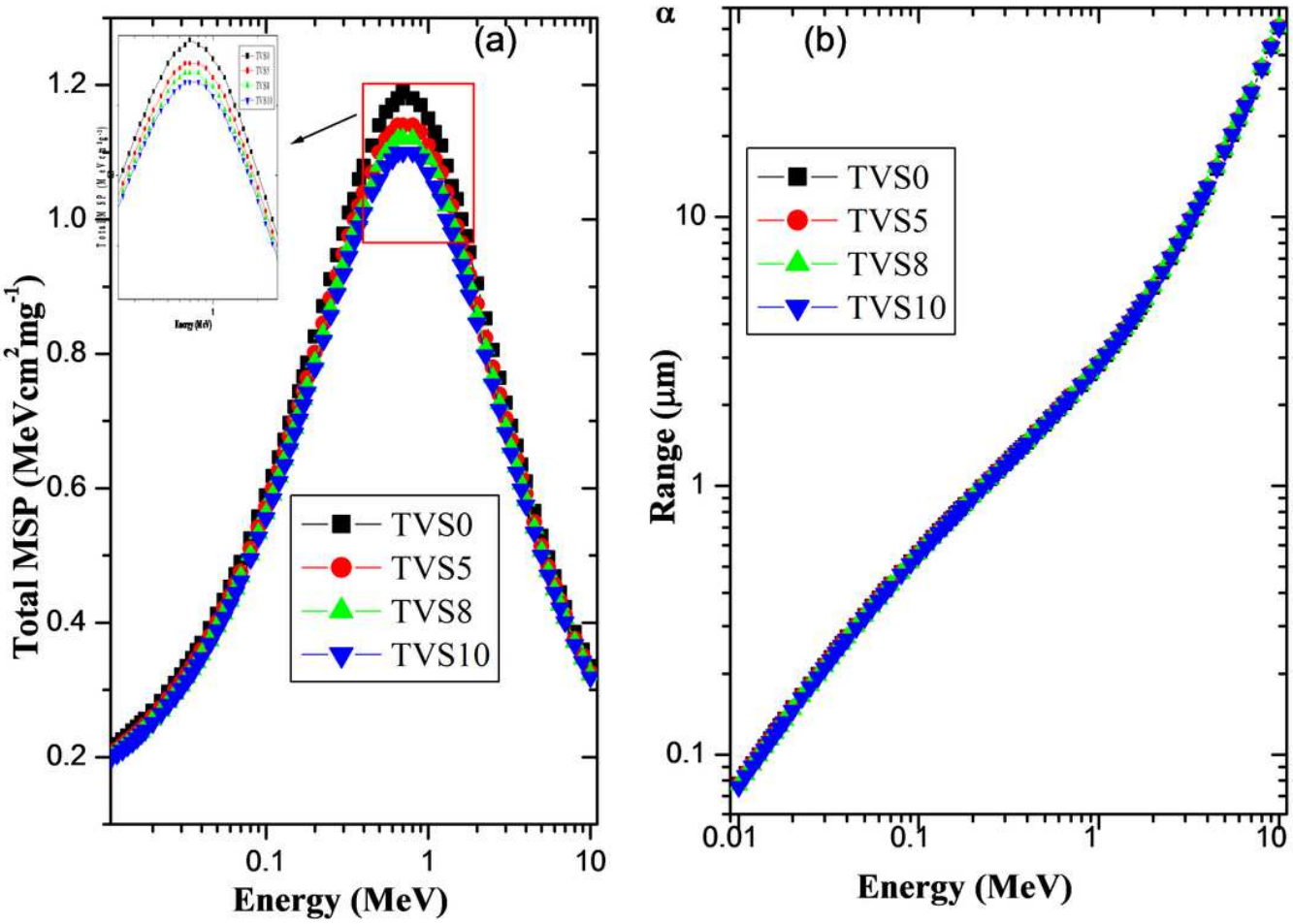

Figure 14

Total MSP (a) and range (b) of α-particle as a function of energy for TVS glasses.

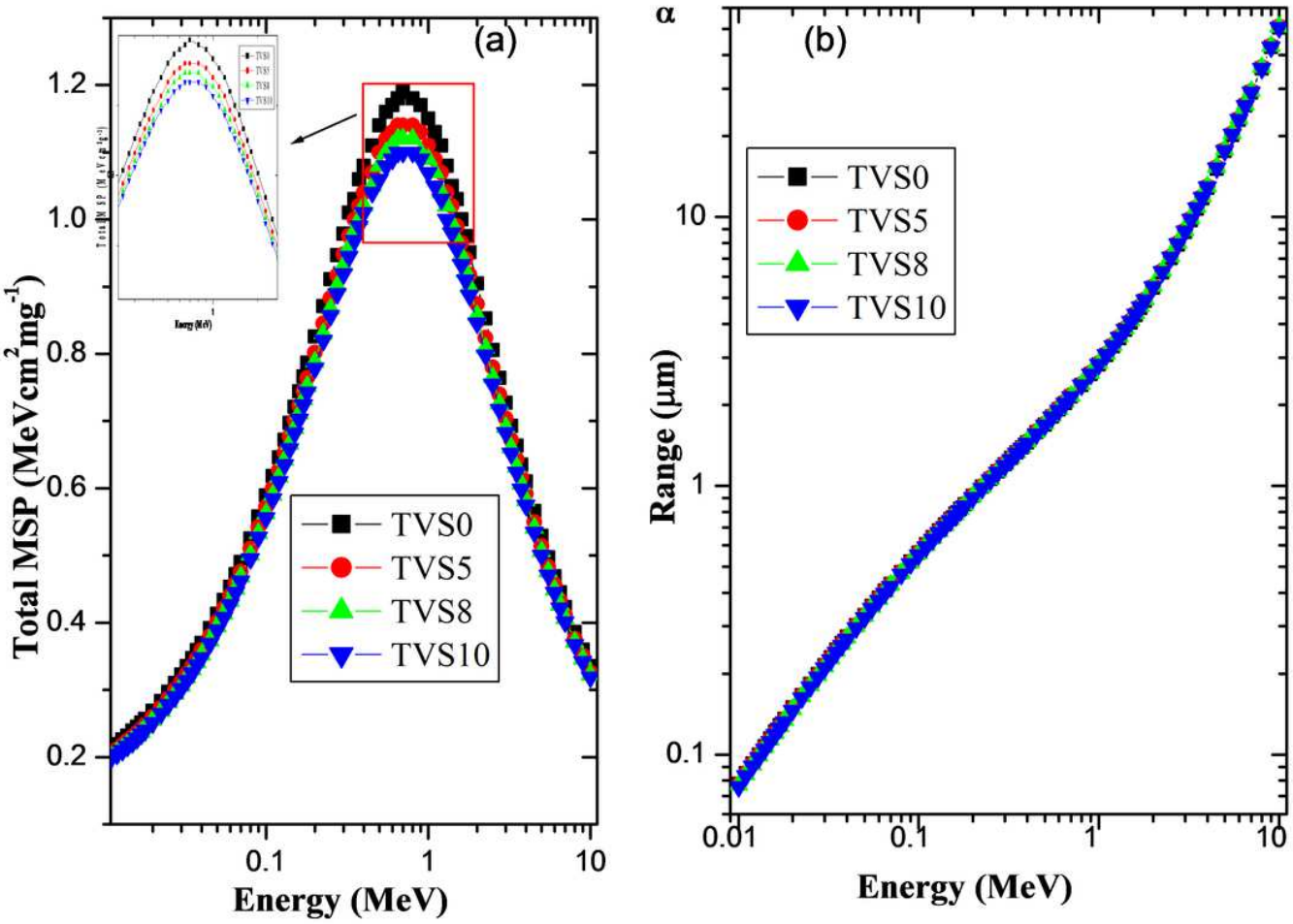

Figure 14

Total MSP (a) and range (b) of α-particle as a function of energy for TVS glasses.

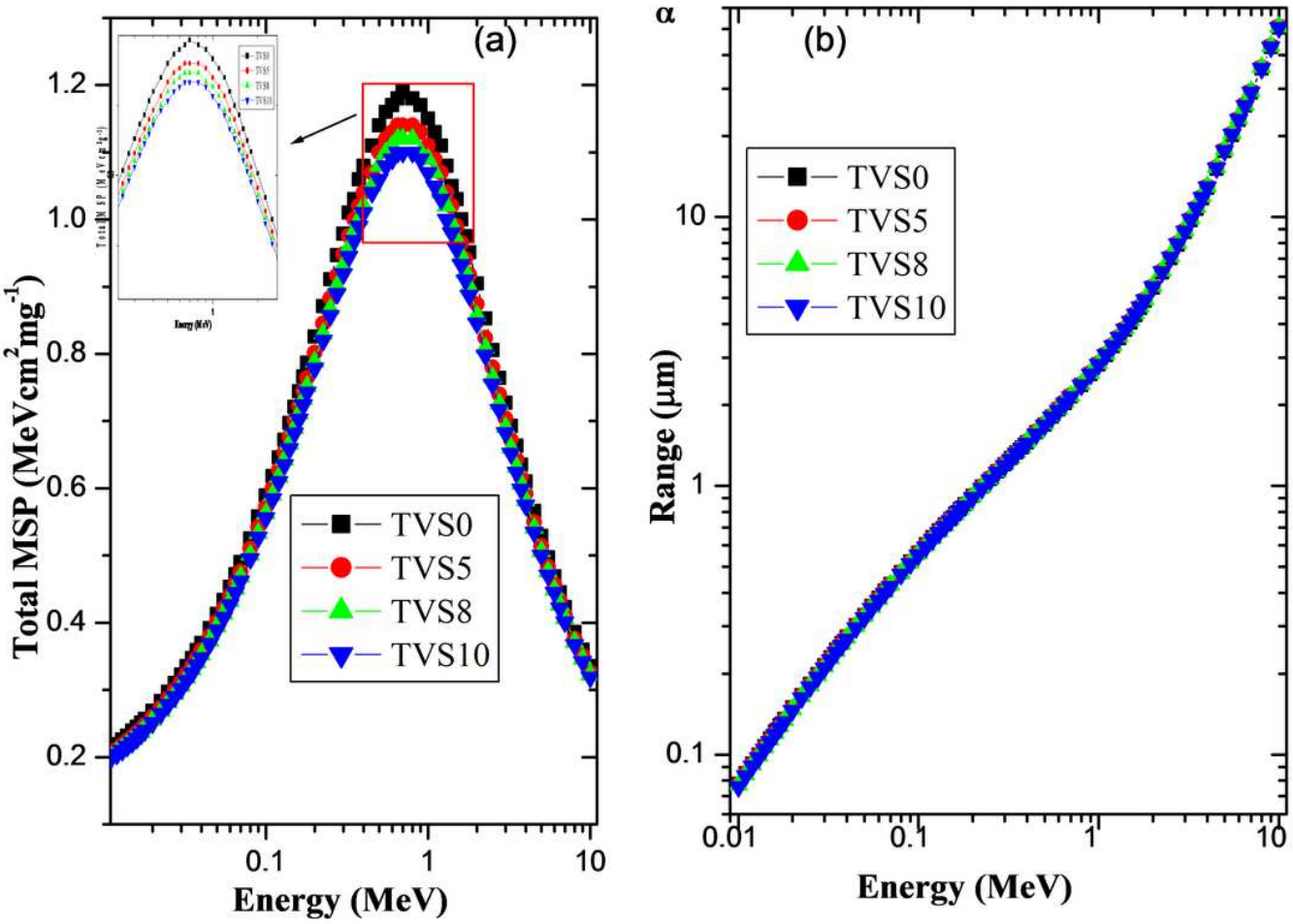

Figure 14

Total MSP (a) and range (b) of α-particle as a function of energy for TVS glasses.

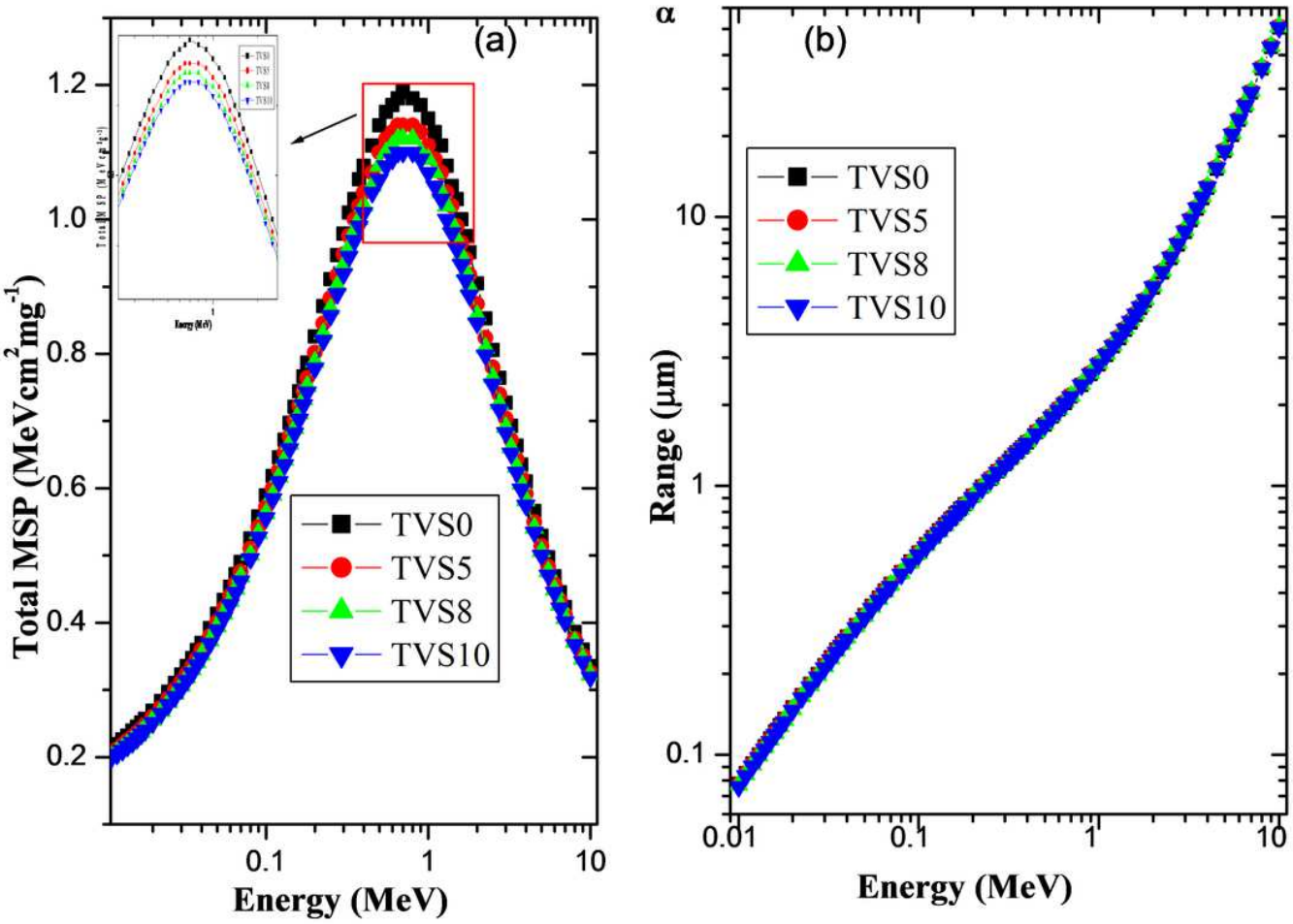

Figure 14

Total MSP (a) and range (b) of α-particle as a function of energy for TVS glasses.